Technical Report

WIND TUNNEL MODELING OF FLOW AND DIFFUSION OVER SAN NICOLAS ISLAND, CALIFORNIA

by

R. N. Meroney and J. E. Cermak

Prepared under
U.S. Navy Research Control N123(61756)50192A(PMR)
U.S. Naval Pacific Missile Range
Point Mugu, California

Unclassified

Fluid Dynamics and Diffusion Laboratory
College of Engineering
Colorado State University
Fort Collins, Colorado

September 1967

CER66-67RNM-JEC44

ABSTRACT

Neutrally and stably stratified flow over a 1:6200 and a 1:12,000 scale model of San Nicolas Island, California, was studied in the Army Meteorological Wind Tunnel of the Fluid Dynamics and Diffusion Laboratory at Coloardo State University. Surface characteristics of wind movement over the island were studied by the use of indicator paints, titanium tetrachloride smoke, and the measurement of mean velocity, mean temperature, mean concentration, and turbulent intensity profiles.

Available field data revealed that similarity was sufficiently achieved to give similar mean flow patterns. Flow in the wake region was self consistent, but no comparative field data are available. Concentration decay rates for diffusing tracers were comparable for neutral flow. Mean velocity, mean temperature, and Richardson number profiles were similar for stably stratified flows; however, the similarity of the diffusion plumes to plumes in the atmosphere is not clear. It is concluded that over complex terrain flow fields may be satisfactorily simulated for stable thermal stratification, but that the characteristics of diffusion in the stable stratifications produced by the Army Meteorological Wind Tunnel should be studied in greater detail.

ACKNOWLEDGMENTS

Many personnel of the Fluid Mechanics Program at Colorado State University have contributed and assisted in this study. The efforts of Messrs. Ching Chi Chih, Tom Nycum, and Jon Peterka were especially appreciated. Cooperation of the Army Materiel Command in giving permission to use the Army Meteorological Wind Tunnel made this study possible.

TABLE OF CONTENTS

TABLE OF CONTENTS - Continued

LIST OF FIGURES

LIST OF FIGURES - Continued

LIST OF FIGURES - Continued

LIST OF SYMBOLS

Symbol	
C	Time mean concentration
g	Acceleration of gravity
h	Typical roughness height
k	von Karman's constant
K_H	Exchange coefficient for heat
K_M	Exchange coefficient for momentum
L	Monin-Obukhov stability length
Q	Source strength
R	Reynolds number
R_f	Richardson number in the flux form
Ri	Richardson number
Ri(Crit.)	Critical Richardson number
u*	Friction velocity - $\sqrt{\frac{\tau}{\rho}}$
u	Local mean velocity
U	Ambient velocity
x, y	Cartesian coordinate
z	Elevation
z_o	Roughness length
ν	Kinematic viscosity
β	Emperical coefficient (see Equation 3-7)
λ	Lateral diffusion characteristic length
η	Vertical diffusion characteristic length
θ_T	Turbulent energy characteristic length (Equation 5-7)
σ_T	Intensity jet width

I. INTRODUCTION

A wind-tunnel study of San Nicolas Island was motivated by the desire to estimate the diffusion characteristics of toxic gases which might be released at the southern tip of the island (point E on Figure 1). The U.S. Navy proposed the island as a site for a series of static-firing tests of rocket motors using solid propellants which in combustion produced a toxic material beryllium oxide. The toxicity of beryllium oxide posed a potential health hazard to personnel on the island and inhabitants on other islands or on the mainland along the downwind trajectory of the combusion product cloud. A field program was instituted to analyze the toxicity problem through study of the diffusion of fluorescent particle clouds released from the proposed test site on San Niclas Island (9). Such a program is inherently difficult and costly due to the vagrancies and unsteadiness of the atmosphere; hence, to supplement and complement the prototype study, a model study in the meteorological wind tunnel of the Fluid Dynamics and Diffusion Laboratory at Colorado State University was initiated. Such a program provided the advantages of steadiness of flow conditions and adequate time to map flow and diffusion fields in three dimensions; however, the scaling of laboratory diffusion and turbulence parameters downstream of the peculiar geometry of San Nicolas Island to the field conditions needed to be studied experimentally.

A necessary condition for the modeling of diffusion characteristics is that mean flow patterns over a scale model of the terrain be established which are similar to those in the prototype. Accordingly, one

primary purpose of this study was to determine if wind patterns observed in a wind tunnel over a 1:6200 scale model of San Nicolas Island are representative of actual wind patterns observed in the field. During this study, emphasis was placed on stably stratified flows. This emphasis was required by the fact that prototype flows are restricted in their dispersive capacity by stable stratification such as is commonly found to occur over San Nicolas Island.

The study was exploratory in nature since few attempts have been made in previous programs to model wind patterns with thermal stratification using such a small scale model with the exception of a 1:50,000 model study of the lee-wave formation downwind of Mt. Fuji by Abe (1), and a 1:12,000 model study of diffusion over Point Arguello, California (3). Other wind-tunnel studies of stably stratified flows have been concerned only with the effect of stratification on turbulence intensity (10,30). The reasons for this narrow range of emphasis were that previously, a wind tunnel capable of creating flow with an adequately controlled density gradient had not been available and adequate field data for comparison with laboratory inversion-flow results had not been obtained.

Specifically, the objectives of the present study were:

1. Determination of the optimum surface roughness, ambient wind speed, and thermal gradient in the approach flow to simulate prototype conditions,
2. Determination of characteristic wind patterns over the 1:6200 scale model,
3. Comparison of wind-tunnel flow measurements with available prototype data,

4. Analysis of the distribution of concentration profiles of tracer gas downstream from the model island, and
5. Analysis of wake characteristics downstream from the model island.

II. EXPERIMENTAL EQUIPMENT

A. Wind Tunnel

The wind tunnel has often been disregarded in meteorology as a fluid flow analogue because of the difficulties in modeling Coriolis effects and temperature stratifications. However, for turbulent shear flows less than 1000 meters from the surface, Coriolis effects are usually small. In the case where the effects of stratification cannot be ignored, it is necessary to employ a wind tunnel installation specifically designed to reproduce magnitudes of stability and stratification as is found in the atmosphere (5). Such a facility is the Army Meteorological Wind Tunnel in the Fluid Dynamics and Diffusion Laboratory at Colorado State University (Figure 2).

The recirculating meteorological wind tunnel, driven by a 250 hp DC motor, contains a 27 meter long test section which is 1.8 x 1.8 m in cross section. A 12.2 meter length of the test-section floor, beginning 10 m from the upstream end, can be heated electrically or cooled by circulating brine through the floor, within a range of 0^{o} C to 210^{o} C. In addition, the ambient tunnel air can be heated or cooled from 0^{o} C to 95^{o} C by passing it over brine-chilled coils.

A set of fine screens reduces ambient turbulence to a level of less than 0.1 percent. A trip fence (turbulence stimulator), located just upstream from the test section, serves to stabilize the flow pattern as well as to provide a thicker turbulent boundary layer than would exist without it. A complete description of the wind tunnel can be found in Reference (4).

B. Instrumentation

1. Velocity and Intensity Profiles -- The velocity distributions were measured with a pitot-static tube of standard (Prandtl) design, 32 mm in diameter. The two pressure ports of the tube were connected to the two ports of an electronic differential pressure transducer (Transonic, Equibar type 120). The D.C. voltage output of this differential capacitor device was recorded on an X-Y plotter (Mosley type 135) versus vertical position. Dynamic pressure profiles were converted to air velocity by evaluating local density from local temperature and barometric pressure measurements.

Longitudinal and vertical turbulence intensity distributions were measured by monitoring the a-c signal of hot wire anemometer probes. The longitudinal turbulence scale for neutrally stratified flows was measured by a single-wire probe (Disa Company). A tungsten wire of .005 mm diameter, 2.54 mm length, and approximately 3.5 ohms cold resistance was used as a sensor. The wire was held at constant temperature by a Colorado State University Solid State Anemometer System (26) and the fluctuating output was presented on an X-Y plotter from a RMS meter (Bruel and Kjaer, type 2409). The vertical turbulence intensities were measured by a cross-wire probe (Disa Company), the fluctuating signals were combined in an electronic difference circuit, averaged by a RMS meter, and finally presented on an X-Y plotter.

Interpretation of the cross-wire signal for thermally stratified flow required calibration of the instrument over a wide temperature and velocity range. The relations used to interpret the data were

$$u = 2.36\sqrt{\frac{\Delta h}{\rho}} \qquad (2\text{-}1)$$

where

Δh = dynamic pressure in mm Hg

ρ = air density in slugs/ft^3;

and

$$\overline{u'} = \left(\frac{\partial U}{\partial E}\right) \overline{e'} \qquad (2\text{-}2)$$

where

$\left(\frac{\partial U}{\partial E}\right)$ is the slope of the single wire calibration

and

$$\overline{w'} = \tfrac{1}{2} \left(\frac{\partial U}{\partial E}\right)_T \quad \overline{(e_1' - e_2')} \qquad (2\text{-}3)$$

where

$\left(\frac{\partial U}{\partial E}\right)_T$ is the calibration coefficient for the inclined hot wire as indicated in Figure 3.

2. Temperature Profiles -- A copper-constantan thermocouple with an ice reference was used to measure mean temperatures. Output of the thermocouple was recorded on an X-Y recorder (Mosely type 135).

3. Surface and Fluid Flow Patterns --

a. Smoke -- Smoke was used to define the flow patterns for the neutral and the inversion flows. Titanium tetrachloride was used to provide the dense smoke required for photographic purposes.

b. Indicator Paint -- Indicator paint was applied to the surface of the model to facilitate recognition of flow patterns. The paint consisted of white water-base latex paint mixed with congo red (an organic indicator of pH intensity). Diluted hydrochloric acid was applied to the painted surface which sensitized the surface to the presence of anhydrous ammonia. Anhydrous ammonia was then released from points of interest on the model surface into the air stream. A trace of the diffusion plume of ammonia, indicating the surface wind direction, showed as a pink streak on the blue background of the model.

c. Camera Equipment -- During this study two cameras were used to record smoke and diffusion traces: (a) a series 100 Polaroid camera with integrating shutter utilizing both color and black and white films which allowed the results to be seen immediately, and (b) a Speed-Graphic camera utilizing 4 x 5 in. black and white film.

4. Simulated Rocket Exhaust Plume Measurements

a. Helium Feet and Sampling System -- The plume gas used in this study was helium because a technique could be devised to measure concentration with the mass spectrometer contained in a Veeco helium leak detector. The feed and sampling system used is schematically illustrated in Figures 5 and 6. The flow rate of helium to the gas source on the San Nicolas Island model surface was controlled by a pressure regulator at the bottle outlet and by a sensitive flowmeter. Source strength was maintained at 630 cc/min. of pure helium throughout this study. The helium exited from a brass tube of radius 3.2 mm which directed the flow vertically upward against a small metal bonnet such that the injected gas had negligible longitudinal velocity. The source outlet was located flush with the island model surface at the proposed rocket test stand site indicated as point E on Figure 5.

The sampling probe was manufactured from small diameter hypodermic tubing and was mounted on a traversing carriage whose horizontal and vertical position was controlled remotely from outside the tunnel. Concentration of the helium in the downwind plumes was measured at ground level along a line normal to the axis of the plume and vertically at the plume centerline.

b. Instruments to Measure Concentration Levels -- Sample gas was continuously drawn into the sampling probe by a small vacuum pump.

Midway between the sampling probe and the vacuum pump a T-connector allowed minute samples to be drawn through a calibrated leak into the evacuated interior of the Veeco mass spectrometer. The helium and other components in the air flow were drawn into a V-tube of the mass spectrometer where the molecules were converted into positively charged ions by electron bombardment. These ions were directed by the repeller grid down through a slit and were accelerated by a pair of focus plates in the V-tube. A magnet which was set outside the tube diverted the helium ions from the other ions in the beam. At the end of the V-tube the charged helium ions were gathered by a collector. An ion current was produced and amplified as a visual indication of the intensity of helium collection on the portable leak-indicator meter.

The DC signal of the charged helium was applied to the Y-axis of an X-Y plotter. The other axis of the X-Y plotter was a time base. However, because of the slow response of the mass spectrometer, a continuous horizontal concentration profile could not be taken. The experimental results in DC voltage were converted into concentration by means of a calibration chart. A typical plume distribution measurement is shown in Figure 7. The full scale of the meter ranged from 1 to 1000. The least count was 0.02 of the 1 scale.

c. Calibration Procedures -- Since a closed circuit wind tunnel was used, the ambient concentration level built up in the wind tunnel with time. Most helium did leak out, thus, the amount of helium in the ambient air flow was never higher than 60 ppm - about 0.2 on the meter scale. Nevertheless, an ambient concentration measurement was taken after each profile. The relative concentration was obtained by subtracting the corresponding ambient concentration from the absolute

concentration. All data presented in the figures and tables are relative concentrations.

A drift in the mass spectrometer due to contamination of the filament of the V-tube often caused a change in the magnitude of the concentration measurements which resulted in a parallel shift of the calibration curve on log-log paper, so the mass spectrometer was re-calibrated before and after each run. A typical calibration curve is shown in Figure 8. Three calibration points were obtained with helium-nitrogen mixtures of known helium concentration (0.05, 0.2 and 0.5%).

Due to the slow response of the mass spectrometer, a period from one to two minutes was allotted for the stabilization of each reading before it was recorded. The concentration signal itself was usually averaged over at least 60 seconds. This method compared favorably with the average of signals integrated over a period as long as 250 seconds by graphical means.

C. San Nicolas Island Models

A 1:6200 scale model of San Nicolas Island was designed and built in the Fluid Dynamics and Diffusion Laboratory. The 1:6200 model (approximately 2½ x 1 meter in actual size was made of laminated 3/16 inch balsa wood sheets set on a stiff fibrex board base. Each balsa sheet was cut to fit a 100 ft contour on a map which had been photographically enlarged to the scale of the model. After lamination of the balsa sheets, the surface was smoothed to the final shape with a power cutting tool using the 100 ft contour outlines as guide lines (Figure 4). The completed model was coated with a plastic sealer and finally with the indicator paint described in II.B.3.b. above.

Subsequently, a smaller 1:12,000 scale model of San Nicolas Island was provided by loan from the Pacific Missile Range for wake measurements. This model had a vertical distortion of approximately 10:3 and was manufactured from a plastic foam with a sealed painted upper surface. This model was sectioned at a sea level contour and remounted on a plywood sheet for use in the Army Meteorological Wind Tunnel.

III. SIMULATION OF ATMOSPHERIC MOTIONS

In order for flow patterns over models of large topographic features to simulate the atmospheric motions over their prototypes, it is generally concluded that geometric, dynamic, and kinematic similarity must be satisfied (5,15). Such similarity is associated with the model-to-prototype equivalence of certain significant dimensional groupings of the system variables. It is now recognized from experience in fluid and hydraulic scaling, however, that physical phenomena not numerically significant for the prototype may become so for the model flow, or vice versa; hence, exploration of the wind tunnel as a laboratory tool often awaits specific comparison of prototype to model measurements for a given category of problems before confidence may be placed in the model results as a predictive device. The state of the art of terrain aerodynamics is at just such an impasse. Current similarity arguments suggest that the required criteria for accurate modeling are geometric similarity, Reynold's number similarity, and similarity in the approaching boundary flows. Once these criteria are established, comparative prototype measurements must be made to determine if they are sufficient.

A. Geometrical Similarity

Geometrical similarity was achieved through use of the primary 1:6200 scale model constructed from balsa wood at Colorado State University. The model scale was undistorted; i.e., the vertical and horizontal scaling were both at 1:6200. A second model of 1:1200 horizontal scale with a 10:3 vertical distortion was provided by the Navy for qualitative wake analysis.

The effect of such vertical distortion on the wake behavior is not well understood; however, it might be expected that vertical convective motions and initial turbulence intensity might be accentuated.

B. Dynamic Similarity

If the Reynolds number is based on the ambient velocity, U, m/sec, the height of a characteristic feature, h, m, and the kinematic viscosity, ν , m^2/sec, then typical values of the Reynolds number for prototype and model are

$$R_p = \frac{U_p h_p}{\nu_p} = \frac{(3)(300)}{1.5 \times 10^{-5}} = 6. \times 10^7 \qquad (3\text{-}1)$$

and

$$R_m = \frac{U_m h_m}{\nu_m} = \frac{(3)(300)}{(1.5 \times 10^{-5})(6200)} = 1.0 \times 10^4 .$$

In other words, when the same fluid, wind speed, and flow regime (either laminar or turbulent) are used for the model flow as are found in the prototype flow, the ratio R_p/R_m becomes equal to the scale ratio -- 1:6200 in this case.

To minimize the apparent dissimilarity suggested by the large difference in R_p and R_m, there are two distinct approaches available. When both flows are in the turbulent state over essentially flat surfaces, the model may be roughened to produce flow characteristics corresponding to those found at Reynolds numbers larger than the actual value. This approach depends upon producing flows in which the flow characteristics become constant (independent of Reynolds number) if a lower limit of the Reynolds number is exceeded. For example, the resistance coefficient for flow in a sufficiently rough pipe as shown in Schlichting (27, p. 521) is constant for a Reynolds number (mean flow

speed x pipe diameter/kinematic viscosity) larger than 2 x 10^4. This implies that the basic flow quantity of surface shear stress, τ_o, is directly proportional to the mean flow speed squared, U^2, times the fluid density, ρ -- $\tau_o \rho U^2$. Thus, if $\rho_m U_m^2 = \rho_p U_p^2$ for such flows, $\tau_{om} = \tau_{op}$. In turn, this condition is the necessary condition for mean turbulence statistics such as root-mean-square values and correlation coefficients of the turbulence velocity components to be equal for the model and the prototype flow. For the case of the San Nicolas Island models, the roughness height scale equivalent to the prototype situation results effectively in a smooth model.

In the case where the laboratory flow speeds must be reduced to satisfy other similarity criteria (such as the thermal criteria described in the following section), the model flow may be actually laminar. When this happens, roughening of the model surface cannot produce the desired similarity between inertial and viscous forces (Reynolds number similarity of the type discussed previously). However, similarity between inertial and viscous forces may still be closely approximated. Basically the concept to use is that described by Abe (1) in which the turbulent prototype fluid is approximated by a fluid of molecular kinematic viscosity equal to an average turbulent eddy viscosity or kinematic turbulent exchange coefficient, K_M. Then a comparison of the Reynolds numbers $(R_m)_{lam}$ and $(R_p)_{turb}$

$$\frac{U_m h_m}{\nu_m} \quad \text{and} \quad \frac{U_p h_p}{(K_M)_p} \quad \text{respectively,}$$

may be made for estimating the degree of dynamic similarity. The ratio of these two Reynolds numbers

$$\frac{R_m}{(R_p)_{turb}} = \left(\frac{U_m}{U_p}\right)\left(\frac{h_m}{h_p}\right)\frac{(K_M)_p}{\nu_m} \qquad (3\text{-}2)$$

can be estimated by selecting typical values for the speed ratio U_m/U_p, the scale ratio h_m/h_p (1:6200 in this study), and the diffusivity ratio $(K_M)_p/\nu_m$. Considering a velocity ratio of unity, a turbulent exchange coefficient of 2.3×10^3 cm^2 sec and a kinematic viscosity for air of 2.3×10^{-1} cm^2/sec, a very favorable value for the Reynolds numer ratio is obtained:

$$\frac{R_m}{(R_p)_{turb}} = (1) \frac{1}{6.2 \times 10^3} 10^4 \simeq 0.5 . \qquad (3\text{-}3)$$

The photographs of smoke-flow patterns show that flow conditions over the laboratory model were essentially laminar near the surface; however, flow downstream of the sharp ridges above the surface appears to be turbulent. This means that the type of Reynolds number similarity proposed in the preceding paragraph should be valid over a large part of the model. One should keep in mind, however, that $(K_M)_p$ is not really a constant; it varies both with height and location over the region, so that the Reynolds number ratio calculated is an average value having a representative order of magnitude.

In the upper region downstream from the ridges, similarity of flow is also expected on the basis of arguments presented in the second paragraph of this section. The argument need only be extended to include the invariance of flow with Reynolds number downstream from "sharp-edged" objects.

The dynamic effects of buoyancy forces due to vertical temperature gradients and the associated vertical density stratifications are of prime importance in determining the flow characteristics around topographical features. If the modifications of vertical motion by atmospheric inversion are to be similar for the laboratory and the prototype

flows, a criterion must be selected to insure adequate temperature variation over the wind-tunnel model. Several parameters could have been chosen, such as a Froude number or the Obukhov stability length; however, a Richardson number, as discussed by Sutton (30), was chosen because of its wide usage by meteorologists and because of its ease of evaluation as a bulk parameter. Batchelor (1953) has shown that in stratified flow close to the ground, dynamic similarity depends entirely on the Richardson number for the atmosphere (19).

The Richardson number, Ri, expressed as a local parameter is defined by

$$Ri = \frac{g}{\theta} \frac{\left(\frac{\partial \theta}{\partial z}\right)}{\left(\frac{\partial u}{\partial z}\right)^2} \quad . \tag{3-4}$$

When a bulk Richardson number is desired to describe the thermal influence over a layer of thickness Δz, the following form is convenient:

$$Ri = \frac{g}{\theta} \frac{\Delta \theta}{(\Delta u)^2} \Delta z \quad . \tag{3-5}$$

For the purpose of obtaining an estimate of Richardson number variation at San Nicolas Island at different heights, use was made of Rawinsonde data taken from selected months over the 33 month period from June 1963 to February 1966. Richardson numbers were computed from profiles of temperature and wind speed taken at 1000 ft increments from 1000 to 10,000 ft and for one 430 ft increment from 570 to 1000 ft. The distributions of Richardson number obtained are shown in Figure 9. Systematic errors result in values abnormally high in computation (i.e., >> 5 etc.). The important observation to be made is, of course, that the atmosphere is very frequently stably stratified.

The meteorological measurements available for flow over San Nicolas Island are unfortunately not suitable for calculation of the exact quantitative variation of Richardson number with height. Accurate analysis required data separated by approximately 30 feet while the separation increment for the Rawinsonde data provided was a minimum of 430 feet. In addition, no information was available for the upstream flow distributions over the ocean. Primary conclusions made from the prototype flow analysis were:

a. Stably stratified inversion layers existed to such an extent that wind tunnel diffusion testing should include their limiting effects to predict dispersion hazards,

b. The average stratified condition consisted of a raised inversion with a base at about 300 meters, and

c. The most common flow direction for the prototype flow was from an azimuth of 315^{o}.

Previous experience in the Army Meteorological Wind Tunnel indicated that a surface based inversion of an appropriate order of magnitude Richardson number could be obtained with the existing thermal controls. Attempts to produce a raised inversion by adding roughness or insulating portions of the cooled floor did not significantly effect the thermal stability. It was concluded that a raised inversion could not be obtained without either a) heating the model island and sea surface after an initial cooling condition, or b) constructing an upstream grid of heating and cooling rods to superimpose the desired temperature profile. Both of these methods would require extensive developmental expenditure; hence, the decision was made to study the surface based inversion as a limiting condition.

Since no accurate data exist for the prototype Richardson number magnitude during stable stratification, the scaling criteria for the wind-tunnel measurements were based on the fact that other atmospheric measurements seem to indicate stable stratification for a value of Richardson number greater than 0.2 (30,19). Thus, it was considered sufficient for dynamic similarity to provide wind tunnel conditions such that the equivalent Richardson number was greater than 0.25 at the 300 meter contour line of the model.

To obtain a Richardson number of 0.25 at the equivalent 300 meter level of the model required the operation of the wind tunnel at the low velocity of 1.6 mps. A further decrease in velocity increases the Richardson number but introduces abnormal tunnel fluctuations.

A typical calculation of the bulk Richardson number for the wind-tunnel flow is shown in Figure 10. In this calculation, the layer over which Ri is calculated corresponds to the actual boundary-layer thickness for the flow.

Local Richardson number distributions were also calculated from measured velocity and temperature distributions in the wind tunnel. In the lower 7 inches of the boundary layer, the local Richardson number behaves in the manner suggested by the meteorological relation

$$Ri = \frac{z/L}{1 + \beta z/L} \tag{3-6}$$

if the log-linear velocity profile holds for the wind profile (see section C) (30,19).

C. Similarity of Approach Flow

The upstream velocity and temperature profiles may be matched rather precisely to those found in the atmosphere by setting the model

at varying distances from the leading edge of the boundary layer in the wind-tunnel test section. Although the momentum and thermal boundary layers begin at different sections it has been found that after a short distance both layers approach the same height. Modeling of the thermally stratified atmospheric boundary layer in a wind tunnel is an area of continued effort in the Fluid Dynamics and Diffusion Laboratory at Colorado State University. It has been found that when the Richardson number is adjusted to correspond to values found in nature, the thermal stratification will also affect the profile shapes in the laboratory. On the basis of several investigations it has been confirmed that the logarithmic linear law of Monin and Obukhov (1954) for atmospheric profiles is also produced by the Army Meteorological Wind Tunnel (7,23).

The logarithmic-linear law was devised by Monin and Obukhov (1954) to describe the mean velocity profile in the atmosphere under various stratification conditions. It has the form

$$u = u^* \left(\ln \frac{z}{z_o} + \beta \frac{z}{L}\right) \tag{3-7}$$

where u^* is the friction velocity, z_o is a roughness length, β is the empirical coefficient, and L is a stability length parameter related to the Richardson number by

$$Ri = \frac{z/L}{1 + \beta z/L} \quad . \tag{3-8}$$

Wind tunnel measurements summarized in Figures 11, 12 and 13 confirm the presence of upstream flow conditions in the wind tunnel that appear to be similar to prototype conditions in atmospheric surface layers (7,17,23).

IV. CHARACTERISTICS OF THE MODEL FLOW AND COMPARISON WITH THE PROTOTYPE FLOW

Having established that geometrical, dynamic and thermal similarity should be attained to a reasonable degree for turbulent and laminar flow over the model, based on arguments outlined in Chapter III, a program of measuring and visualizing flows over the model was undertaken. Since inversion flows were of primary interest, the laboratory study was confined primarily to low-speed flow 1.6 m/sec with a maximum attainable temperature difference (the wind-tunnel floor was 103^{o} F cooler than the ambient air). Flow patterns for the stable stratification were well documented in the cases of flow approaching from an azimuth of 315^{o}. This direction was selected because it represents the most common flow direction for the prototype flow. Flow data for an azimuth of 315^{o}, with no thermal stratification, were obtained to determine flow-pattern differences between neutral and inversion flows.

A. Boundary-Layer Characteristics Upwind from the Model

One of the first objectives of this study was to determine the nature of the boundary-layer flow approaching the model. The bulk Richardson number based on the thermal boundary layer gave an indication of the overall stability of the flow. As shown in Figure 10, this Richardson number for the inversion flow in the wind tunnel was approximately $Ri = 0.477$. For 5.1 cm from the wall, equivalent to the 310 m contour in the prototype, the local Richardson number for the same flow was 0.25.

A detailed description of typical upstream inversion velocity profiles is given by Figure 14. In this figure, velocity profiles measured with a pitot-static tube are shown for a set of stably stratified flows over a range of Richardson numbers. The profile for an ambient velocity near 1.6 m/sec has a power-law distribution of the form

$$u \alpha z^{1/5}$$

where u is the velocity and z is the height above the floor. A power-law velocity distribution with this exponent is characteristic of low Reynolds number or nearly laminar boundary-layer flows. Velocity measurements for flows less than 0.6 m/sec were very difficult to obtain reliably; hence, the ambient flow speed was not reduced below 1.6 m/sec in order to realize a larger value of the Richardson number.

A typical temperature profile is shown in Fig. 15. This profile depicts an inversion flow with an ambient velocity of 1.8 m/sec. Variations in temperature profiles were much smaller than for the velocity profiles. In a given day, temperature data were reproducible to within $1 - 2^{o}$ F. Temperature profiles for the approach flow also appear to follow a power-law distribution.

The temperature profiles were very insensitive to the presence of the model or other barriers near the floor level. Efforts to use additional roughness on the floor or to insulate portions of the cooled floor to obtain a raised inversion effect at ground level were not successful, although Richardson number profiles were modified due to variations in the velocity gradients.

B. Temperature and Velocity Fields Over the Model

Measurements were taken for the velocity and temperature profiles directly over the island on a line extending upwind from the proposed launch site (Point E, Figure 1). The temperature profiles did not vary significantly either upstream, over, or downstream of the island model. Surface temperatures on the island were 25^{o} F higher than the surrounding model sea surface; however, any adjustments in temperature occurred too close to the surface to measure with the thermocouple. Reduction of field infrared surface temperature measurements made by an airplane about noon on a clear day over San Nicolas Island reveals that the land surface is maintained approximately 20^{o} F hotter than the sea surface (Figure 16) (data and instrument calibration curves provided by PMR). Hence, the higher model island surface temperatures do provide an approximation to the prototype condition.

Velocity profile variation over the island was insignificant except in the lee of the steep cliff features on the southwestern edge of the island. The details of these variations are discussed in Chapter VI as wake flow.

C. Flow Patterns Over the Model

As discussed in Chapter II, B, Section 3, two types of flow visualization techniques were used to obtain flow patterns. Photographs of surface flow directions using the indicator paint on the model gave an indication of local flow directions at the surface. Figure 17 shows typical examples of these flow patterns. Patterns such as those shown were produced by one release of ammonia at the upstream end of each streak.

A study of the model surface after each ammonia plume release revealed gradations in the color of indicator paint tints which allowed interpretation of the surface flows. These results are summarized graphically in Figures 18, 19 and 20. Surface flow lines generally agree with the ambient flow directions of 315^{o} for neutral conditions. Inversion conditions (Figure 20) result in a deviation of the flow to the west in the lee of the steep cliffs to the south of the island.

A description of the flow pattern above the surface was also obtained by photographing smoke over the model. Figures 21 through 30 show smoke traces for an ambient flow direction of 315^{o}, ambient velocity of 1.6 m/sec, and temperature difference of 115^{o} F. The photographs reveal a fairly simple flow over the island proper with interesting secondary flows downstream produced by the southern ridge. Mean flow patterns were deduced from these photographs and dominant features were represented in graphic form on topographic maps.

The northwest to southeast ridge which runs the length of the island reaches from 150 to 275 meters in height on the prototype and forms a barrier to the marine layer flow. Photographs in Figures 21 and 22 reveal the large-scale vortex motion induced by the ridge which produces large local mixing rates. Several photographs (especially those in Figures 21, 23 and 27) reveal a regularity of disturbances downstream of the island most typical of ground waves or laminar flow; hence, it should be expected that any transport phenomena may be more laminar than turbulent in character for the model flow. Figures 24 through 30 all reveal the laminar characteristics of the fluid motion over the upstream portion of the island. Figure 30 presents the laminar character of the flow upstream of the island, in which no turbulent mixing is evident.

The tendency of the island to direct atmospheric motions slightly to the east may be seen in Figures 23, 27 and 28. Smoke follows the lee edge of the island ridge eastward before it releases and continues downstream along a 315° azimuth.

Figures 31 through 34 show the basic flow patterns established with photographs of the smoke. The double cross-hatched regions indicate flow in which smoke released near the ground tended to stay close to the surface and was laminar in character. The single cross-hatched regions indicate where the flow, once at the surface, had separated and was somewhat above the surface with a turbulent vortex or ground-wave character to the motion. In general, the smoke remained attached to the surface until the flow passed over the downstream edge of the island, separated after following the ridge line, and either became turbulent or underwent laminar oscillations downstream from the ridge.

The side views of oil fog plumes released from the proposed rocket test stand site, shown in Figure 35, compare favorably to Figures 21 and 22 over the model. Oil fog pictures were provided by PMR and are evidently from series of tests performed by GCA Corporation on January 22, 1964 (9). The flow patterns indicated by Figures 18, 19, 20, 31, 32, 33 and 34 are in agreement with wind measurements made by PMR personnel at various sites indicated on Figures 36 through 38.

A total of twelve Berkeley Instruments, Micro-Meteorological field stations, Model W54631, measuring temperature, wind direction and wind speed were located on San Nicolas Island. These instruments operated continuously from February 1965 until August 1965. The data provided by PMR consisted of a printout of the raw data as collected with subhourly and hourly averages. Figures 36 through 38 display mean

wind directions and standard deviations from April and May of 1965 as averaged over approximately thirty days of neutral or stably stratified thermal conditions.

V. DIFFUSION CHARACTERISTICS OF MODEL FLOW

Diffusion in a disturbed boundary layer is of great practical importance. An atmospheric boundary layer disturbed by obstacles such as hills, mountains, canopies, or buildings, is much more common than the ideal case of a flat undisturbed boundary. Theoretically, a disturbed boundary layer might be interpreted as a conventional nonisotropic wall shear layer with a superimposed field of decaying turbulence produced by the disturbance. Certainly, in such a flow, the diffusion solutions produced for the simpler undisturbed boundary layer are not applicable (8,13,30).

Since disturbances can be generated by infinitely many different types of obstructions, it is not satisfactory, practically, to wait until all aspects of such a flow are understood and predictable. Indeed, it is doubtful if diffusion over complex terrain will ever be completely definable by such a synthesis. Hence, it is appropriate to consider if diffusion characteristics in the presence of such disturbances can be satisfactorily modeled in meteorological wind tunnels. The investigation of the concentration profiles downstream from the island model were directed toward determination of similarity law behavior comparable with prototype measurements and a specification of deviations from the non-disturbed dispersion behavior.

A. Neutrally Stratified Flow Over the Model

Measurements made downstream from the model hill (maximum height $\sim$ 3 cm) follow the trends set by the smooth flat plate. There seem to

be no significant differences. This result is in agreement with the velocity distirubution and flow development discussed in Chapters IV and VI, where it is affirmed that only the lower few centimeters of the boundary feel the presence of the island, and the effect of the hill on the concentration profile can easily be hidden by random experimental errors. This conclusion was also reached by Plate and Sheih in experiments on line-source diffusion downstream from two-dimensional model hills (25).

Vertical and horizontal concentration distributions for neutral stratification are plotted in Figures 39 and 40. These profiles have been nondimensionalized and compared for various distances downstream from the release point. The vertical and horizontal distances, z and y, have been divided by the characteristic lengths η and λ, respectively. The local concentration, $C(x, y, \tau)$ has been divided by the local maximum $C(x, o, o)$. The length scales λ and η were defined as the distance from the wall on plume centerline to the position where the local concentration has decreased to half its maximum level.

The concentration distribution can be described by a dimensionless universal curve,

$$\frac{C(x,y,z)}{C_{max}(x,oo)} = \exp 0.693 \left\{ - \left(\frac{y}{\lambda(x)} \right)^{a} - \left(\frac{z}{\eta(x)} \right)^{b} \right\} \qquad (5\text{-}1)$$

where $\lambda(x)$ and $\eta(x)$ are the lateral and vertical similarity lengths. The constants a and b were chosen equal to two. The agreement with this universal curve in the presence of the model island is of the same order observed by other investigators under various flow conditions (10, 17,21,25). The vertical and lateral growth of the plumes as characterized by the similarity lengths $\lambda(x)$ and $\eta(x)$ were proportional to

downstream distance x as

$$\lambda(x) \sim x^{h} \quad , \quad \text{where} \quad h \simeq 0.53 \text{ to } 0.65;$$

and (5-2)

$$\eta(x) \sim x^{p} \quad , \quad \text{where} \quad p \simeq 0.50 \text{ to } 0.77 \, .$$

Data were taken several times on different days; data scatter was of the same order each time.

The corresponding variation of $C_{max}(x,o,o)$ can be approximated by

$$C_{max}(x,o,o) \sim x^{-m} \quad , \quad \text{where} \quad m \simeq 1.11 \text{ to } 1.38. \tag{5-3}$$

These values fall below those obtained previously for point source diffusion utilizing an ammonia gas in the smaller Colorado State University tunnel (10,21). It was considered desirable to determine whether this was an effect of the source gas, the wind tunnel, or the test configuration. The test configuration described by Maholtra and Cermak, in Reference (21) was duplicated in the small Colorado State University wind tunnel, with a helium source release. Measurements made reproduced the previous results for plume growth rates within experimental error, except for a slight tendency to diffuse faster vertically due to the lower density of helium (see Figure 41). It was concluded that the ammonia and helium detection techniques gave essentially the same results.

Subsequently, a thorough survey was made of the diffusion of a helium plume in a neutrally stratified boundary layer for the entire length of the Army Meteorological Wind Tunnel. Measurements were made for two different scales of free-stream turbulence, 0.03 and 16.0%, and velocities ranging from 7 to 30 feet per second. The experimental results indicated an order of variation in the growth of plume characteristics not predicted by the Lagrangian similarity hypothesis of Cermak (2).

Figures 42, 43 and 44 summarize the effect of tunnel position on plume characteristics. The effects noted may be the result of secondary flow or boundary layer growth. A complete tabulation of these results was included in Reference (28).

Kai Kao and Cermak developed an expression for the maximum ground-level concentration for a continuous point source released at height $\bar{z} = h$ in a neutrally stratified boundary layer (16). This relation was developed upon the hypothesis of Lagrangian similarity and a logarithmic velocity profile. They suggest that

$$\frac{u^* z_o C_{max}}{Qk} = \frac{1}{\pi \zeta^2 F(\zeta)} \exp - \frac{H^2}{2\zeta^2} \qquad (5\text{-}4)$$

where

$$\zeta = \frac{z}{z_o} = f(\xi)$$

$$\xi = k^2 \frac{x}{z_o}$$

$$F(\zeta) = \frac{1}{\zeta} \int_1^{\zeta} \ln \zeta \, d\zeta \text{ , and}$$

$$H = \frac{h}{z_o} \text{ .}$$

Figure 45 compares the measurements made downstream from the San Nicolas Island model with this theory. Again, it is apparent that the model island has negligible effect on plume dispersion.

B. Stably Stratified Flow Over the Model

Several sets of tracer concentration measurements were made to determine the degree of similarity between diffusion in the stably stratified model flow and the corresponding neutrally stratified flow. A

comparison of the relative rates of concentration decay with distance downstream from the model and prototype sources is not possible because of the failure of the prototype study to provide usable data (9). Model results, therefore, are made nondimensional and compared with existing theories.

Nondimensional vertical and horizontal concentration profiles for the stably stratified flow are plotted in Figures 46 and 47. These data may be approximated by Equation 5-1 with coefficients a and b equal to 2 and 2.8, respectively. The increase in value of the coefficient b from the neutral lapse situation is related to the increase in Richardson number with vertical height for stratified flow.

The effect of the temperature stratification is also evident in the variation of the characteristic lengths λ and η with downstream distance. The growth of the characteristic lengths λ and η decreases with increase of longitudinal distance; hence, exponents in Equation 5-2 vary from 0.6 to 0.2 for n and from 0.8 to 0.4 for p. The variation with distance downstream may be indicative of the effect of a raised source. Koehler measured n equal to 0.33 and p equal to 0.44 under similar thermal and velocity conditions over a smooth flat plate for a ground source (17).

The maximum ground concentration varied with downwind position as x^{-m} with $m \simeq 0.9$ to 1.30. Koehler's measurements for a ground source under the same stratified conditions resulted in $m = 1.2$. Hence, in this respect it appears that the diffusion plume downstream from the model island behaves as if the island was not present.

Koehler derived an expression from Lagrangian similarity theory for the variation of maximum ground concentration with downwind distance

in a stratified boundary layer (17). When this expression is rederived to account for source height, the following equations are obtained:

$$\varepsilon = \eta \ln \frac{\eta}{\eta_o} - H \ln \frac{H}{\eta_o} - (\eta - H) - \beta\eta_o(\eta - H)$$

$$+ \frac{\beta}{2} \ln \frac{\eta}{\eta_o} (\eta^2 - H^2) - \beta^2 \frac{\eta_o}{2} (\eta^2 - H^2)$$

$$- \frac{\beta}{4} (\eta^2 - H^2) + \frac{\beta^2}{3} (\eta^3 - H^3) + \frac{\beta}{2} (\eta^2 - H^2)$$

$$+ kH \left(\ln \frac{H}{\eta_o} + \beta(H - \eta_o)\right) \qquad (5\text{-}5)$$

and

$$\tilde{C}_{max} = \frac{C_{max} u^* L^2}{Qk} \simeq \frac{\text{const exp } (-H^2/2\eta^2)}{\pi\eta^2 \left(\ln \frac{\eta}{\eta_o} - 1 + \frac{\beta}{2} (\eta - 2\eta_o + \frac{\eta_o^2}{\eta}) + \frac{\eta_o}{\eta} \right)} \qquad (5\text{-}6)$$

where

$$\varepsilon = k^2 x/L \ ,$$

$$\eta = z/L \ ,$$

$$H = h/L \ .$$

The other symbols are defined in the table of symbols. The relation between $\tilde{C}$ and ε has been determined for a characteristic roughness $\eta_o = 0.0001$ on a CDC 6600 computer and compared with the concentration plume measurements in Figure 48. The island source had a release height of H = 0.11. Agreement between theory and data is very good despite the presence of the San Nicolas Island model.

VI. WAKE CHARACTERISTICS DOWNSTREAM OF THE MODEL

Experimental investigations of the atmospheric surface layer over a flat terrain and of the boundary layer along a flat plate in a wind tunnel have shown that both flows are similar (5,7,23). Flat terrain is normally the exception, however, on the earth's surface, and flows may be dominated by mountains, hills, islands, or other obstructions. These obstructions affect the mean velocity distributions in the atmospheric surface layer and strongly influence the order of magnitude of the turbulence structure. Both effects are important to the rate of dispersion of pollutant clouds near such structures.

Terrain aerodynamics has been studied for several prototype obstructions, including Mt. Fujiyama, Japan; Rock of Gibraltar; Bear Mountain, Pennsylvania; and Pt. Arguello, California (1,3,12,14). In general, simulation was most complete for the complex terrain of sharp-edged geometry. A series of studies have also been instigated at Colorado State University to synthesize the effects of terrain (6,22, 24,25).

Measurements of velocity and turbulent intensity were made downstream of the two San Nicolas Island models (1:6200 and 1:12,000 scale) for wind direction of 315^{o} and a velocity of 1.6 m/sec. Data were examined for wake growth rates and turbulence decay.

A. Wake Characteristics in Neutral Flow

Velocity, vertical turbulence intensity, and longitudinal turbulence intensity were measured along a line projected downstream

from site E on San Nicolas Island model and parallel lines east and west of this projection. The shallow island heights generally had very little effect on the velocity profiles; however, the wake growth and dispersion was obvious through the turbulence measurements.

The wake behind the 1:6200 scale model was extremely weak and not evident at all in the velocity measurements. The wake appeared to be deflected slightly to the east by the model orientation to the general flow and was most intense just downstream from the island tip. The wake turbulence had effectively disappeared by one meter (6.2 km on prototype) downstream distance (see Figure 49).

The smaller 1:12,000 scale model of San Nicolas Island had a 10:3 vertical distortion; hence, although the model was more convenient for wake measurements, the vertical height was greater than for the 1:6200 model. The vertical distortion was evidenced by the marked deviation of the velocity profiles, Figure 50, and the large scale of the turbulence intensities measured, Figures 51 and 52. Although the total length of downstream distance affected by the wake was appreciably longer for the 1:12,000 scale model ($x \simeq 3$ meters) there was no noticeable wake drift to the east.

B. Wake Characteristics of Stable Flow

Wake behavior behind the 1:6200 scale model again was not evident in velocity measurements. Vertical turbulence intensity data indicated, however, that although the strength scale of the eddies was much decreased by stable stratification, the eddies persisted to three meters downstream from the model, Figure 53.

Deviations in the velocity profile were evident in the 1:12,000 scale model, Figure 54. In this case, separation may have occurred. The vertical turbulence intensity measurements were similar to those for the 1:6200 model with a larger scale, Figure 55.

C. Wake Growth and Dissipation

The profiles of $\sqrt{\overline{u'^2}}$ / U_∞ and $\sqrt{\overline{w'^2}}/U_\infty$ for neutral flow shown in Figures 49, 51, and 52 have a very similar appearance to those of a two-dimensional jet. This similarity includes a linear spread of the intensity profiles for distance downstream. An intensity jet width σ_T was defined as that distance from the floor at which the value of $\sqrt{\overline{u'^2}}$ had dropped to half the maximum value, see Figure 56. The amount of turbulence present is determined, of course, by the balance of production and dissipation of turbulent energy.

A convenient measure of the integral characteristics of the intensity distribution was suggested by Plate as

$$\theta_T = \int_0^\delta \frac{\overline{u'^2}}{u_\infty^2}\, dy \quad . \tag{5-7}$$

This characteristic length should scale as a spreading parameter of the turbulent energy (24). Figure 57 indicates the rapid generation of turbulent energy near the island lee bluffs and its subsequent decay.

For stably stratified flow, the intensity jet width does not grow linearly with downwind distance, Figure 58. The temperature inversion tends to limit vertical growth of the shear effects to a definite height. Figure 57 also displays the characteristic energy length θ_T for the stably stratified flows. The length has decreased by an order of magnitude, but the general shape of the curve is similar.

VII. CONCLUSIONS

On the basis of the experimental work completed in the meteorological wind tunnel, comparison with prototype data, and interpretation of the measurements, the following comments can be made:

1. Comparison of wind tunnel and prototype temperature data established at least a qualitative similarity in the structure of the model and prototype temperature field over the San Nicolas Island ground surface, for surface-based inversion conditions.

2. Comparison of surface-flow directions and smoke traces for neutral and surface-based inversion flows established that similarity existed in wind flow patterns over the San Nicolas Island and its model for neutral and surface-based inversion flows.

3. Diffusion downstream from a smooth, non-complex terrain may be approximated by the assumption of a theoretically flat surface. The island will not deflect a diffusion plume appreciably from the general circulation directions.

4. Maximum ground concentrations downstream from a continuous point source may be predicted by a diffusion theory based on Lagrangian similarity for both neutral and inversion flows.

5. The wake downstream from San Nicolas Island will not contain a strong separation, will result in only minor deviations from the normal mean velocity profiles for flat terrain, and will effectively dissipate in less than two to three island lengths.

6. Turbulence intensity characteristics in the wake of the model island decay and spread in a manner similar to the theoretical half jet flow.

BIBLIOGRAPHY

BIBLIOGRAPHY

1. Abe, M., Mountain Clouds, Their Forms and Connected Air Currents, Part II, Bull. Central Met. Obs., Japan, 7, (3), 1941.

2. Cermak, J. E., Lagrangian Similarity Hypothesis Applied to Diffusion in Turbulent Shear Flow, Journal of Fluid Mechanics, 15, Part I, pp. 49-64, 1963.

3. Cermak, J. E., and Peterka, J., Simulation of Wind Fields Over Point Arguello, California, by Wind-Tunnel Flow Over a Topographical Model, Final Report, U.S. Navy Contract N126(61756)34361 A (PMR). Fluid Dynamics and Diffusion Laboratory Report CER65JEC-JAP64, Colorado State University, December, 1965.

4. Cermak, J. E., and Plate, E. J., Micrometeorological Wind-Tunnel Facility, Final Report, Contract No. DA-36-039-SC-80371, U.S. Army Electronic Research and Development Activity, Fort Huachuca, Arizona.

5. Cermak, J. E., Sandborn, V. A., Plate, E. J., Binder, G. H., Chuang, H., Meroney, R. N., and Ito, S., Simulation of Atmospheric Motion by Wind Tunnel Flows, Fluid Dynamics and Diffusion Laboratory Report CER66-17, Colorado State University, May, 1966.

6. Chang, Shih-Cheng, Velocity Distribution in the Separated Flow Behind a Wedge Shaped Model Hill, Fluid Dynamics and Diffusion Laboratory Report No. CER65SCC66, Colorado State University, March, 1966.

7. Chuang, H., and Cermak, J. E., Similarity Profiles in Thermally Stratified Shear Flows, Fluid Dynamics and Diffusion Laboratory Report No. CER66-67-HC-JEC-4, Colorado State University, July, 1966.

8. Cramer, H. E., A Practical Method for Estimating the Dispersal of Atmospheric Contaminants, Proceedings of First National Conference on Applied Meteorology, American Meteorological Society, C, pp. 33-35, October, 1957.

9. Cramer, H. E., Hamilton, H. L., Jr., and DeSanto, G. M., Atmospheric Transport of Rocket Motor Combustion By-Products, Vols. I, II, and III, Final Report Contract No. N123(61756)34567(PMR), GCA Corporation, Bedford, Mass., December 1965.

10. Davar, K. S., and Cermak, J. E., Characteristics of Diffusion Plumes for a Point Source within a Turbulent Boundary Layer, Int. Jour. of Air Wat. Poll., 8, pp. 339-354, 1964.

11. Ellison, T. H., Laboratory Measurements of Turbulent Diffusion in Stratified Flows, Jour. Geophys. Res., 67, 3029, 1962.

12. Field, J. H., and Warden, R., A Survey of Air Currents in the Bay of Gibralter, 1929-1930, Geophysics Memoirs, No. 59 (R and M 1963), Published by Her Majesty's Stationery Office.

13. Frenkeil, F. N., Turbulent Diffusion: Advances in Applied Mechanics, 3, pp. 61-107, 1953, Academic Press, New York.

14. Halilsky, J., et al., Wind Tunnel Study of Turbulence in the Bear Mountains Wake, Quarterly Progress Report No. 1, New York University, Dept. of Meteorology and Oceanography, 1962.

15. Hidy, G. M., ed., On Atmospheric Simulation: A Colloquium, National Center for Atmospheric Research, NCAR-TN-22, November, 1966.

16. Kao, Kai, and Cermak, J. E., Turbulent Diffusion in the Neutral Surface Layer, Fluid Dynamics and Diffusion Laboratory, Colorado State University, Unpublished Report, July 1966.

17. Koehler, S. B., Turbulent Diffusion in a Stably Stratified Boundary Layer, Fluid Dynamics and Diffusion Laboratory Report CER66-67SBK-41, Colorado State University, March, 1967.

18. Lettau, H. H., and Davidson, B., Exploring the Earth's First Mile, Pergamon Press, New York, 1957.

19. Lumley, J. L., and Panofsky, H. A., The Structure of Atmospheric Turbulence, Interscience Publishers, New York, 1964.

20. Lyons, R., and Panofsky, H. A., and Wollaston, S., The Critical Richardson number and its Implications for Forecast Problems, Jour. of Applied Meteorology, 3, 136, 1964.

21. Maholtra, R. C., and Cermak, J. E., Mass Diffusion in Neutral and Unstably Stratified Boundary Layer Flows, Int. Jour. Heat Mass Transfer, 7, pp. 169-186, 1964.

22. Plate, E. J., Diffusion from a Ground Level, Line Source into the Disturbed Boundary Layer Far Downstream from a Fence, Int. Jour. Heat and Mass Transfer, 10, pp. 181-194, 1967.

23. Plate, E. J., and Lin, C. W., Investigation of the Thermally Stratified Boundary Layer, Fluid Mechanics Paper No. 5, Colorado State University, February 1966.

24. Plate, E. J., and Lin, C. W., The Velocity Field Downstream from a Two-Dimensional Model Hill, Fluid Dynamics and Diffusion Laboratory Report, CER65EJP14, Colorado State University, February, 1965.

25. Plate, E. J., and Sheih, C. M., Duffusion from a Continuous Point Source into the Boundary Layer Downstream from a Model Hill, Fluid Dynamics and Diffusion Laboratory Report CER65EJP-CMS60, Colorado State University, December, 1965.

26. Sandborn, V., and Finn, C., Operating and Maintenance Manual, CSU Hot Wire Anemometer, Fluid Dynamics and Diffusion Laboratory Report, CER66-67VAS-CLF16, Colorado State University, 1967.

27. Schlichting, H., Boundary Layer Theory, Fourth Edition, McGraw-Hill, New York, 1960.

28. Shih, Ching-chi, Continuous Point Source Diffusion in a Turbulent Shear Layer, Master of Science Thesis, Dept. of Civil Engineering, Colorado State University, August 1966.

29. Smith, T. B., et al., Micrometeorological Investigation of Naval Missile Facility, Point Arguello, California, Final Report on Contract N123 (61756) 32885 A (PMR), 2 Vols., July 31, 1964.

30. Sutton, O. G., Micrometeorology, McGraw-Hill, New York, 1953.

31. Wiskind, H. K., A Uniform Gradient Turbulent Transport Experiment, Jour. Geophys, Res., 67, 3033, 1962.

FIGURES

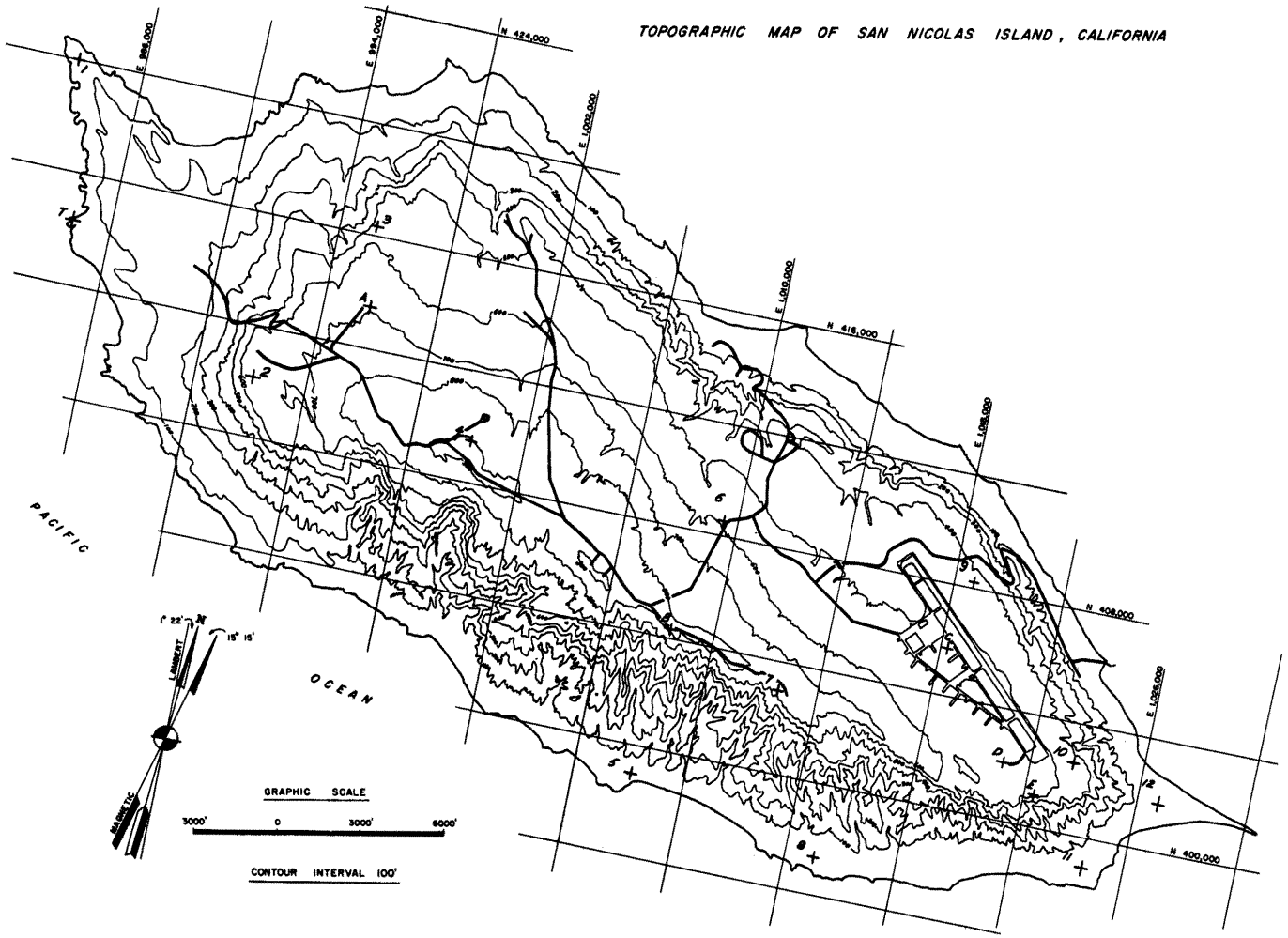

Figure 1. Topographic maps of San Nicolas Island, California

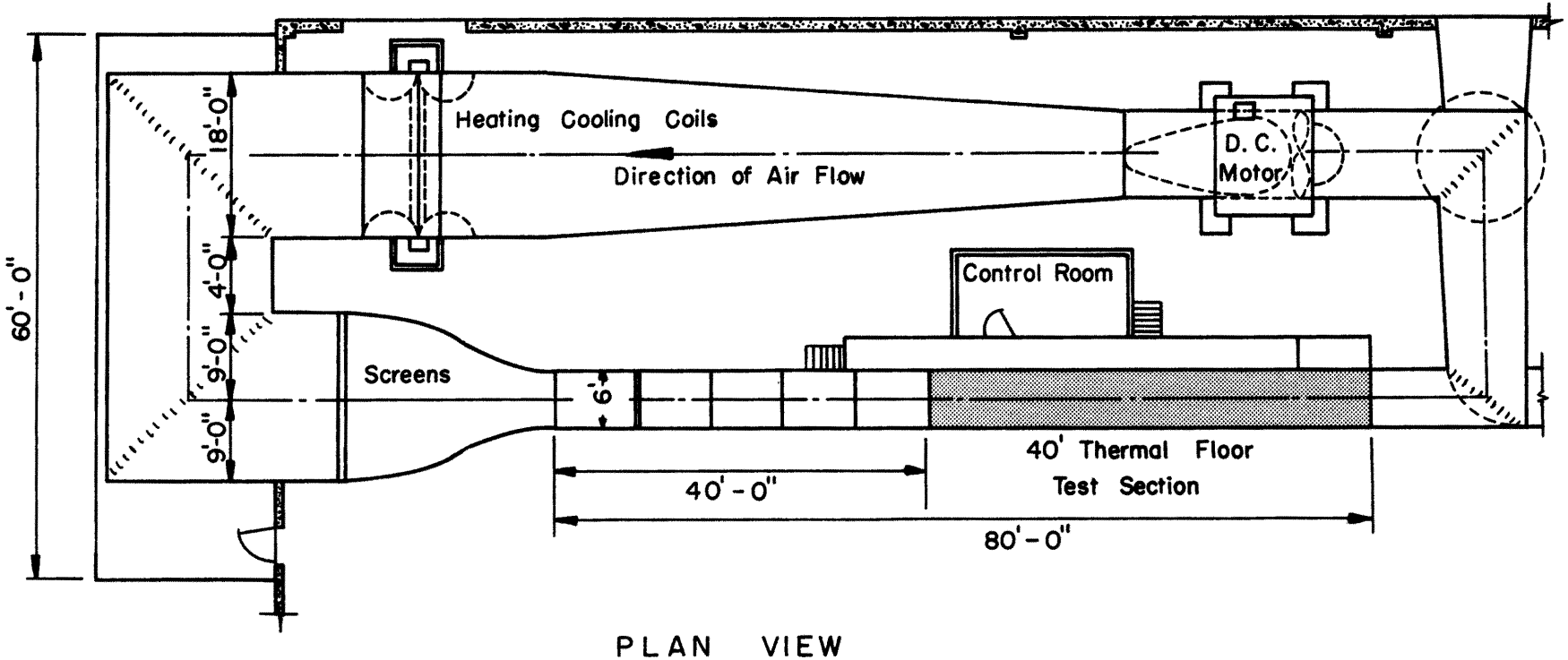

Figure 2. Plan view of the Army Meteorological Wind Tunnel

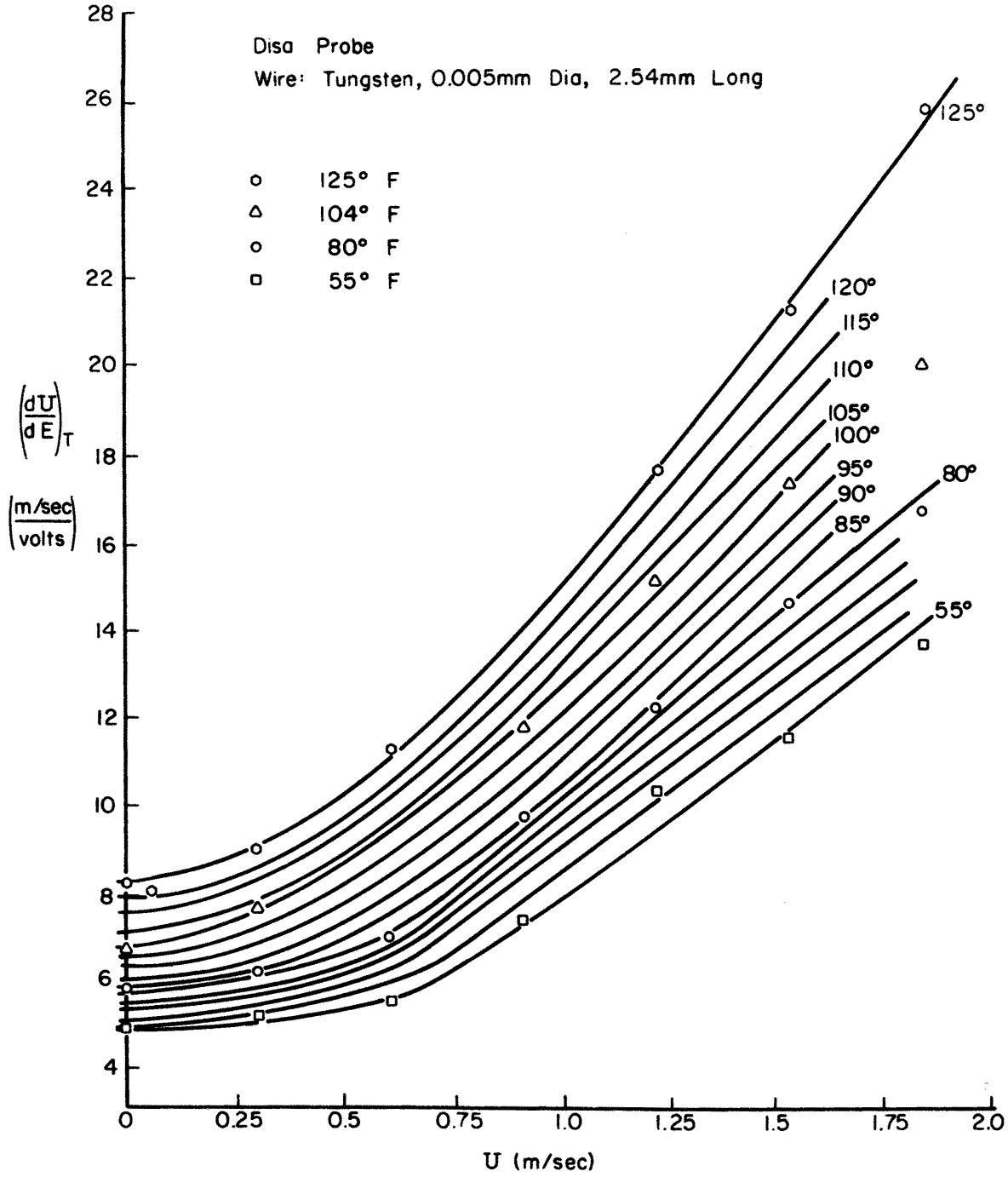

Figure 3. Cross-wire anemometer calibration for stratified flows

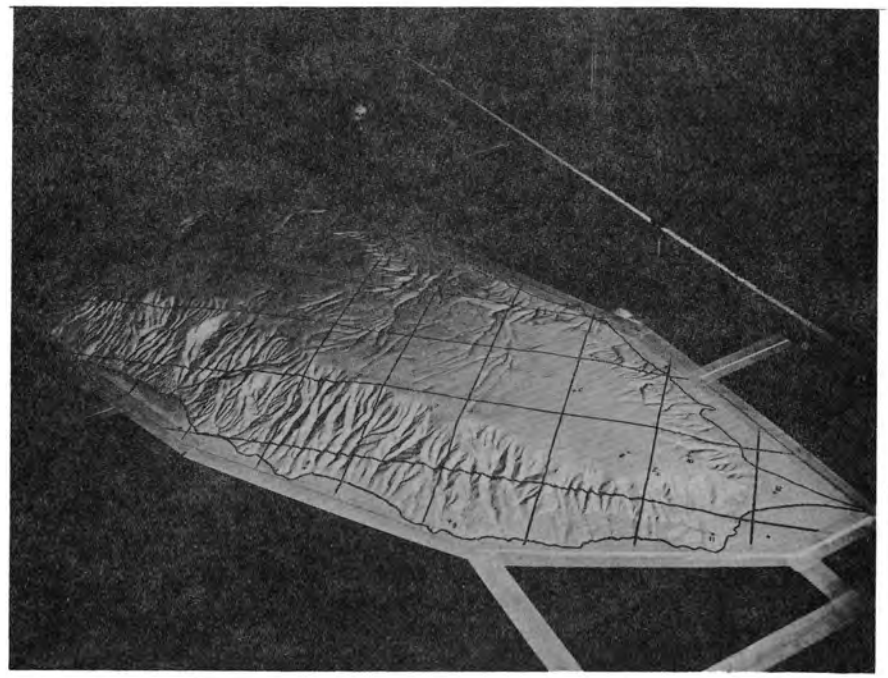

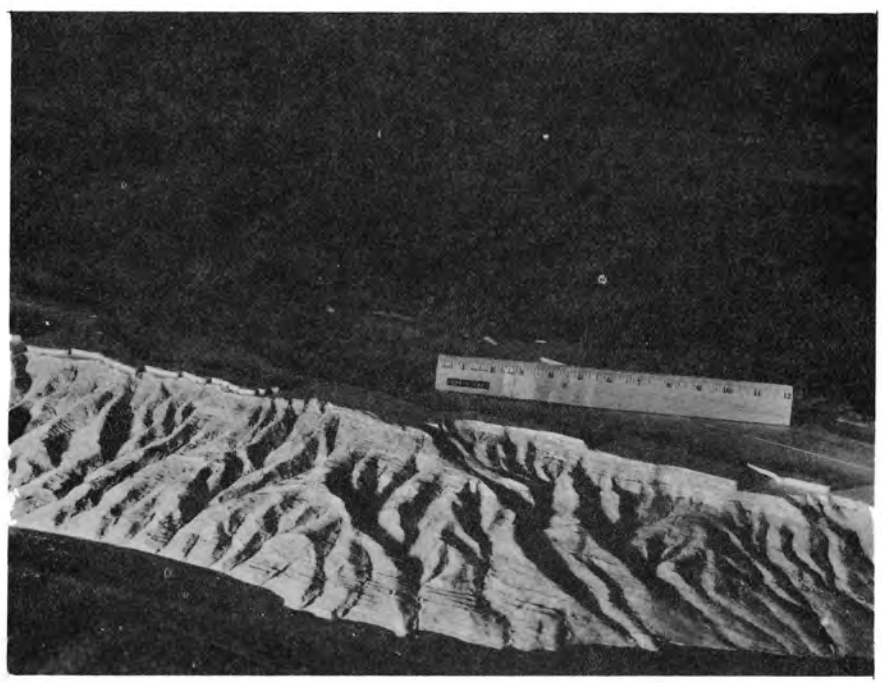

Figure 4. Construction of the 1:6200 scale model of San Nicolas Island

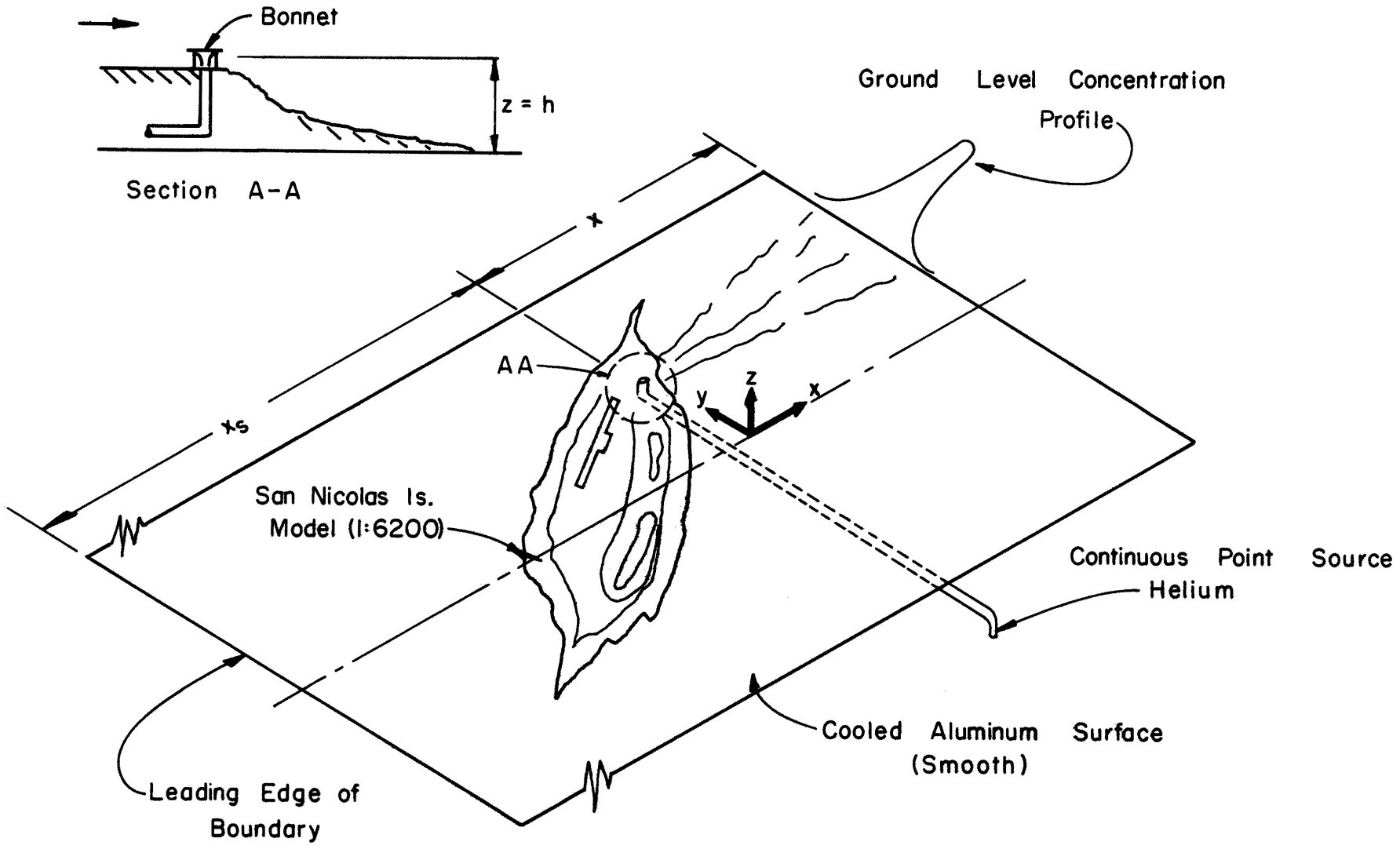

Figure 5. San Nicolas Island model orientation

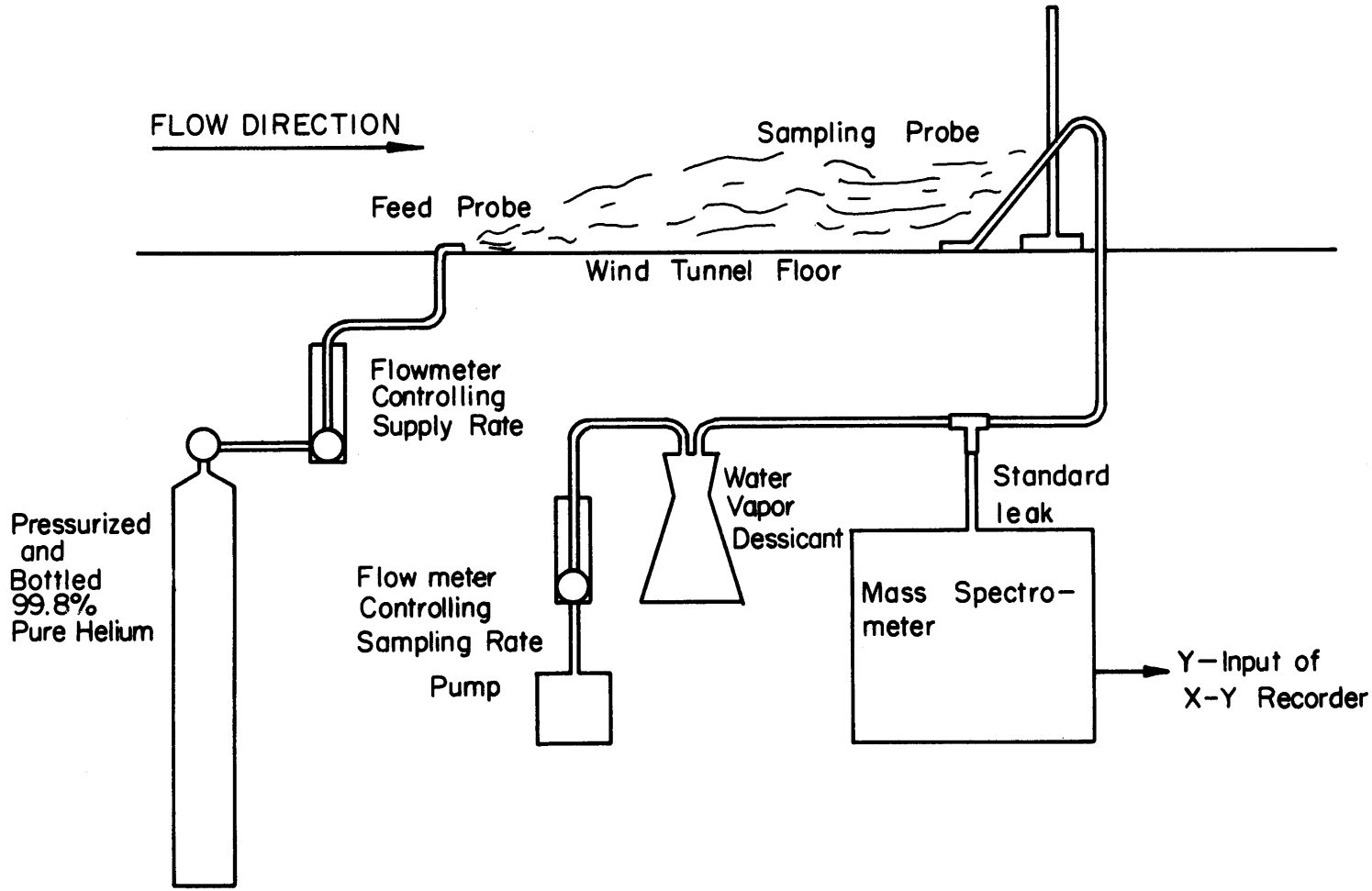

Figure 6. Feed and sampling systems

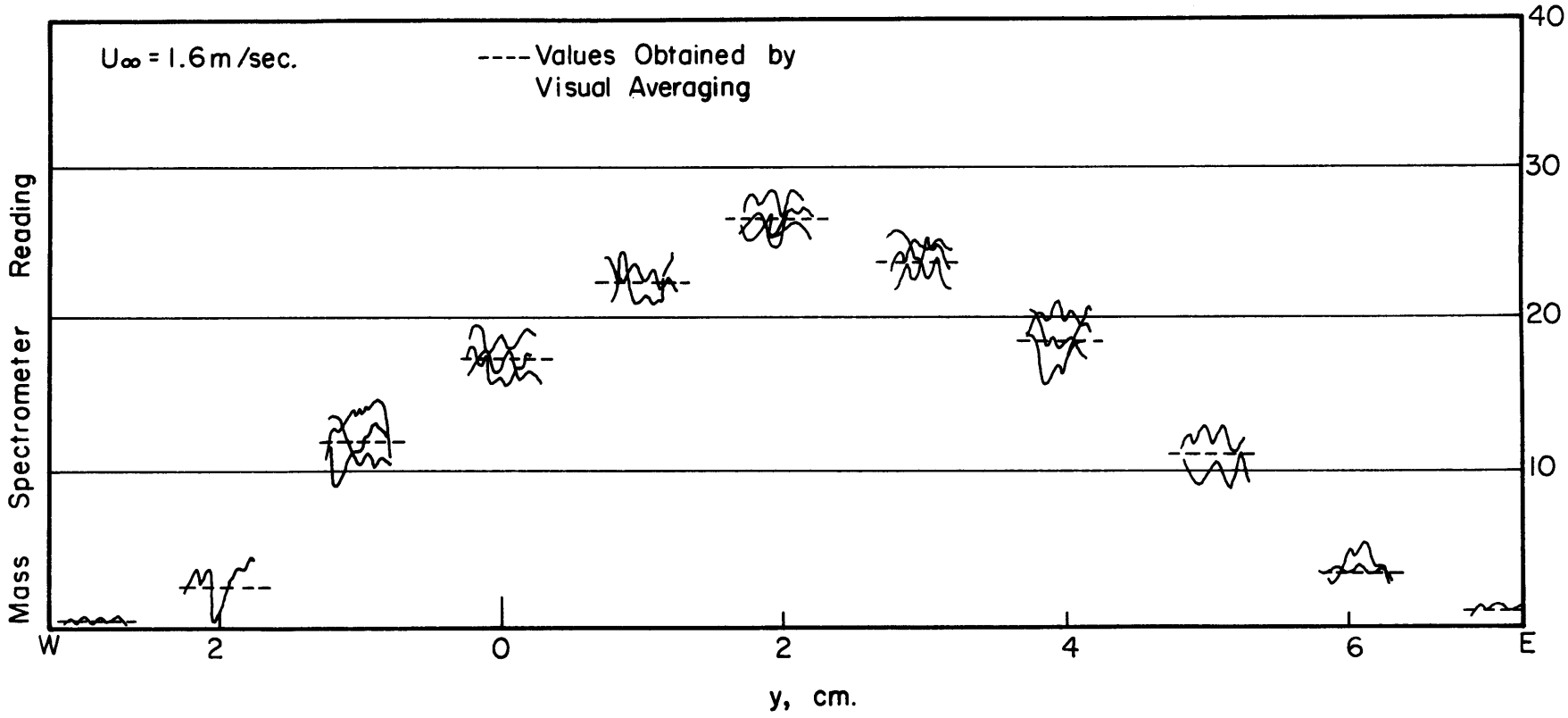

Figure 7. A typical ground level concentration profile

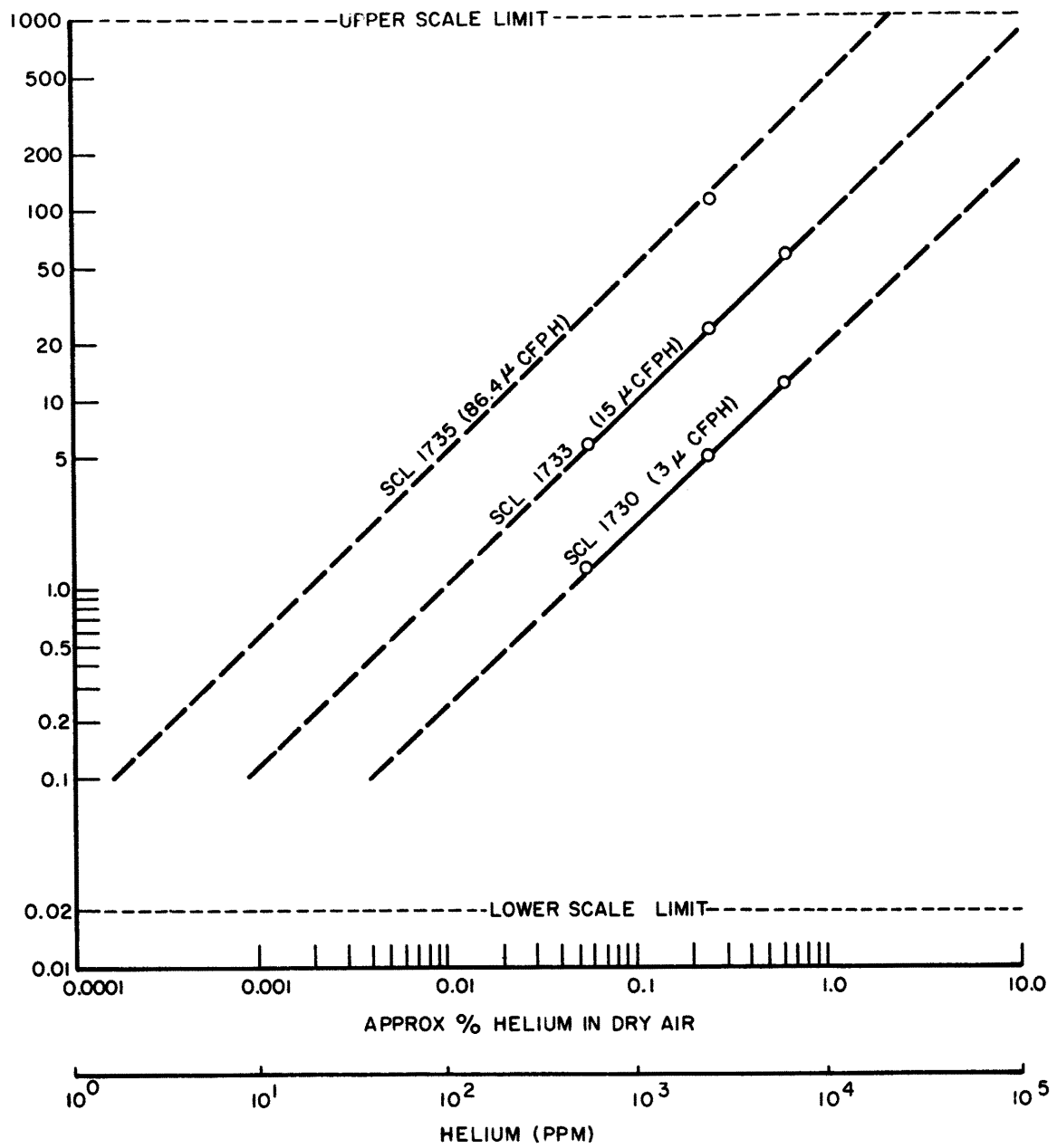

Figure 8. Leak detector calibration

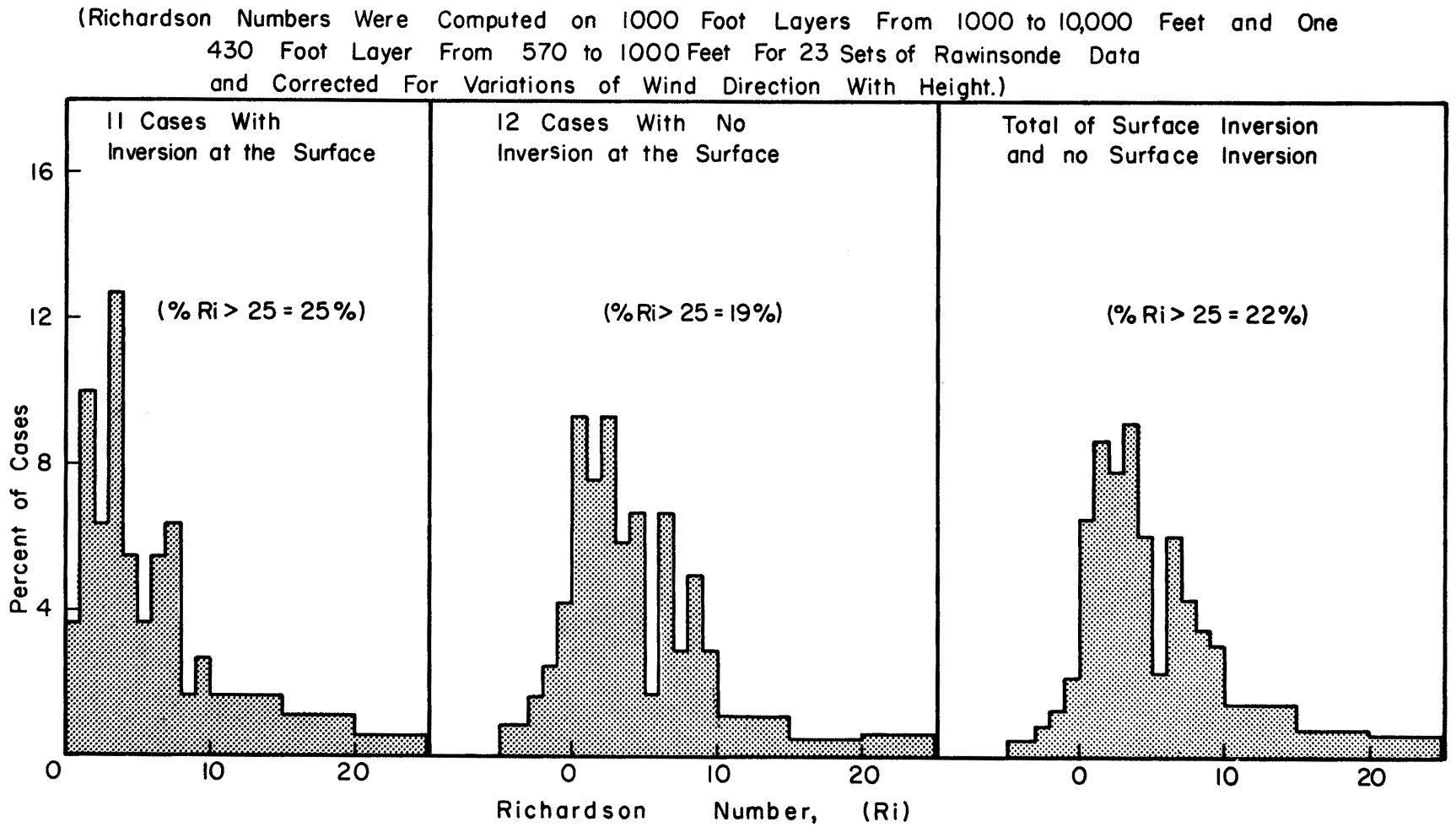

Figure 9. Distribution of Richardson numbers for San Nicolas Island, California

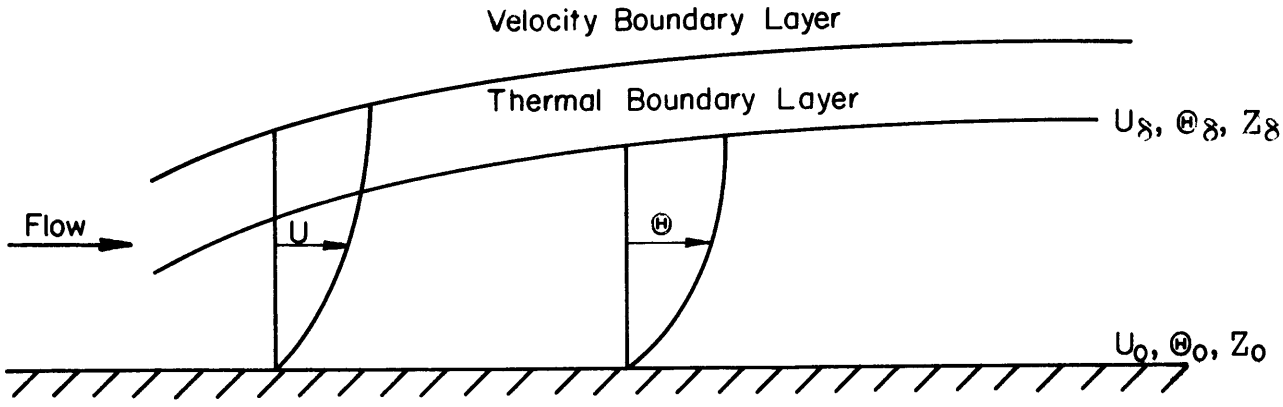

$$R_i = \frac{g\left(\frac{\partial \Theta}{\partial Z}\right)}{\Theta\left(\frac{\partial U}{\partial Z}\right)^2} \qquad \text{but } \frac{\partial \Theta}{\partial Z} \cong \frac{\Theta_\delta - \Theta_0}{Z_\delta - Z_0} \qquad \frac{\partial U}{\partial Z} \cong \frac{U_\delta - U_0}{Z_\delta - Z_0}$$

$$R_i \cong \frac{g}{\Theta_{av}} \frac{(\Theta_\delta - \Theta_0)(Z_\delta - Z_0)}{(U_\delta - U_0)^2}, \quad \text{where } \Theta_{av} = \frac{\Theta_\delta + \Theta_0}{2}$$

Data for Wind Tunnel Flow Approaching the Model

$\Theta_\delta = 140°F = 600°R$, $\Theta_0 = 30°F = 490°R$, $\Theta_{av} = 545°R$

$Z_\delta = 22" = .56m$, $Z_0 = 0$ $\qquad$ $U_\delta \cong 1.5mps$, $U_0 = 0$

$$R_i \cong \frac{g}{\Theta} \frac{(\Theta_\delta - \Theta_0)(Z_\delta - Z_0)}{(U_\delta - U_0)^2} \cong \frac{9.81}{545} \frac{(110)(0.56)}{(1.5)^2}$$

$$R_i \cong 0.477$$

Figure 10. Bulk Richardson numbers for boundary layer flow

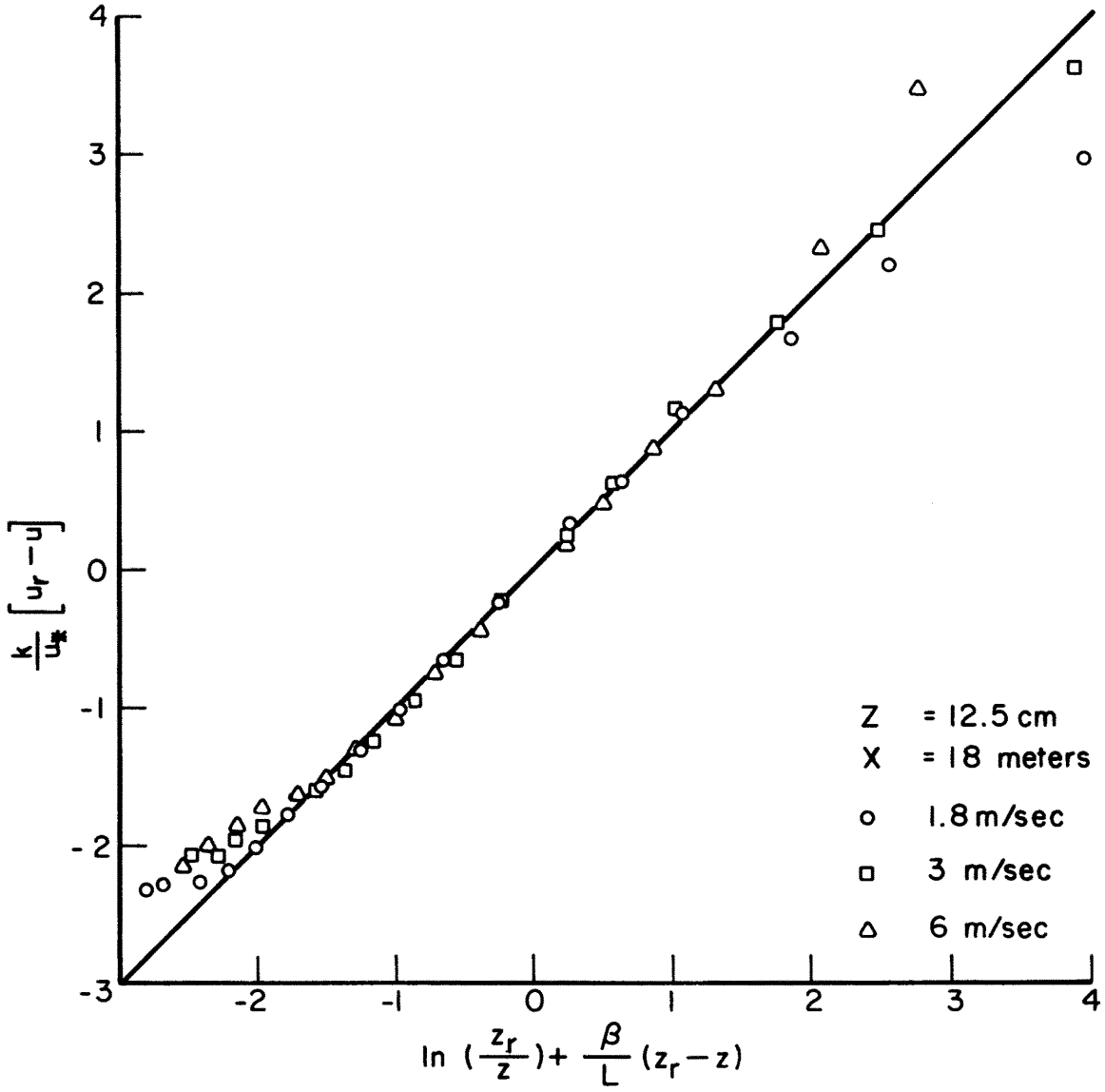

Figure 11. Monin-Obukhov velocity model comparison

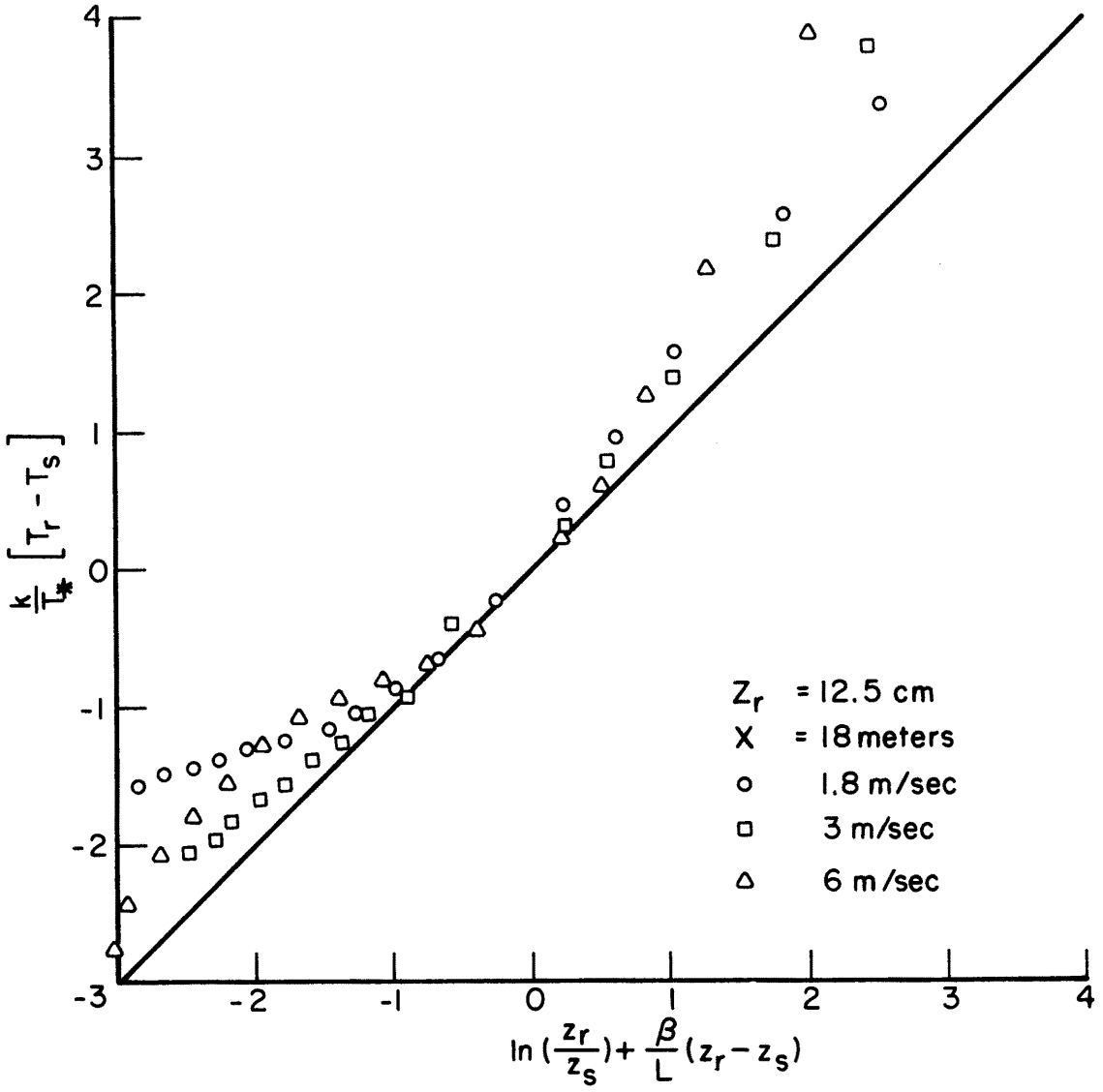

Figure 12. Monin-Obukhov temperature model comparison

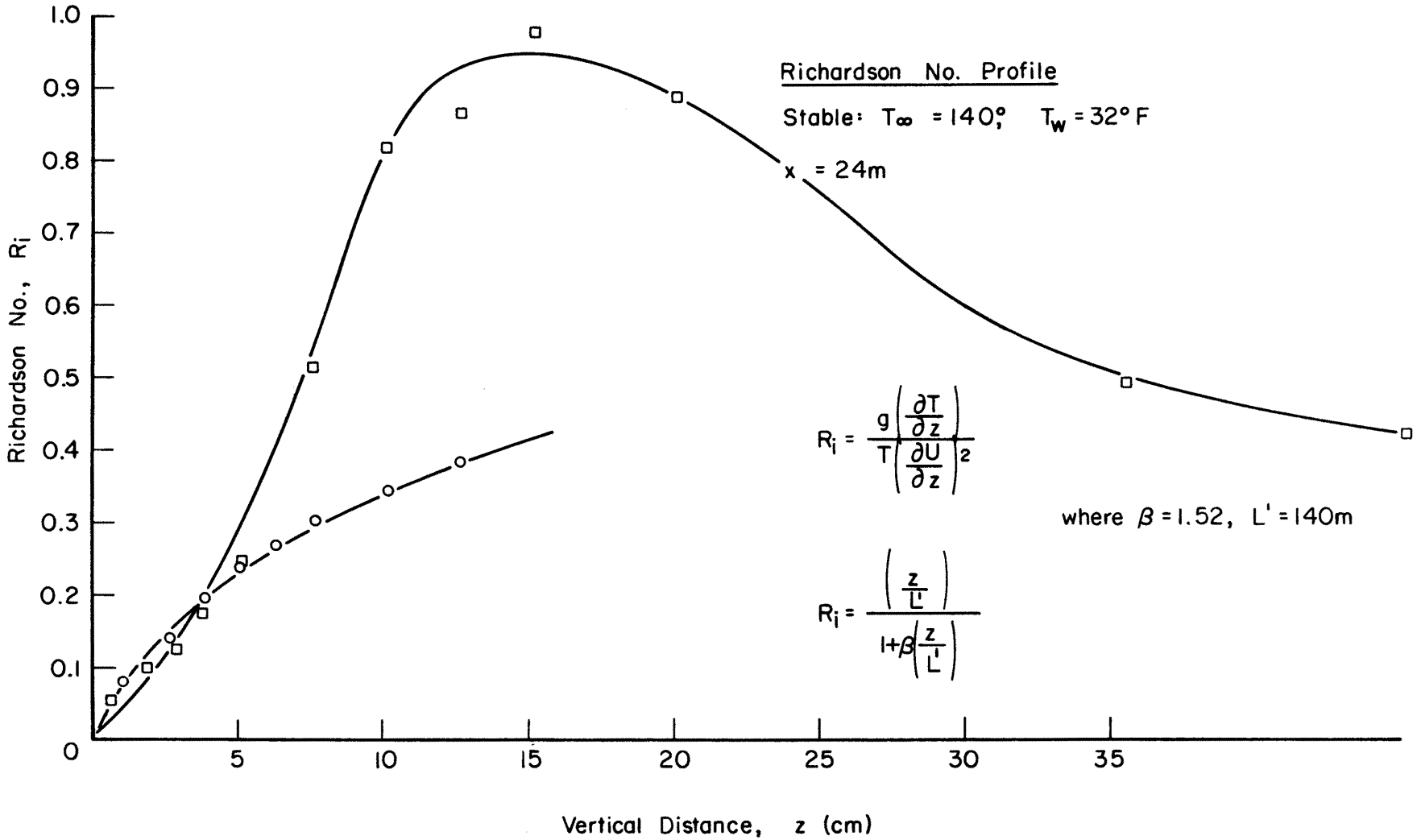

Figure 13. Richardson number distribution over model

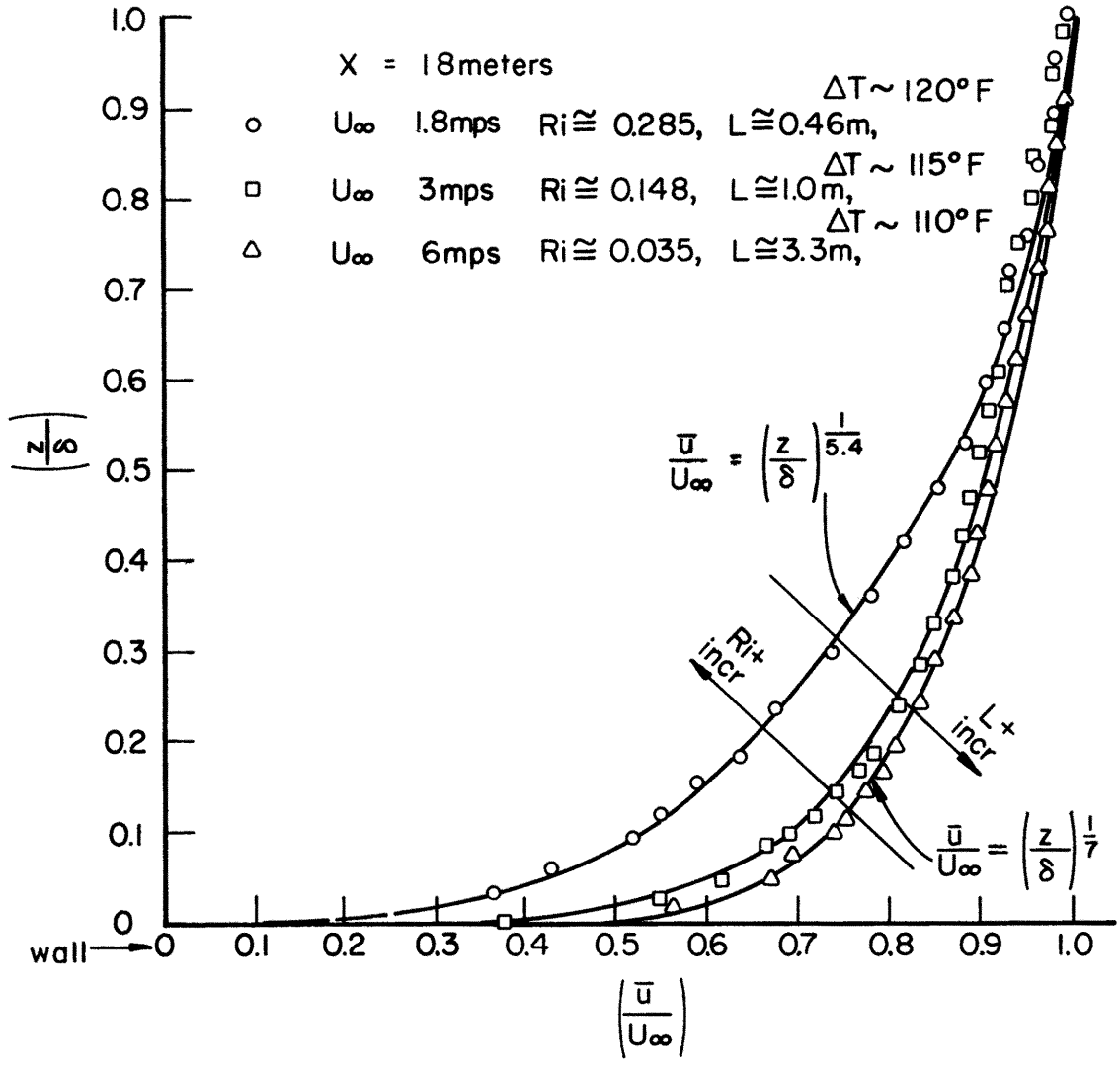

Figure 14. Velocity profile for stratified boundary layers

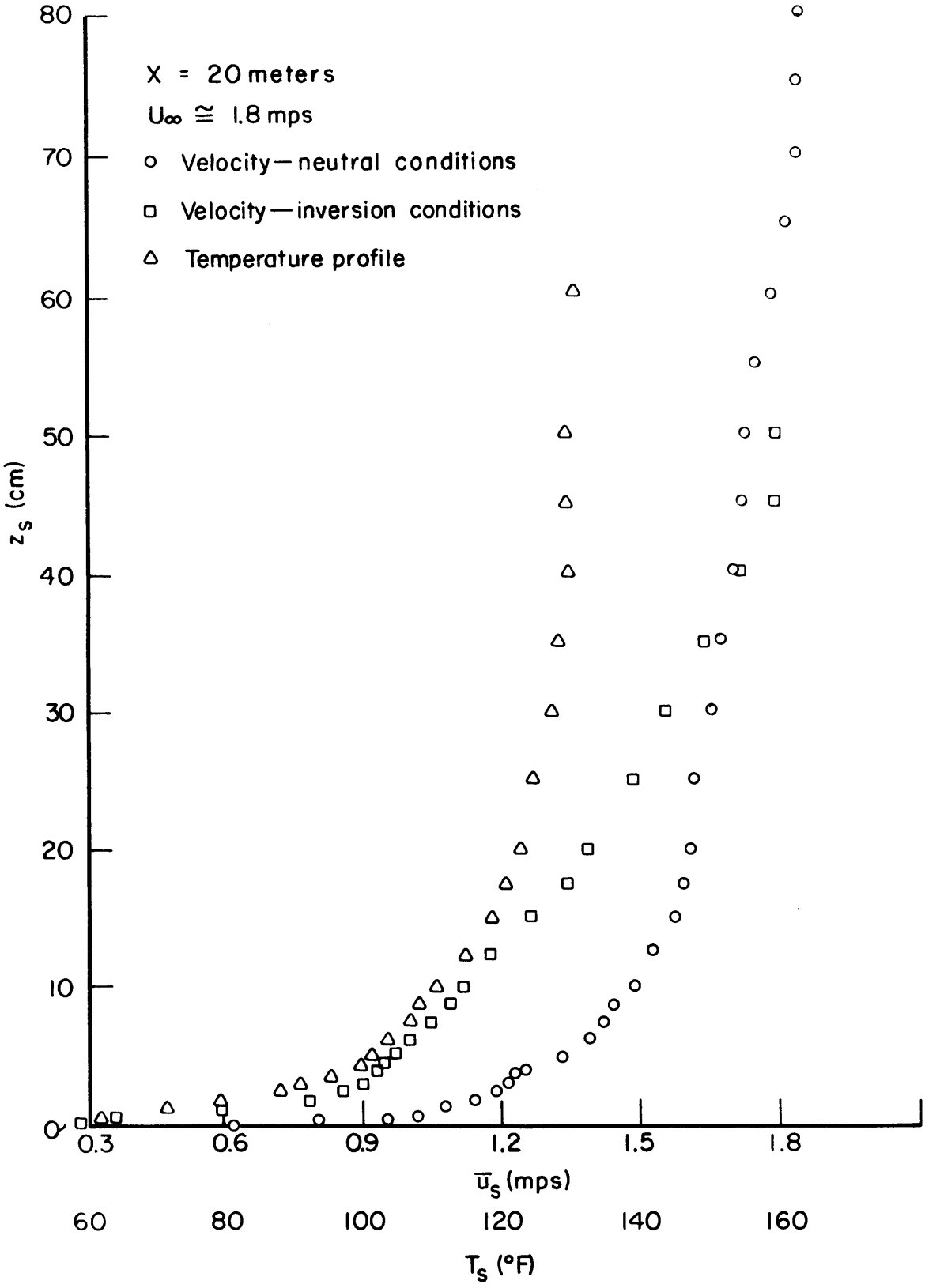

Figure 15. Typical approach flow velocity and temperature profiles

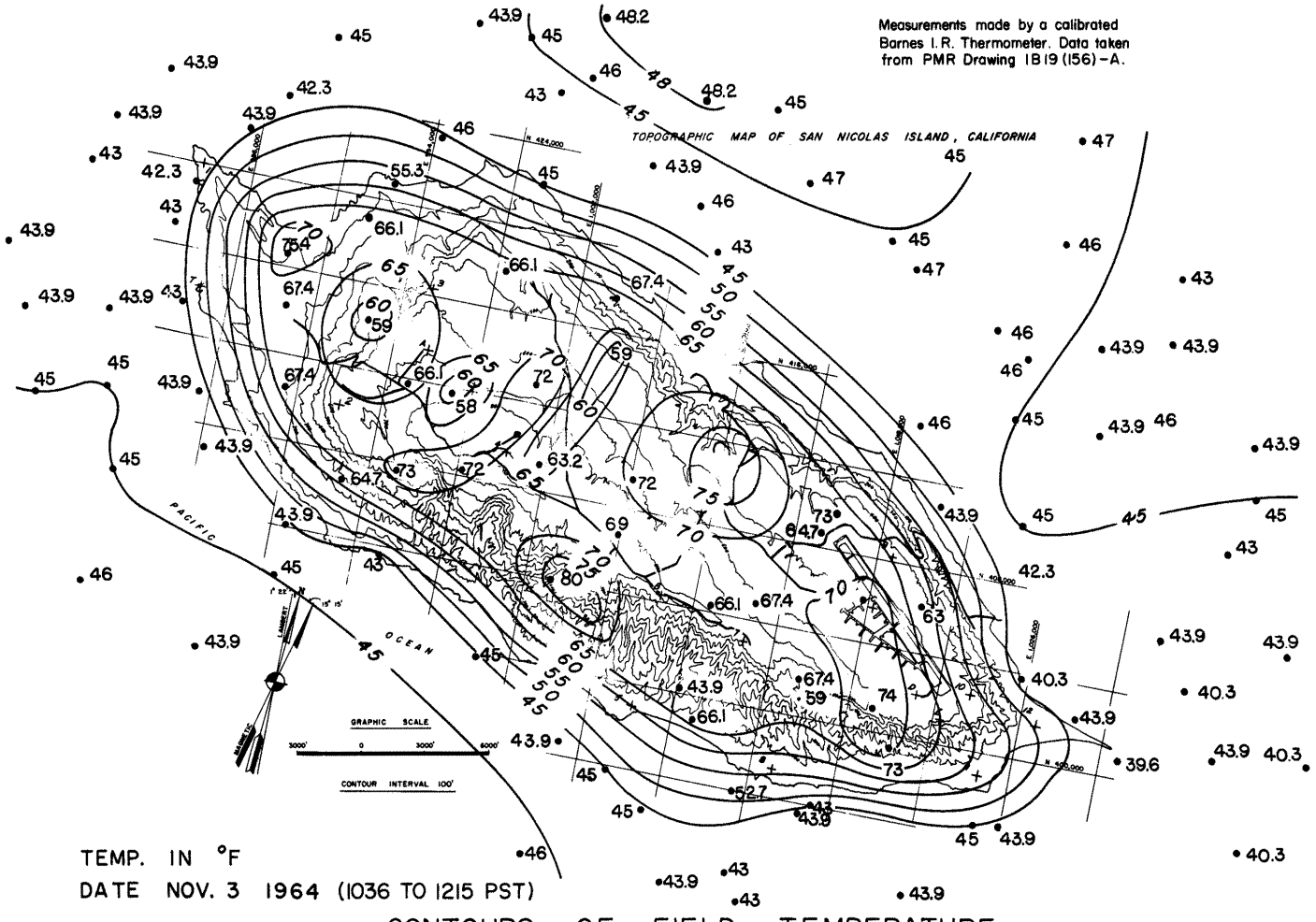

Figure 16. Contours of field temperature

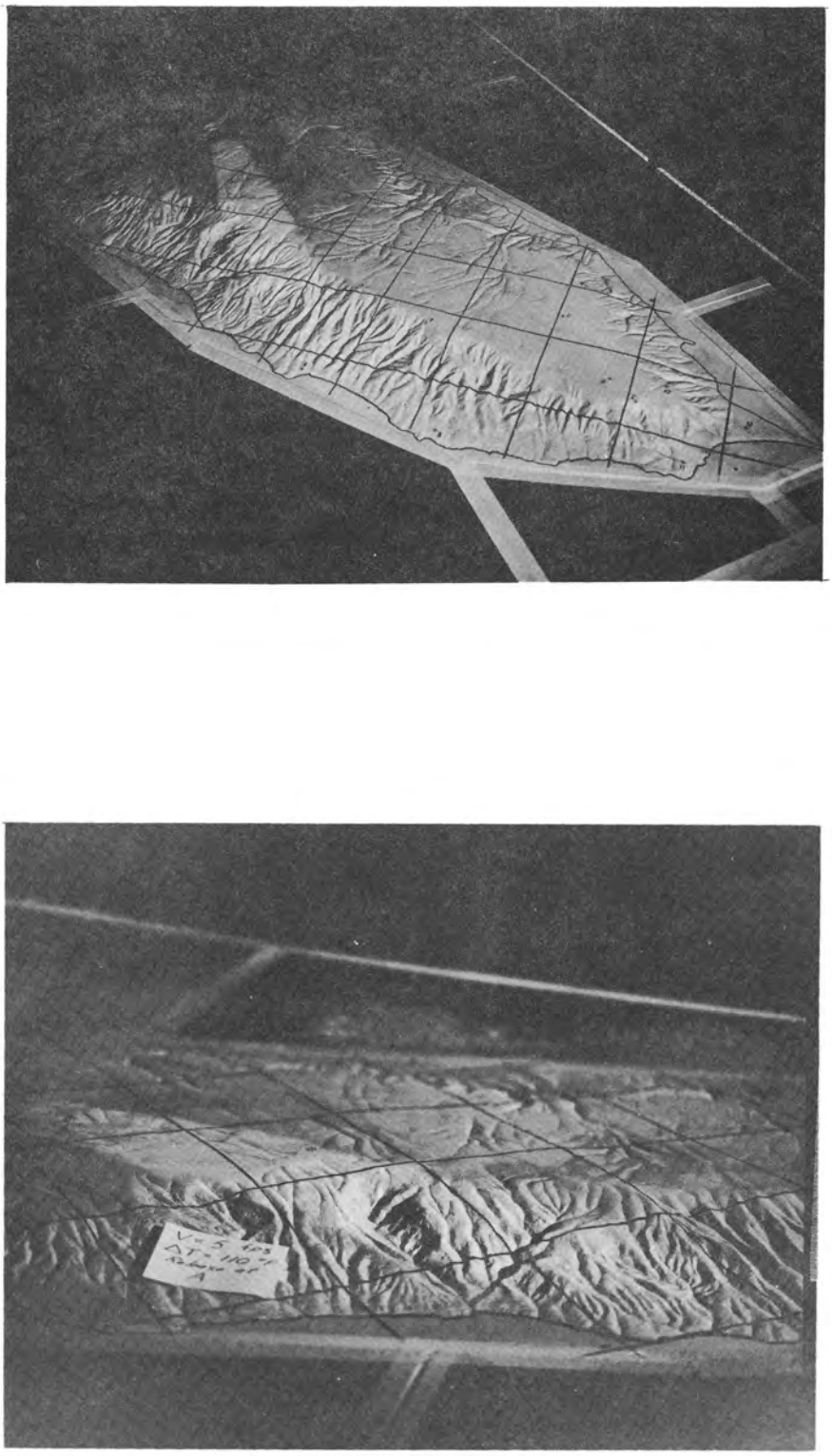

Figure 17. Single release ammonia trace data

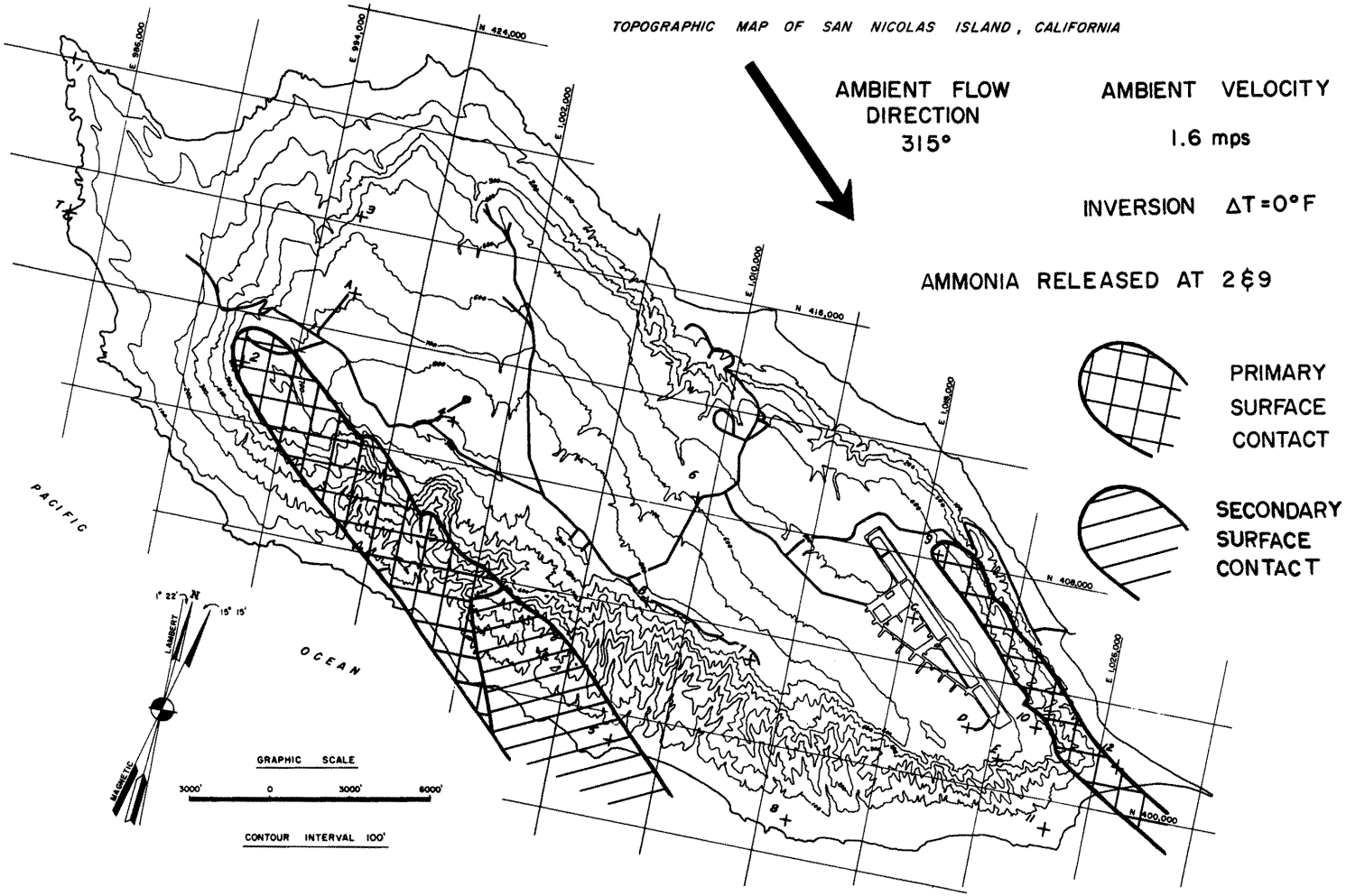

SURFACE DISTRIBUTION TRACE OF AMMONIA FOR NEUTRAL FLOW

Figure 18. Surface distribution trace of ammonia for neutral flow

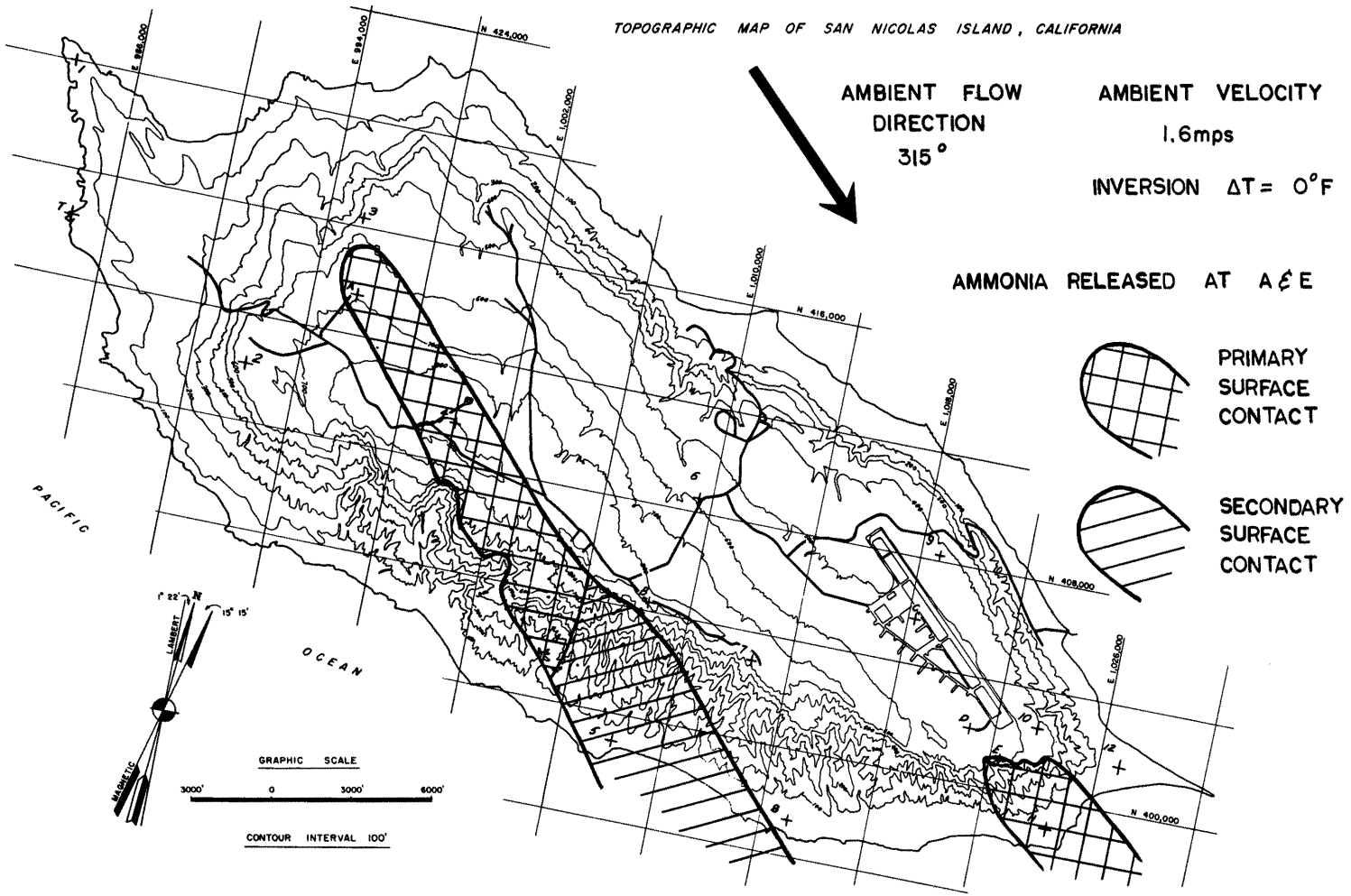

SURFACE DISTRIBUTION TRACE OF AMMONIA FOR NEUTRAL FLOW

Figure 19. Surface distribution trace of ammonia for neutral flow

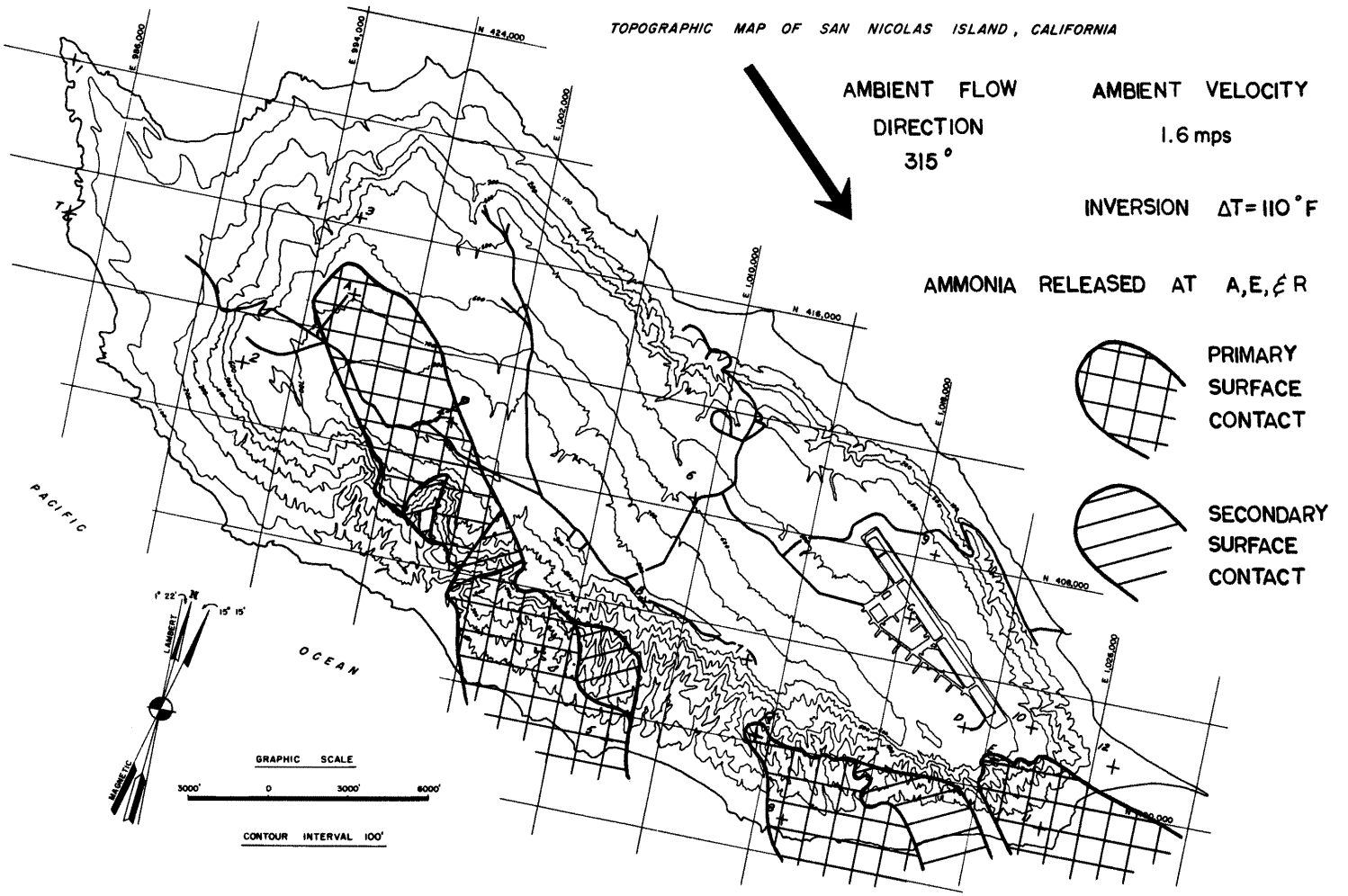

SURFACE DISTRIBUTION TRACE OF AMMONIA FOR INVERSION FLOW

Figure 20. Surface distribution trace of ammonia for inversion flow

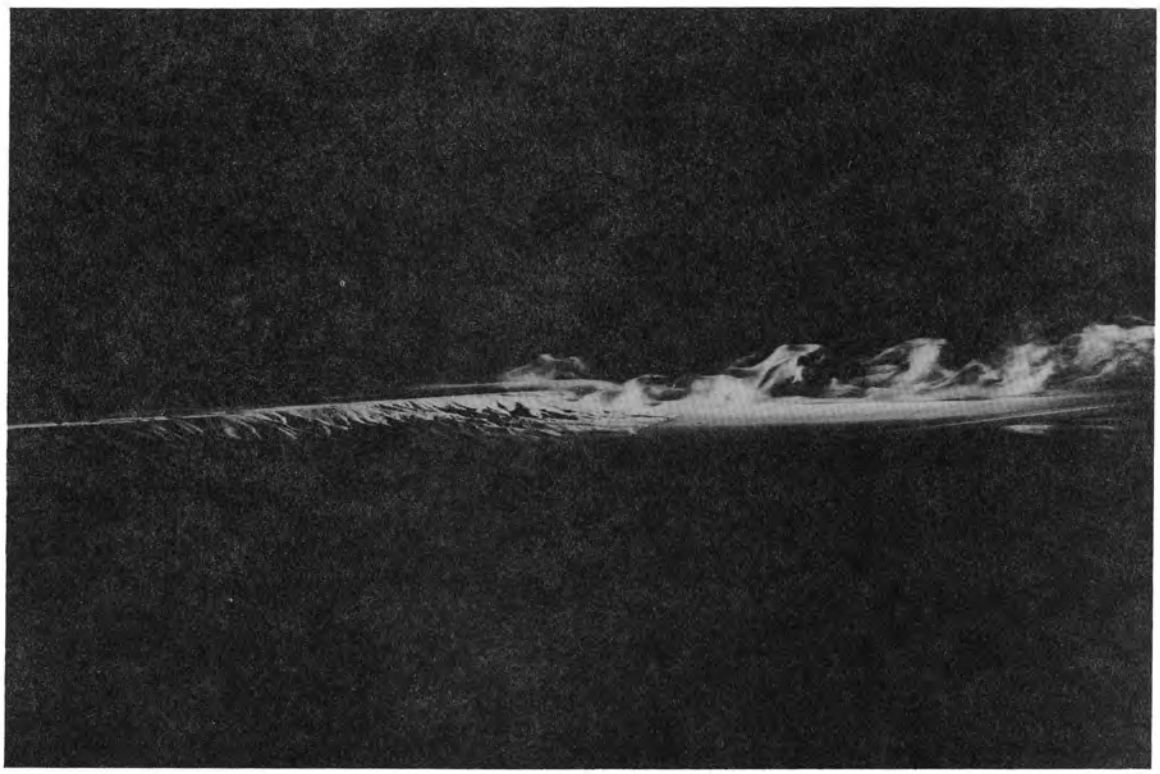

Figure 21. Smoke flow patterns; inversion $\Delta T = 115^{o}$ F, azimuth 315^{o}, velocity U ≃ 1.6 mps; camera direction, east

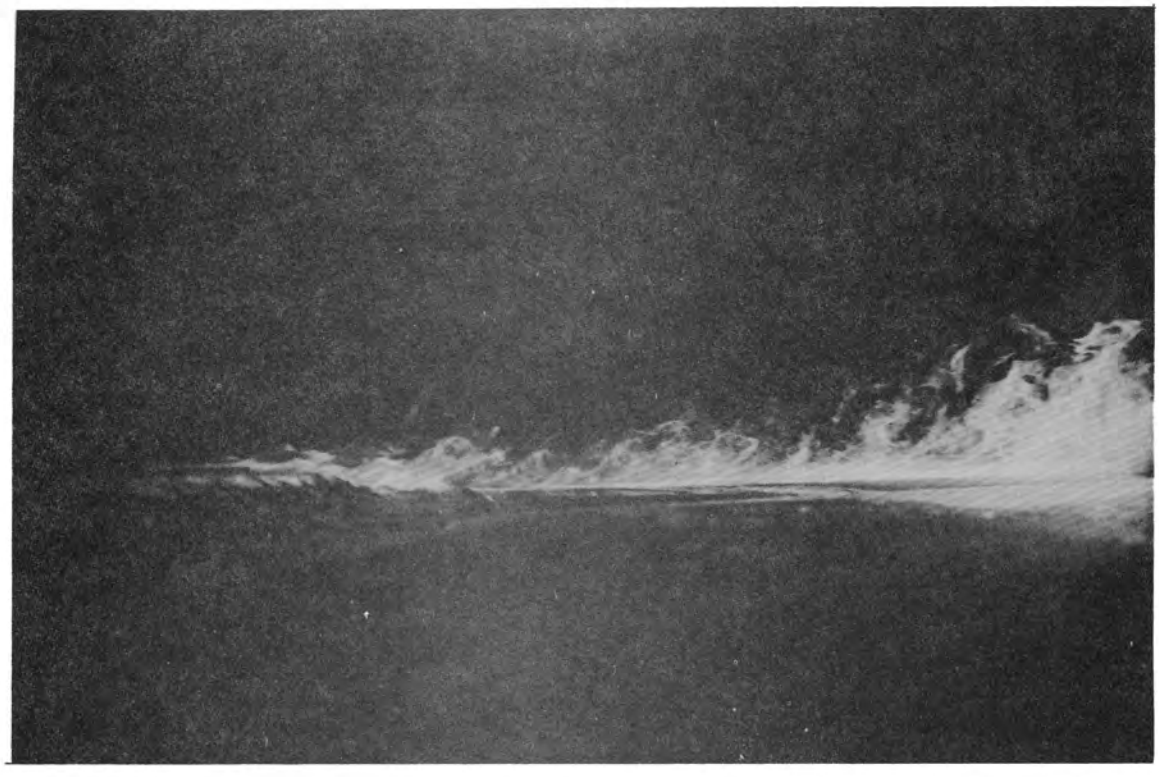

Figure 22. Smoke flow patterns; inversion $\Delta T = 120^{o}$ F, azimuth 315^{o}, velocity U ≃ 1.6 mps; camera direction, east

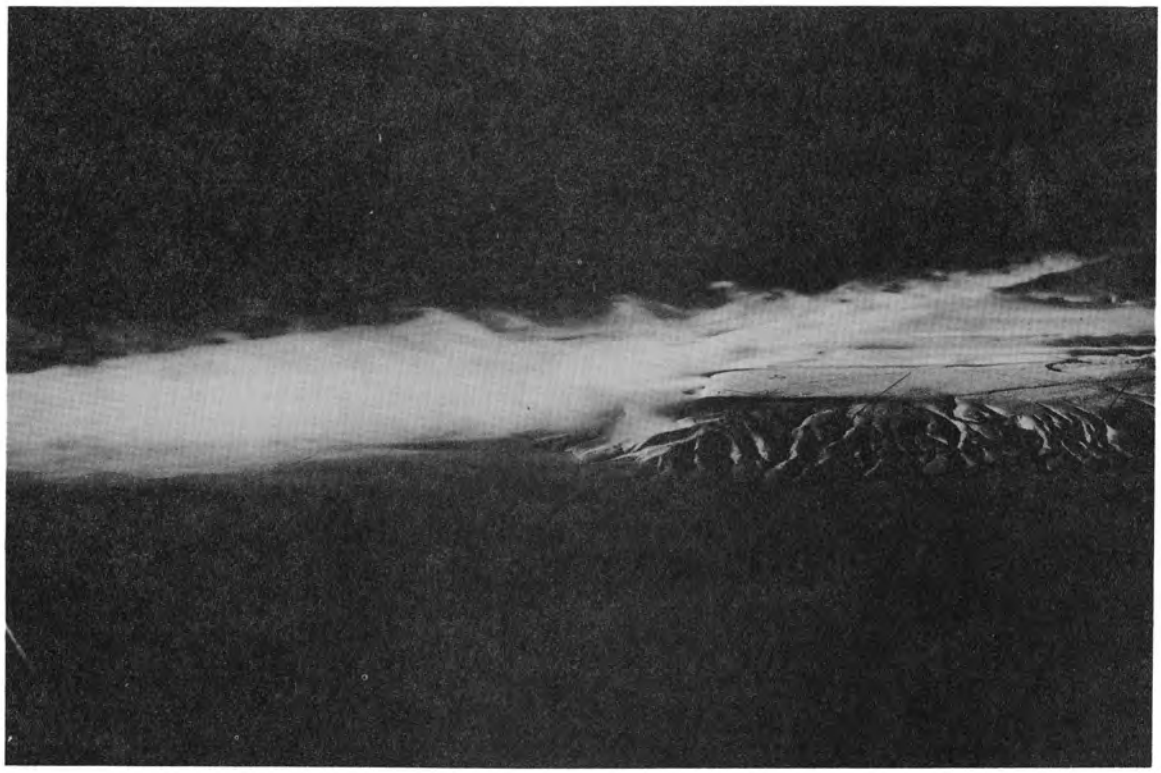

Figure 23. Smoke flow patterns; inversion $\Delta T = 115^{o}$ F, azimuth 315^{o}, velocity U $\simeq$ 1.6 mps; camera direction, west

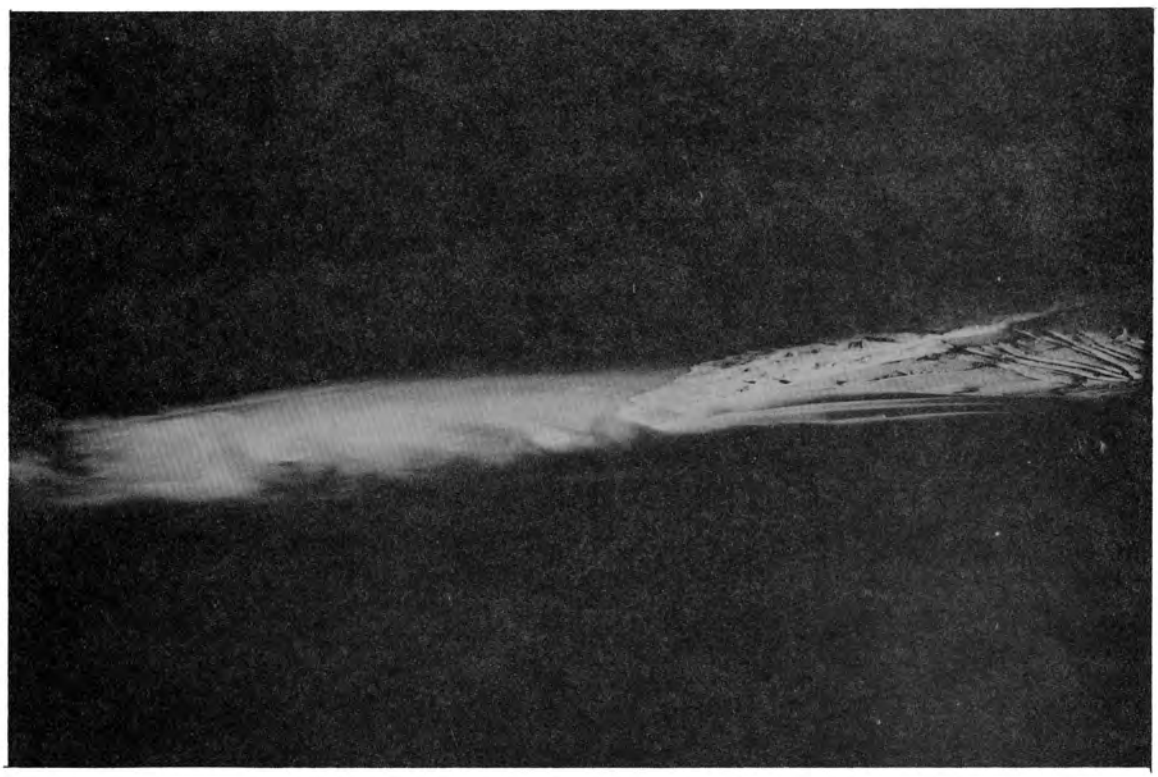

Figure 24. Smoke flow patterns; inversion $\Delta T = 115^{o}$ F, azimuth 315^{o}, velocity $U \simeq 1.6$ mps; camera direction, west

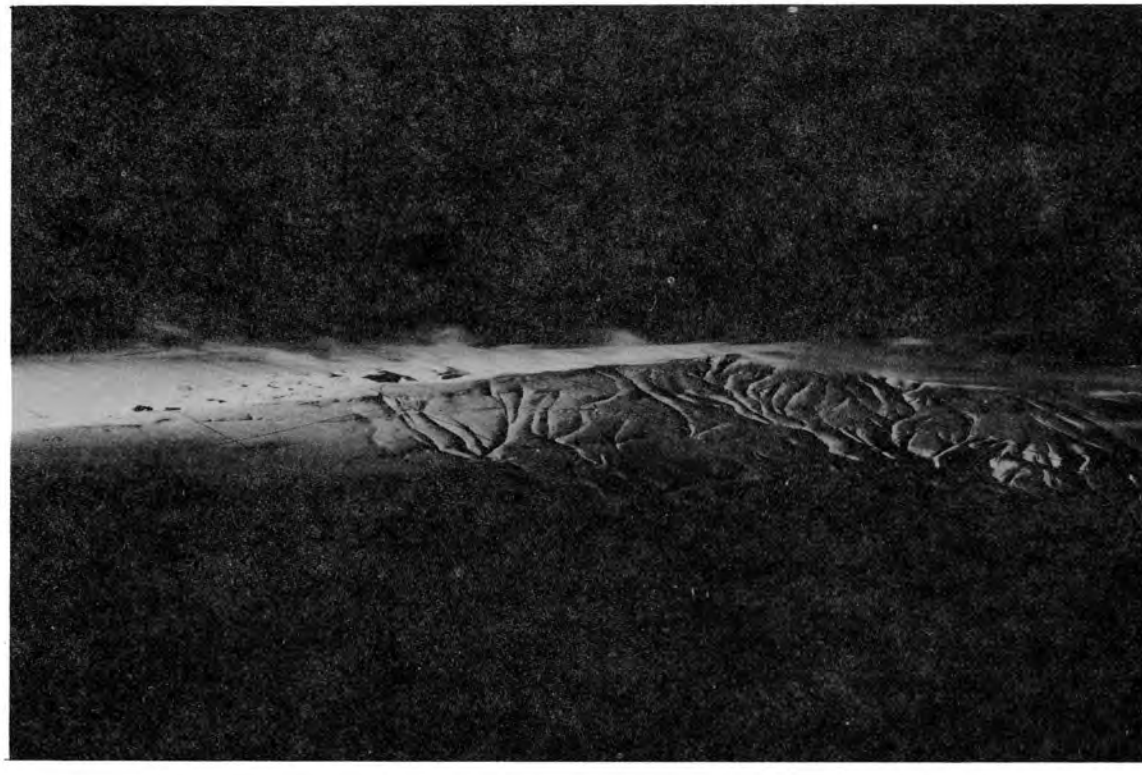

Figure 25. Smoke flow patterns; inversion $\Delta T = 115^{o}$ F, azimuth 315^{o}, velocity U $\simeq$ 1.6 mps; camera direction, south

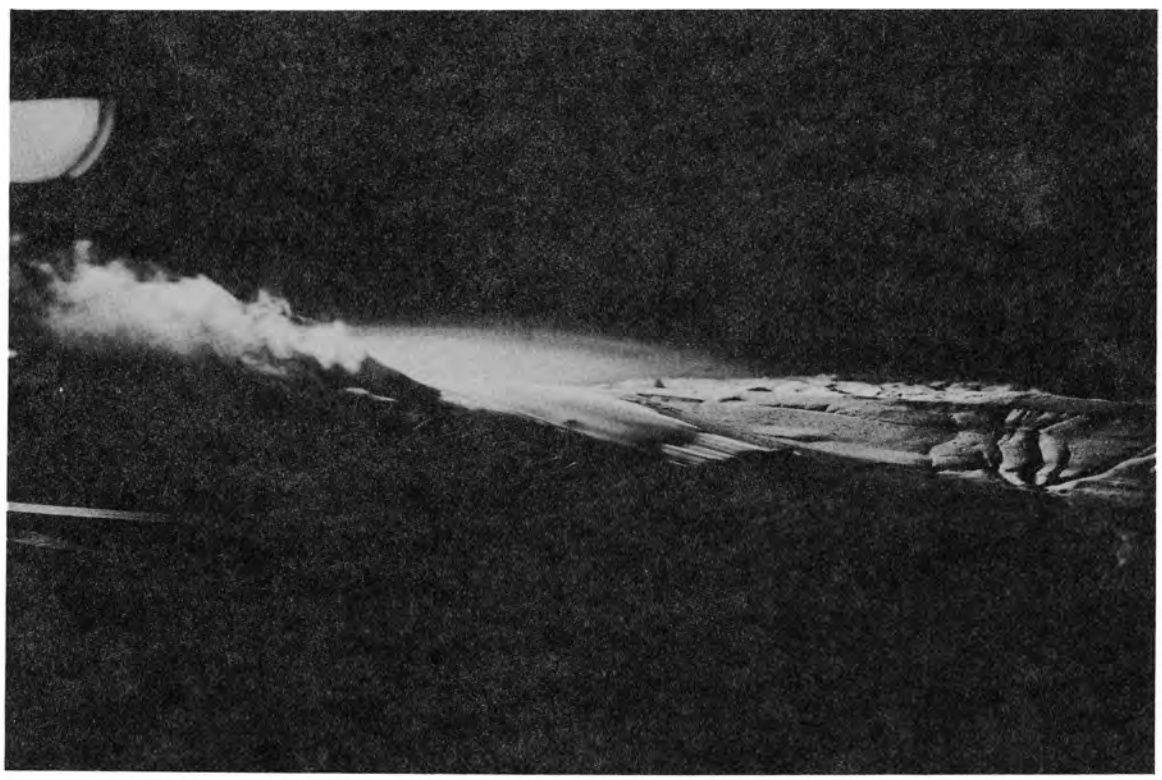

Figure 26. Smoke flow patterns; inversion $\Delta T = 115^{o}$ F, azimuth 315^{o}, velocity U ≃ 1.6 mps; camera direction, southwest

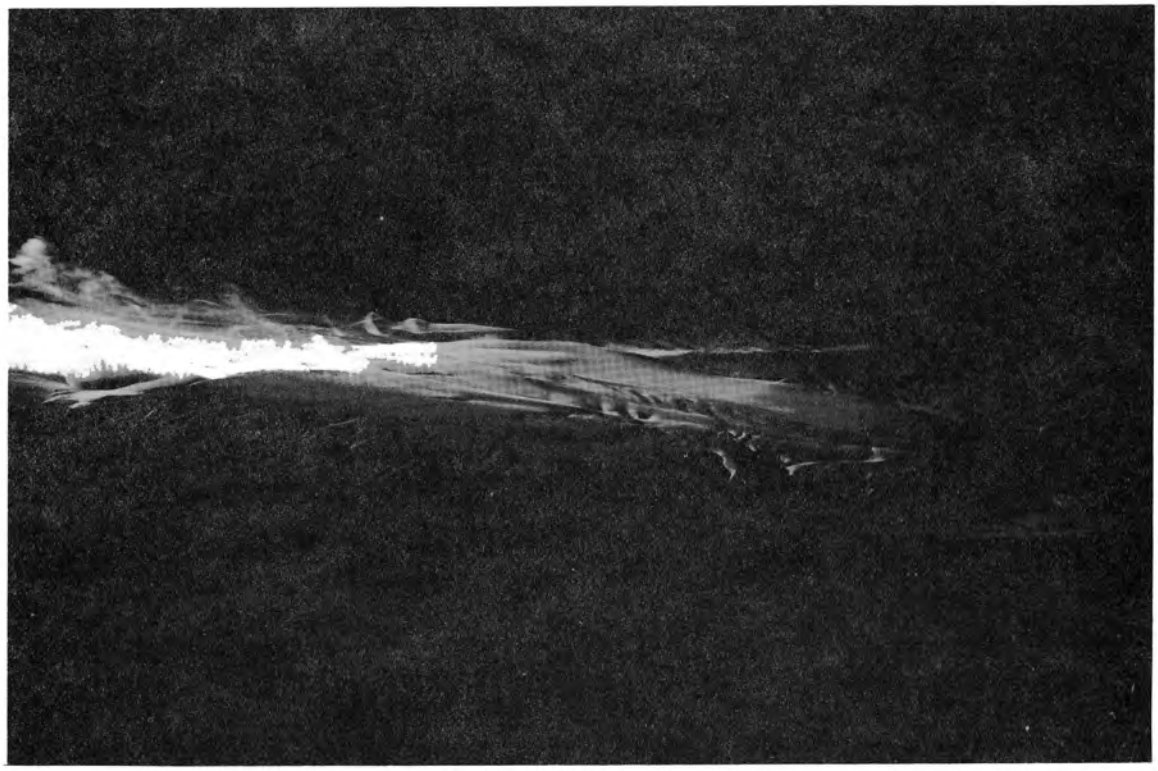

Figure 27. Smoke flow patterns; inversion $\Delta T = 115^{o}$ F, azimuth 315^{o}, velocity U ≃ 1.6 mps; camera direction, southwest

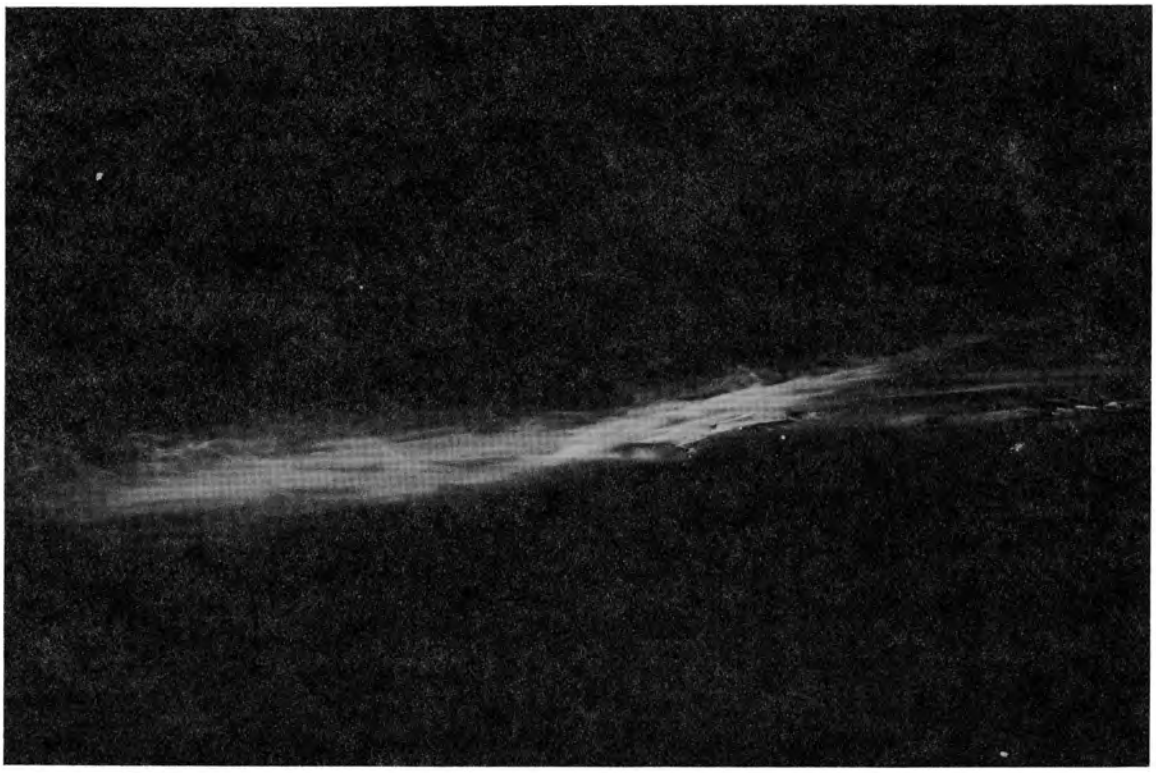

Figure 28. Smoke flow patterns; inversion $\Delta T = 115^{o}$ F, azimuth 315^{o}, velocity U ≃ 1.6 mps; camera direction southwest

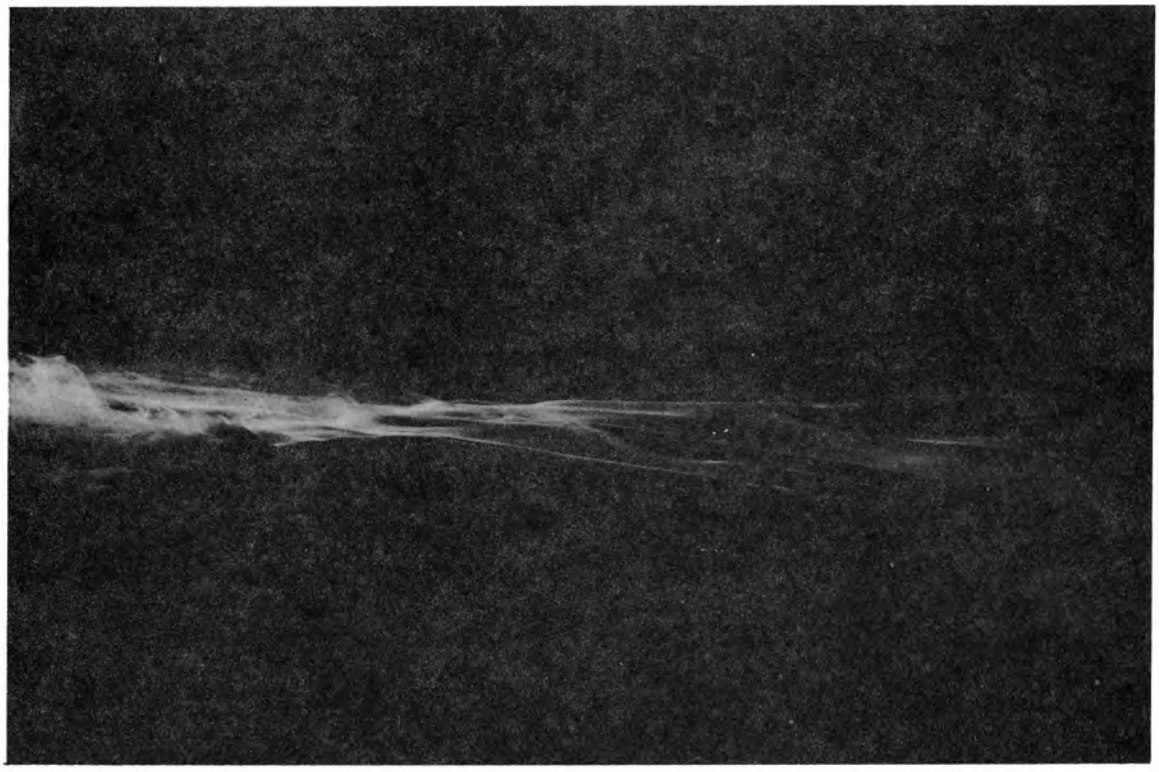

Figure 29. Smoke flow patterns; inversion $\Delta T = 115^{o}$ F, azimuth 315^{o}, velocity U ≈ 1.6 mps; camera direction, southwest

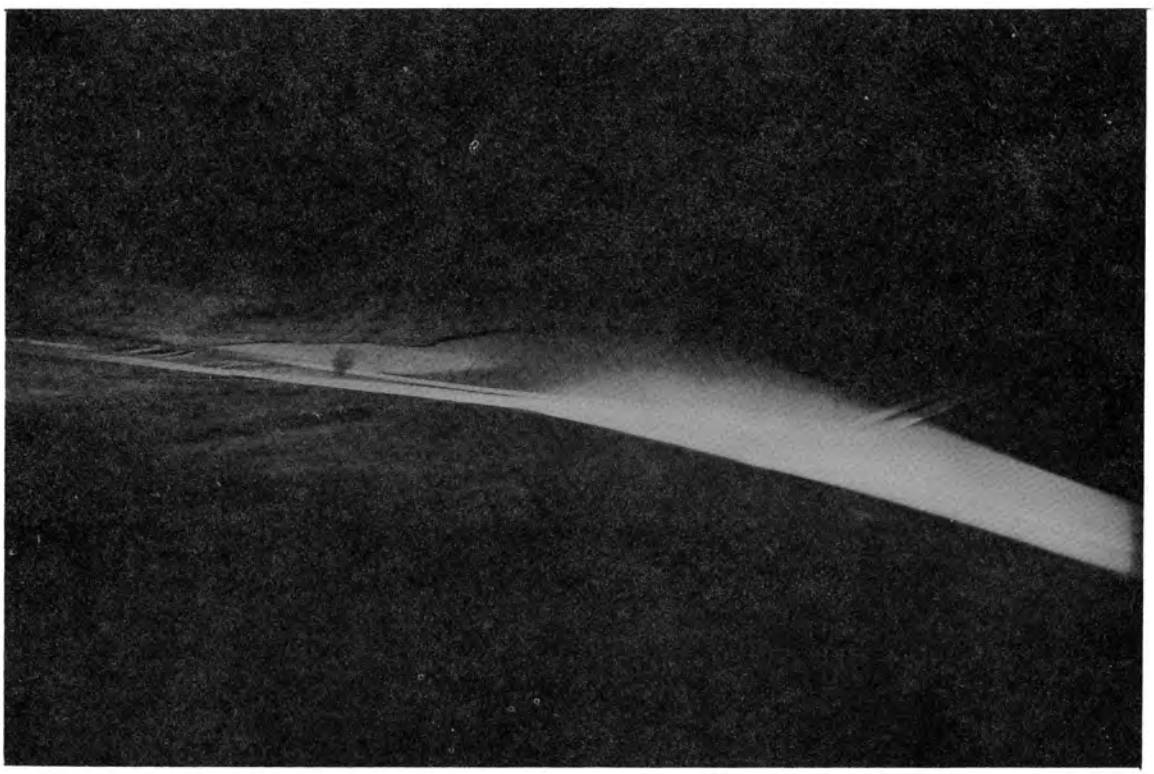

Figure 30. Smoke flow patterns; inversion $\Delta T = 115^{o}$ F, azimuth 315^{o}, velocity U ≈ 1.6 mps; camera direction, south

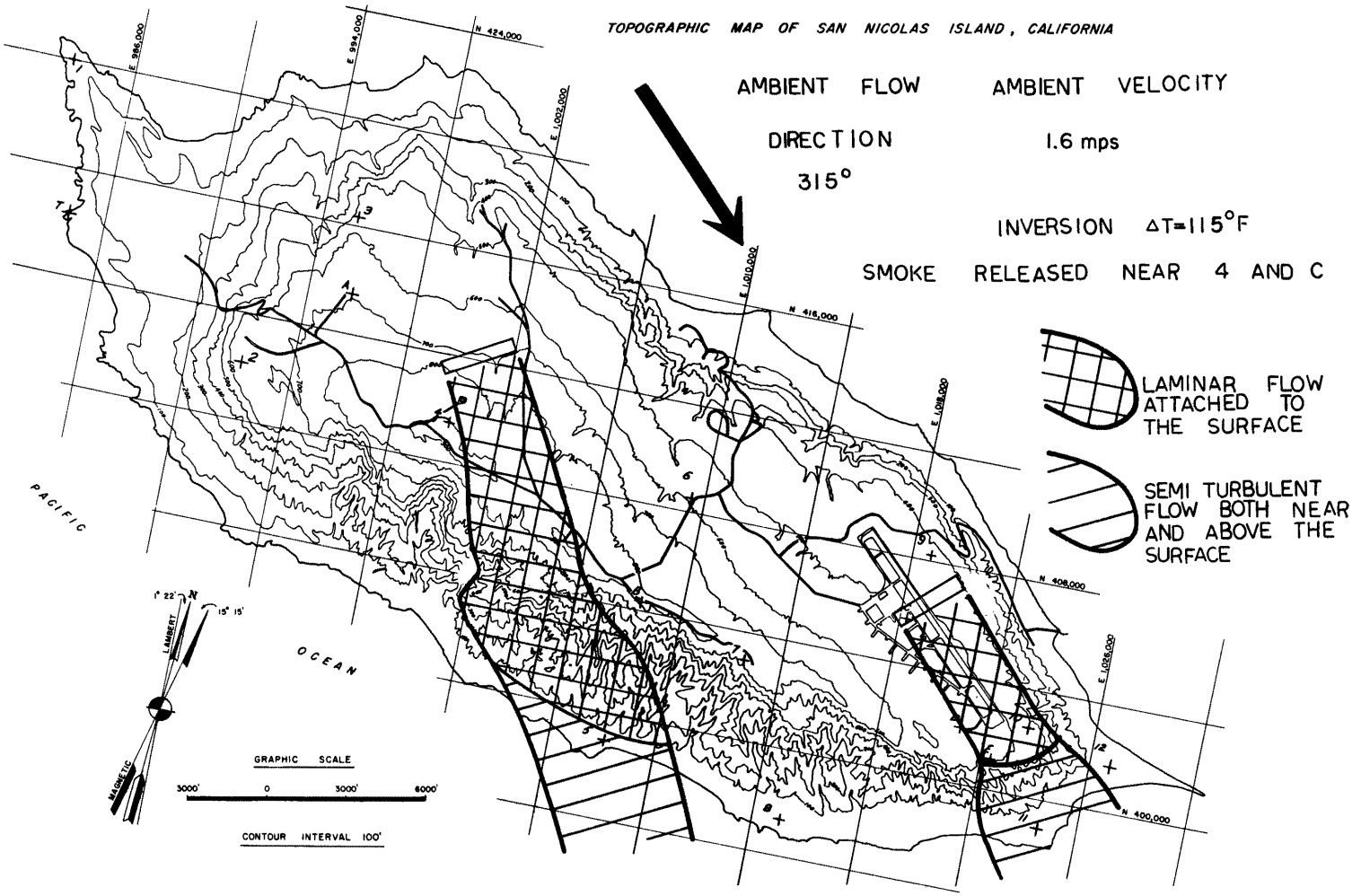

FLOW PATTERNS DEFINED BY SMOKE TRAILS FOR INVERSION FLOW

Figure 31. Flow patterns defined by smoke trails for inversion flows

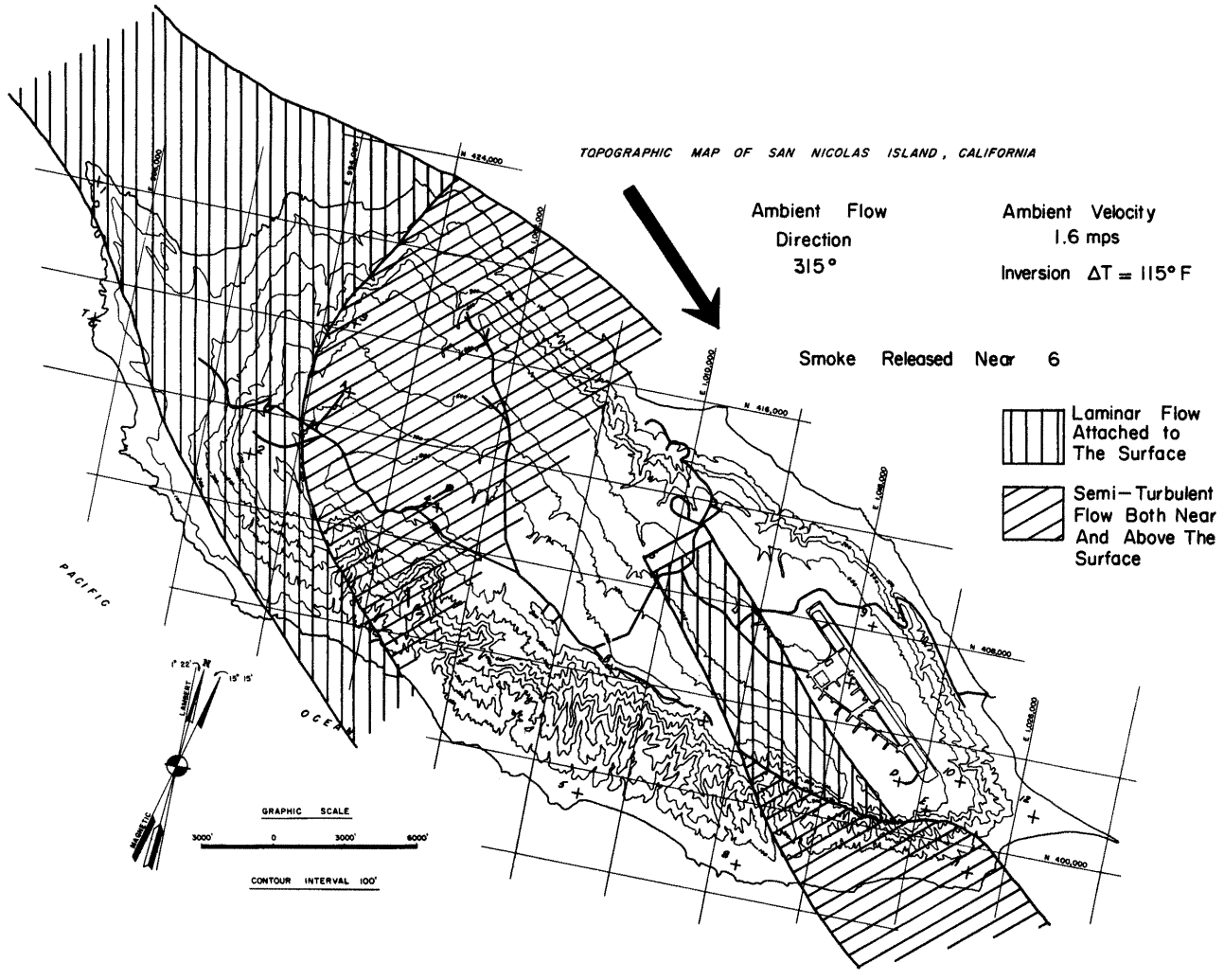

Figure 32. Flow patterns defined by smoke trails for inversion flows

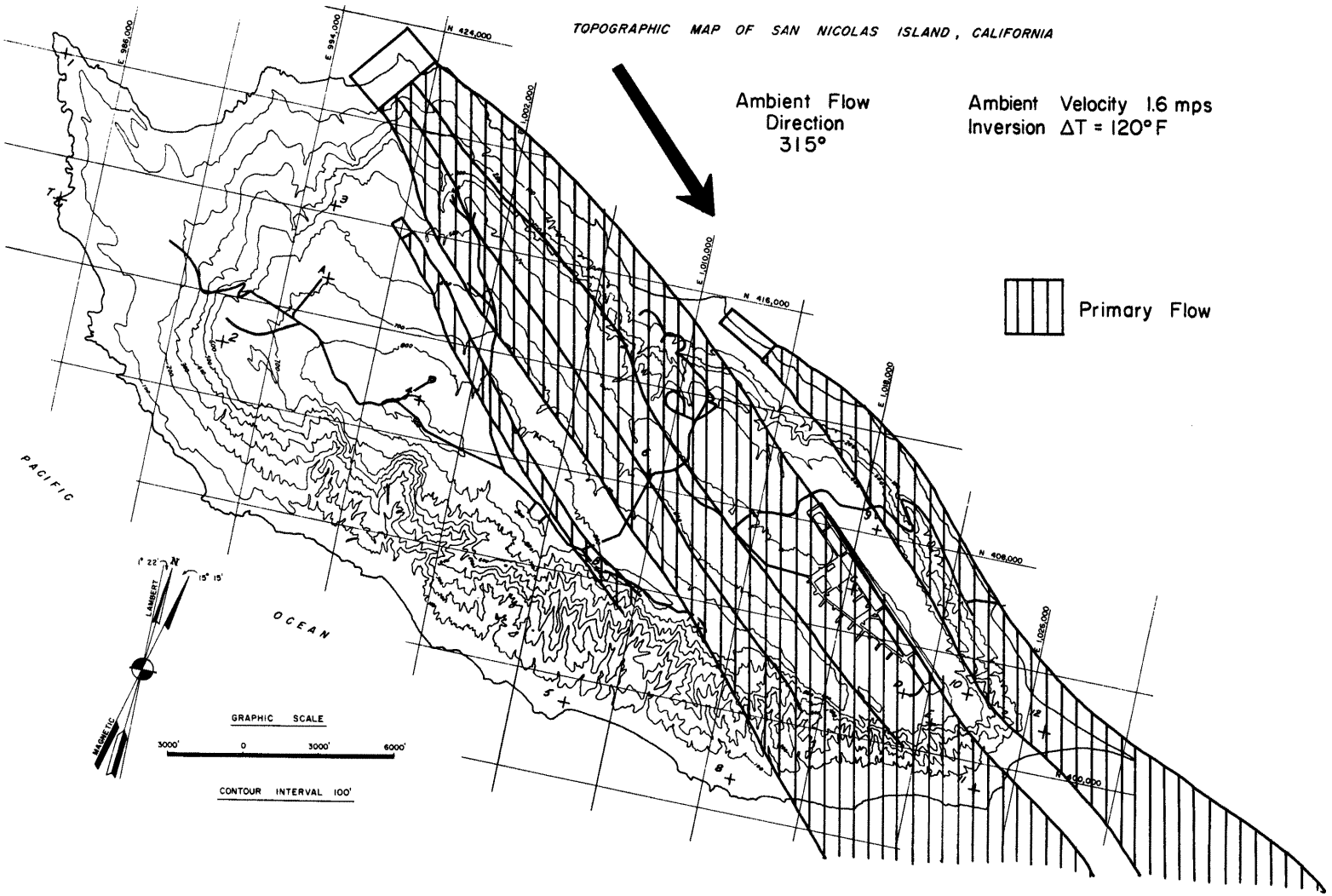

Figure 33. Flow patterns defined by smoke trails for inversion flows

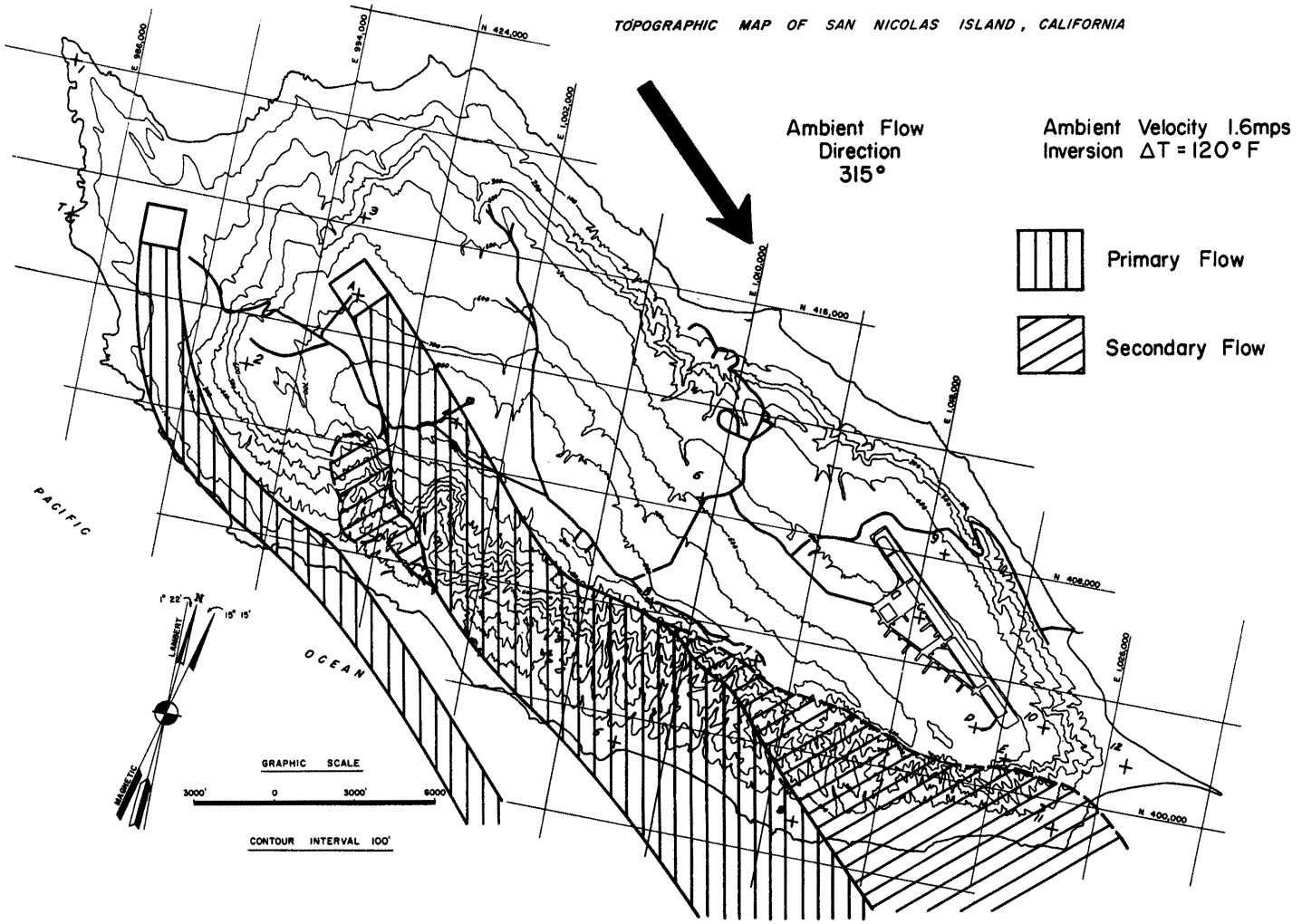

Figure 34. Flow patterns defined by smoke trails for inversion flows

Figure 35. Oil-fog smoke plume released from rocket test stand site

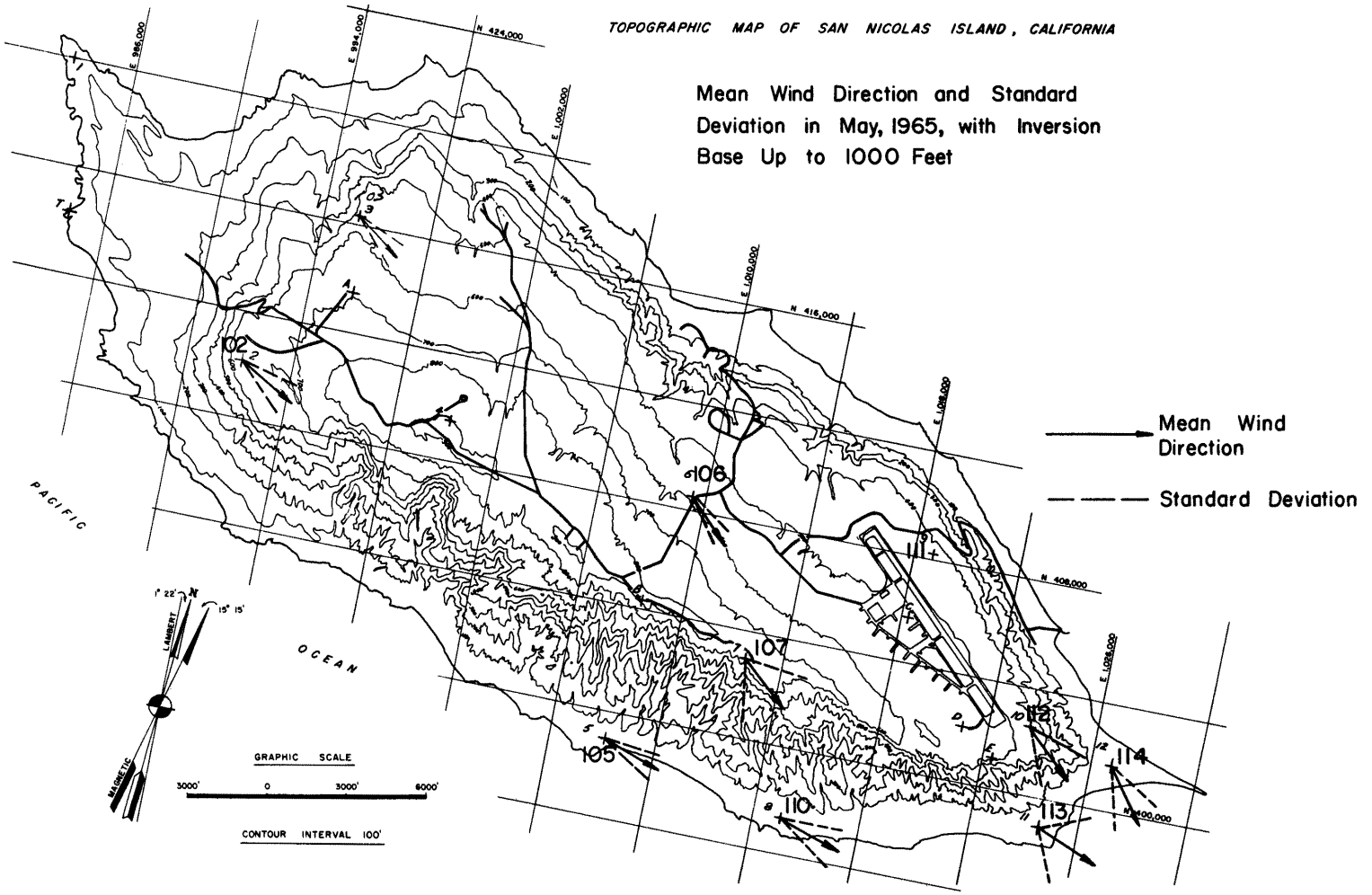

Figure 36. Prototype flow conditions, San Nicolas Island

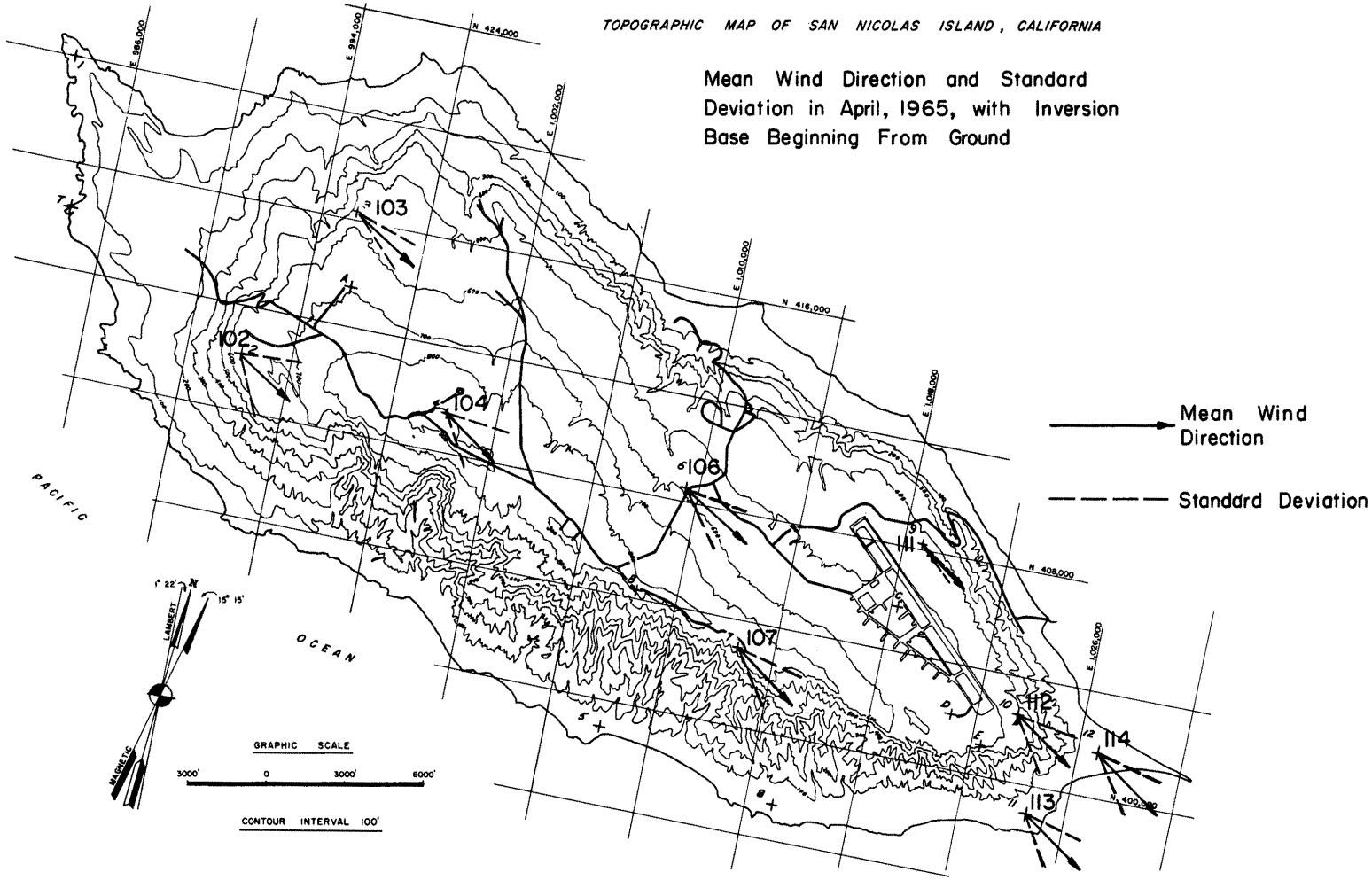

Figure 37. Prototype flow conditions, San Nicolas Island

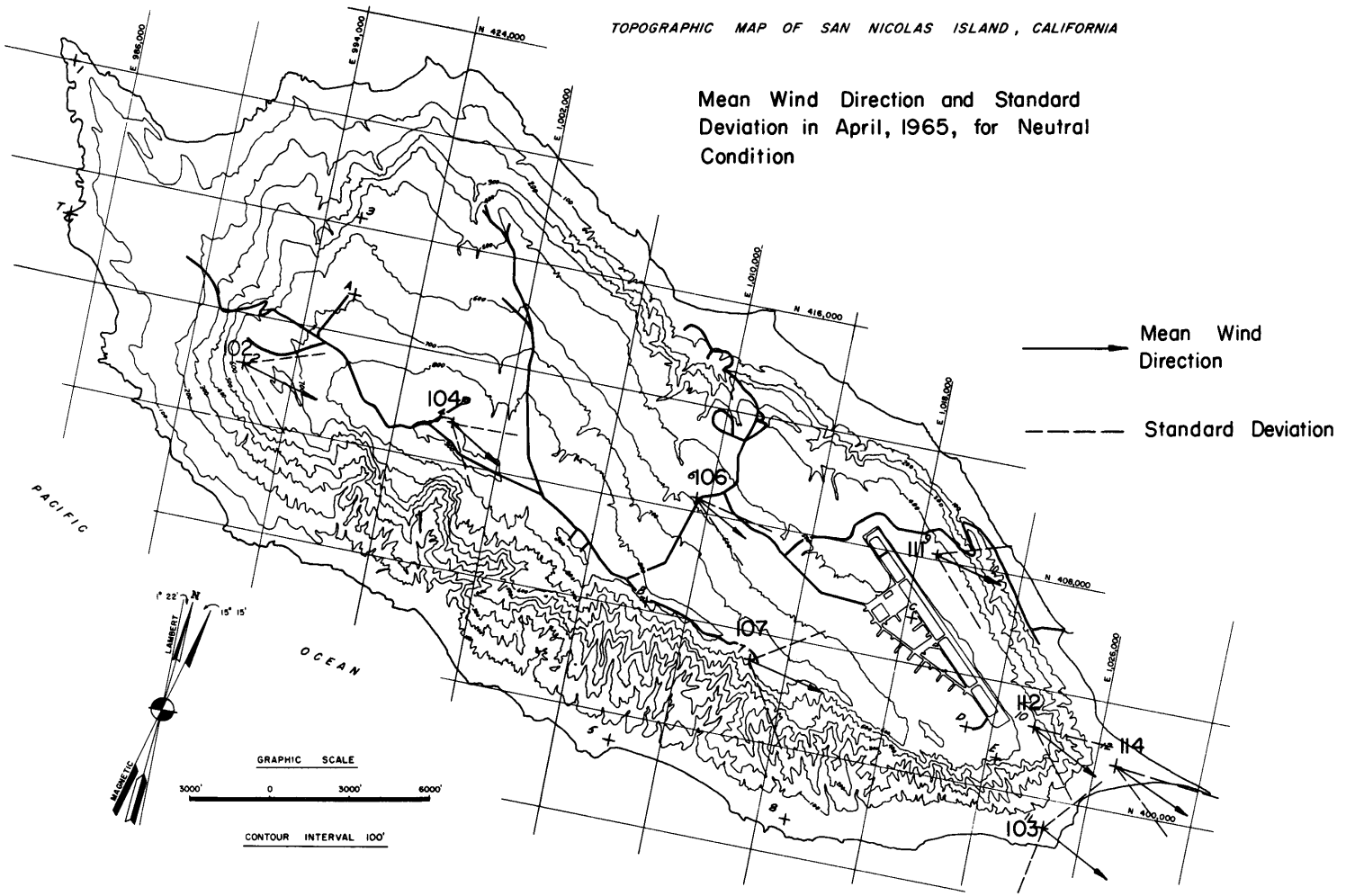

Figure 38. Prototype flow conditions, San Nicolas Island

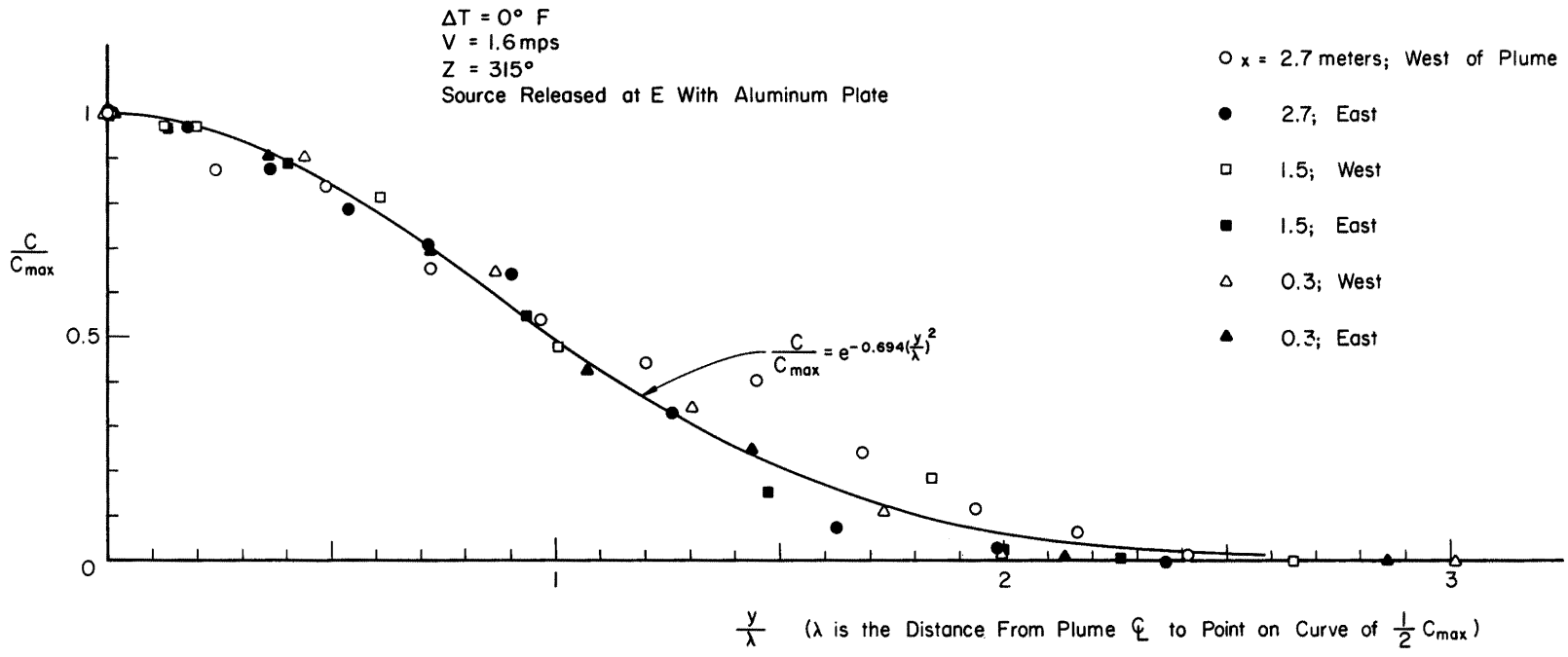

Figure 39. Non-dimensional horizontal concentration profiles

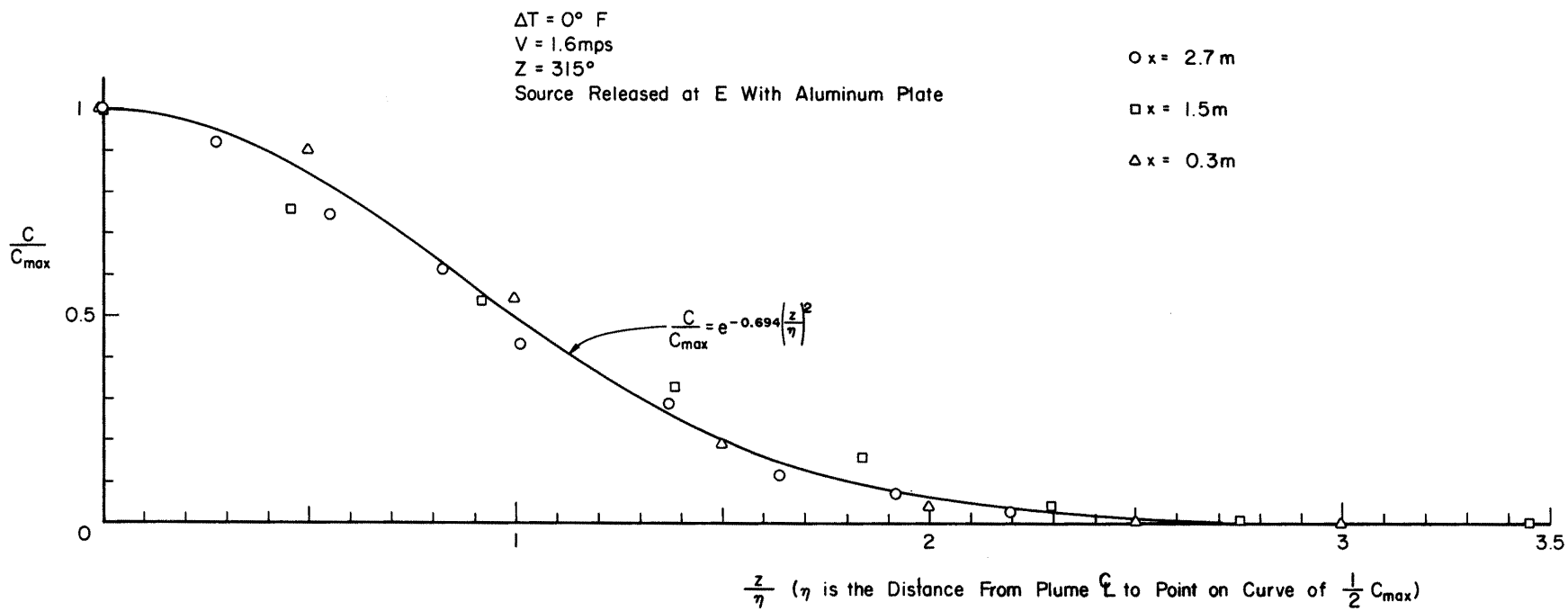

Figure 40. Non-dimensional vertical concentration profiles

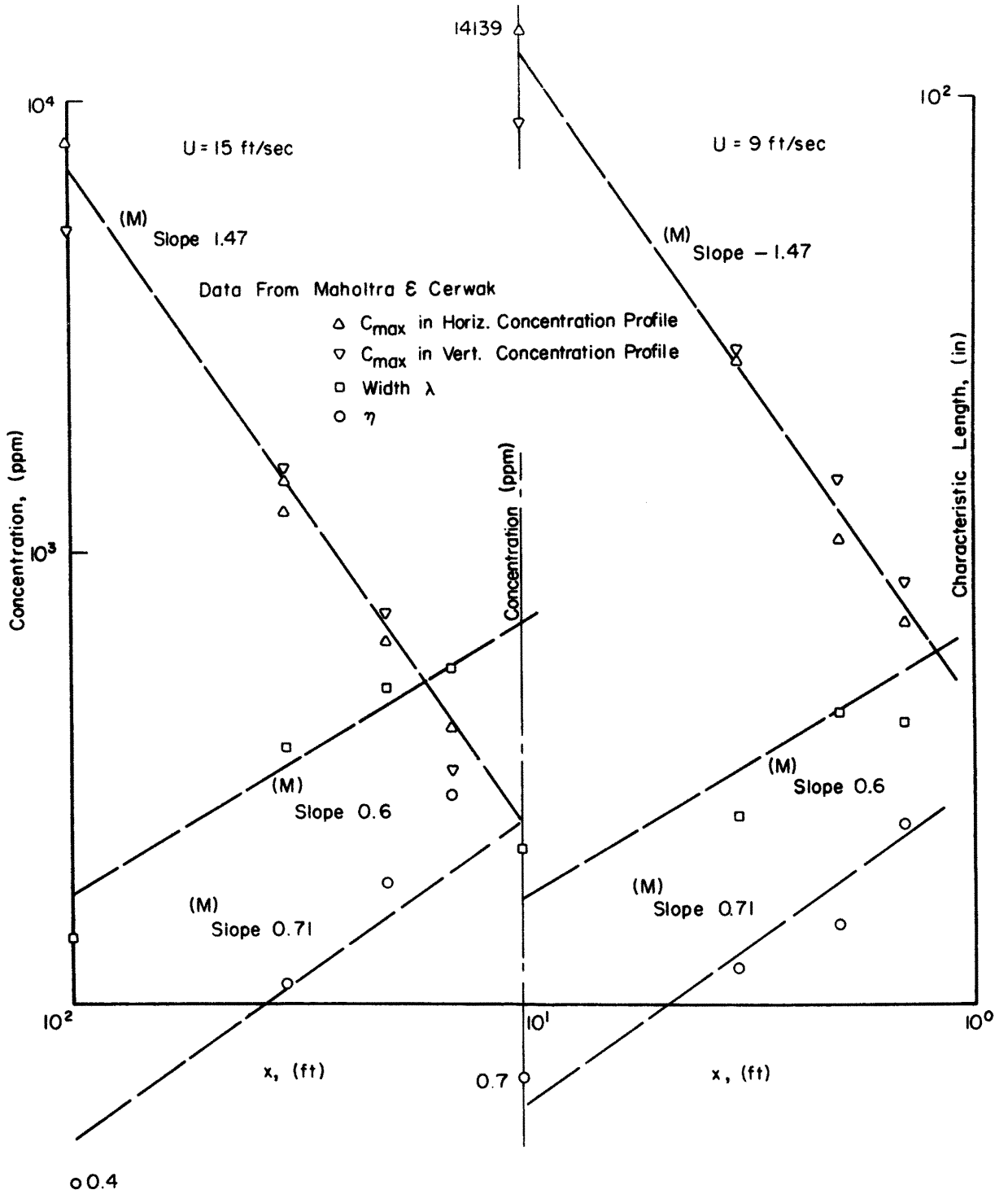

Figure 41. Comparison of ammonia and helium release results

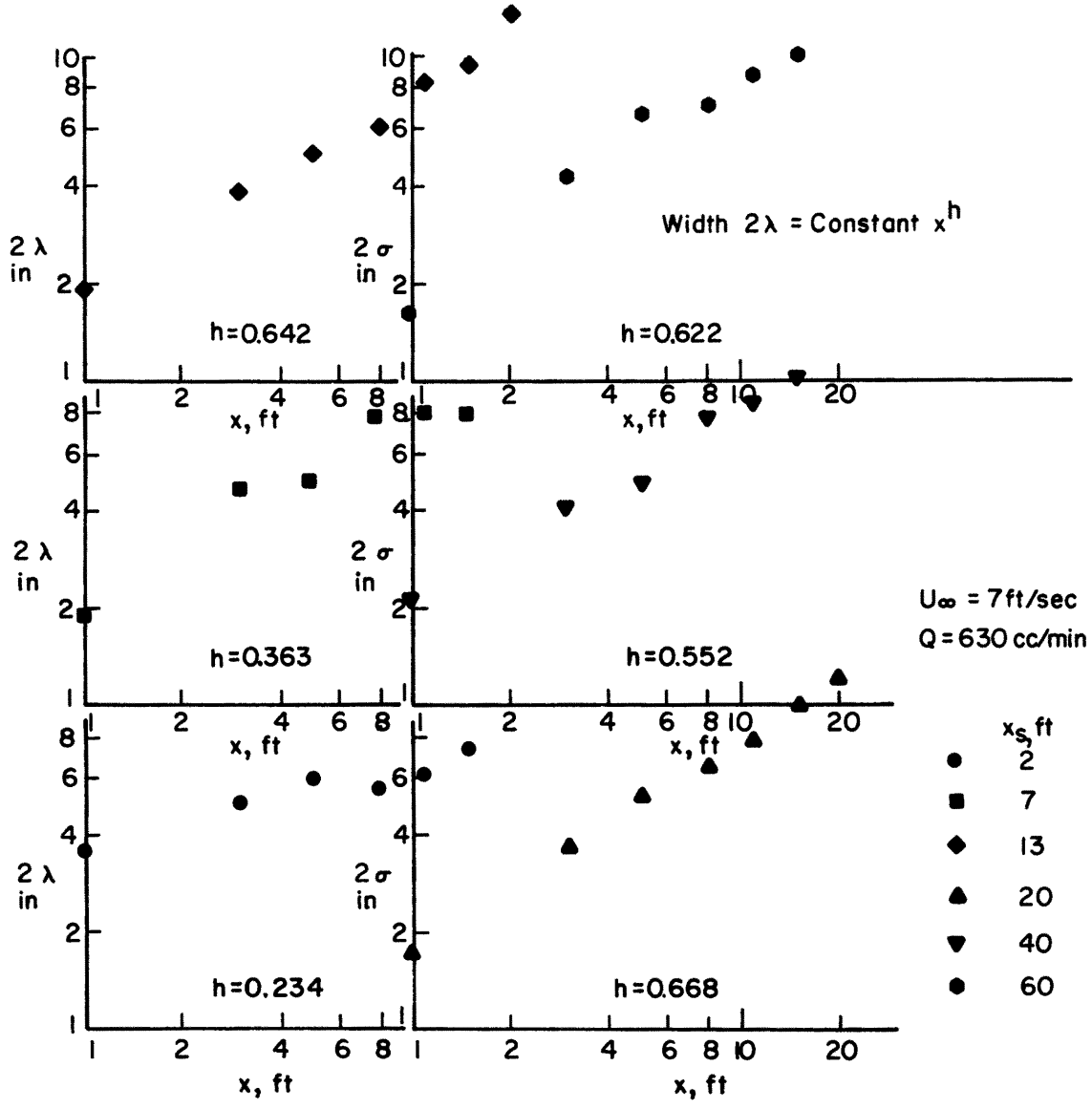

Figure 42. Variation of characteristic plume width λ

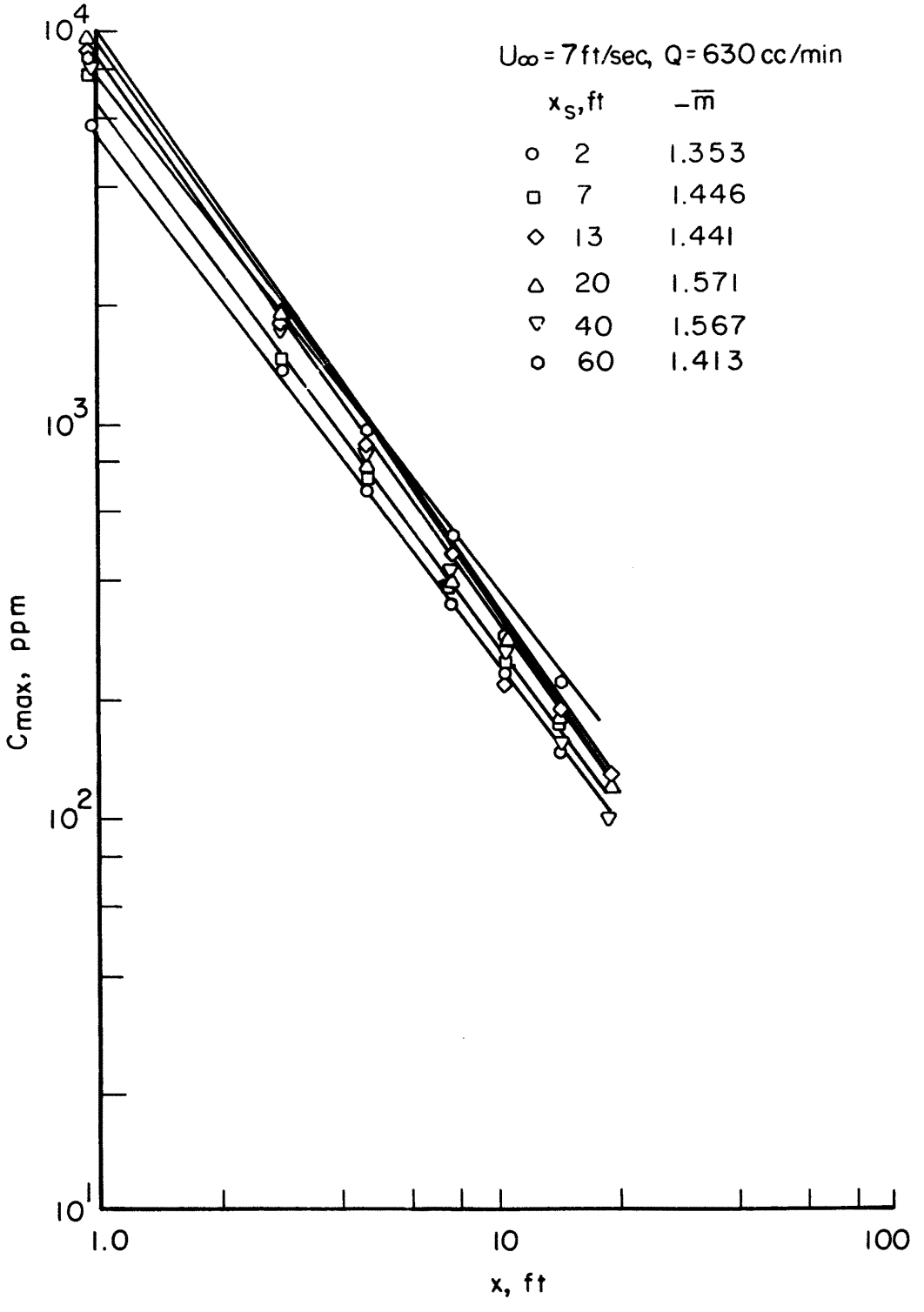

Figure 43. Variation of maximum plume concentration

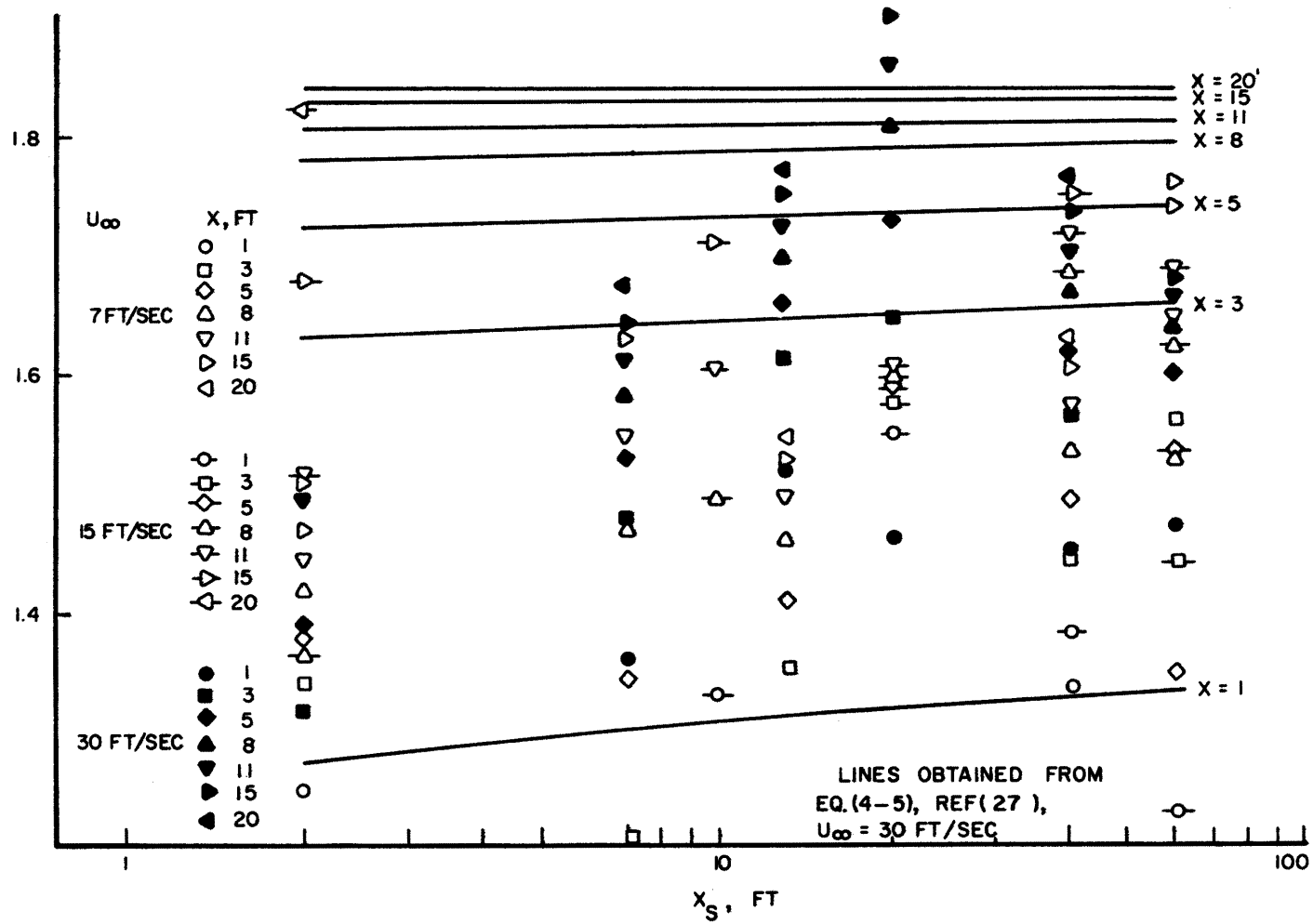

Figure 44. Variation of exponent m for continuous point source plumes in meteorological wind tunnel

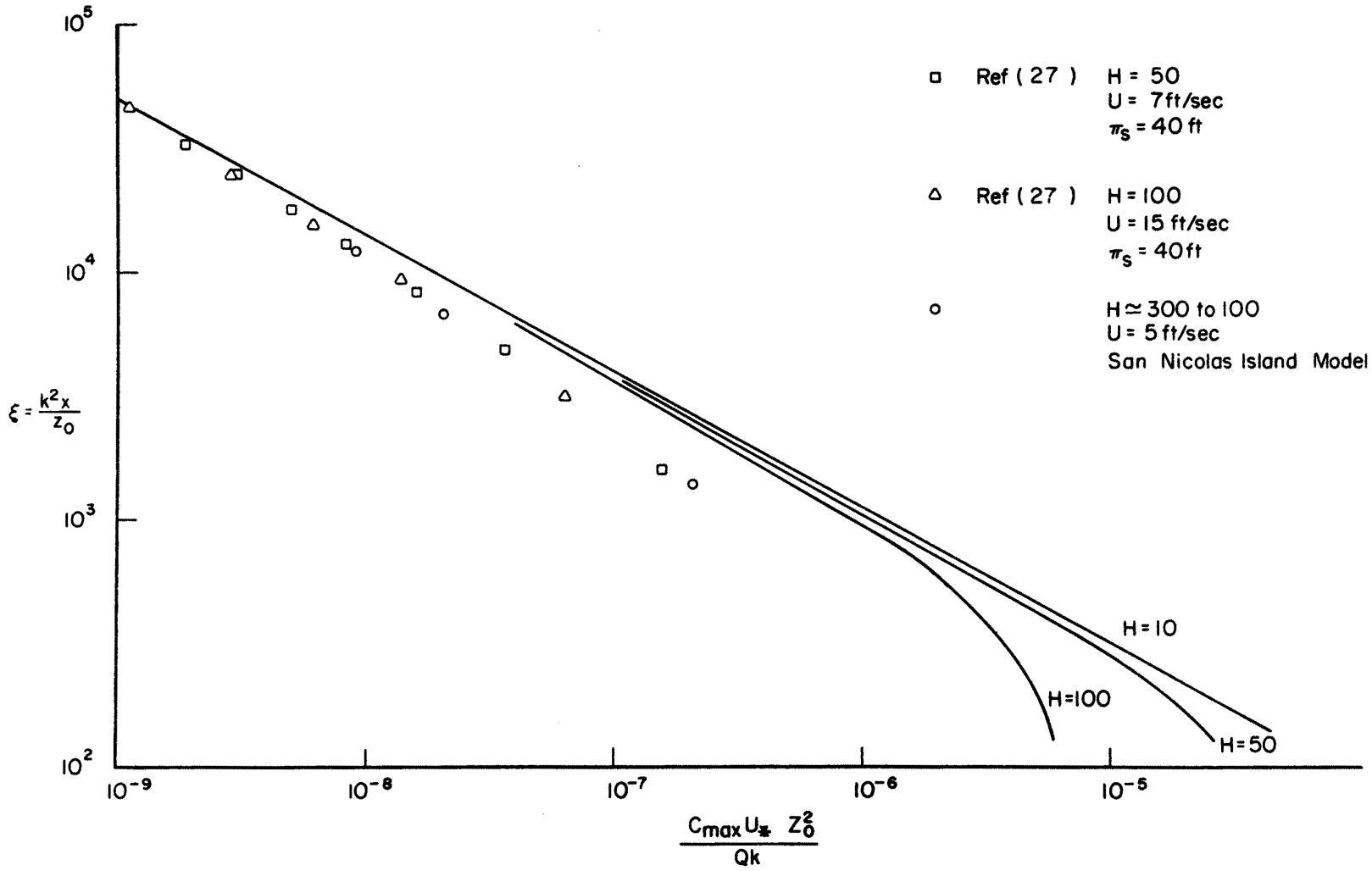

Figure 45. Dimensionless maximum concentration versus dimensionless downwind distance: neutral stratification

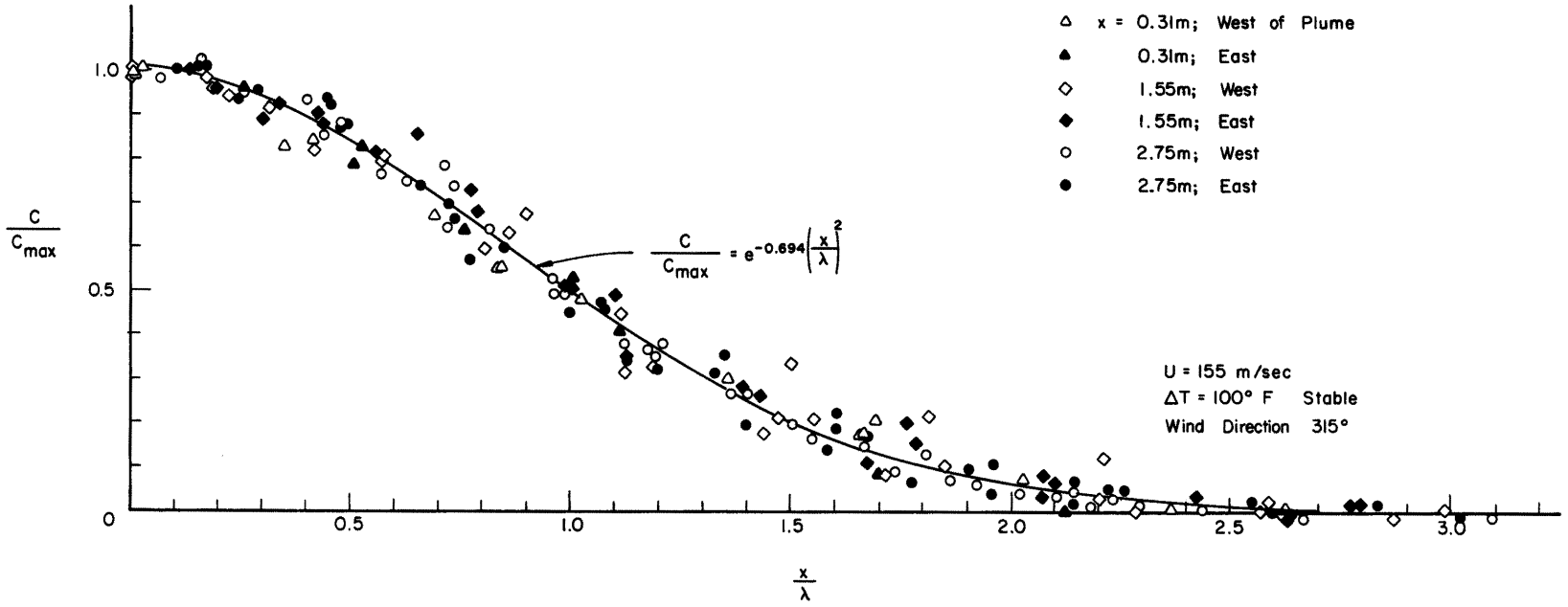

Figure 46. Non-dimensional horizontal concentration profiles

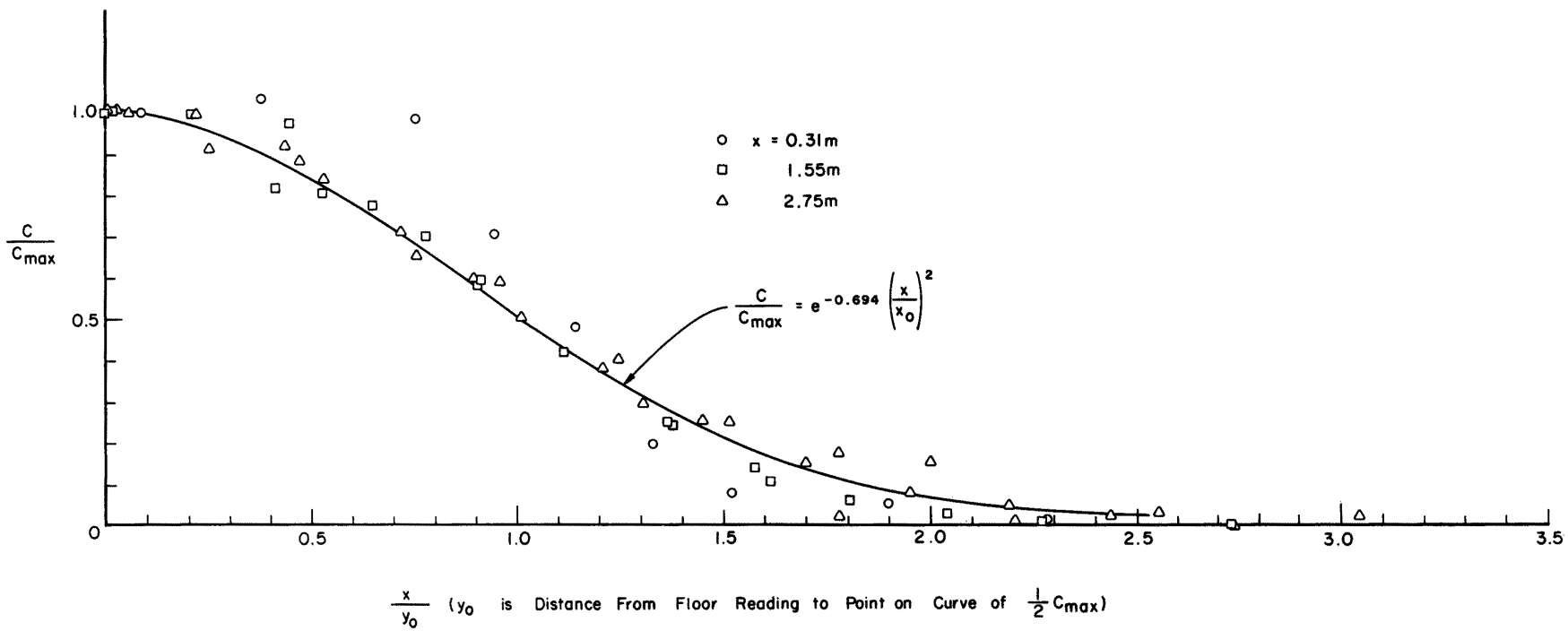

Figure 47. Non-dimensional vertical concentration profiles

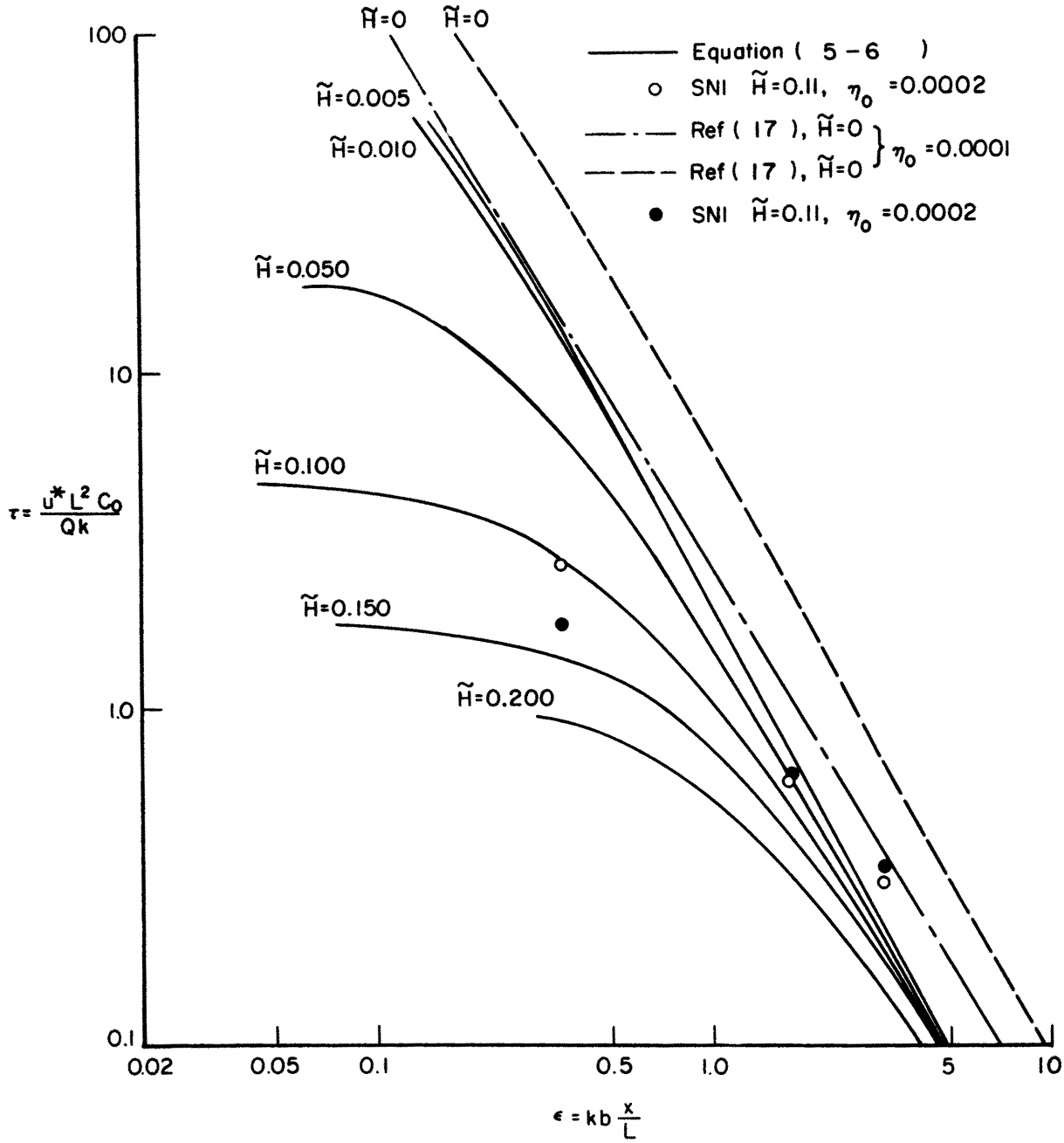

Figure 48. Dimensionless maximum concentration versus dimensionless downwind distance: stable stratification

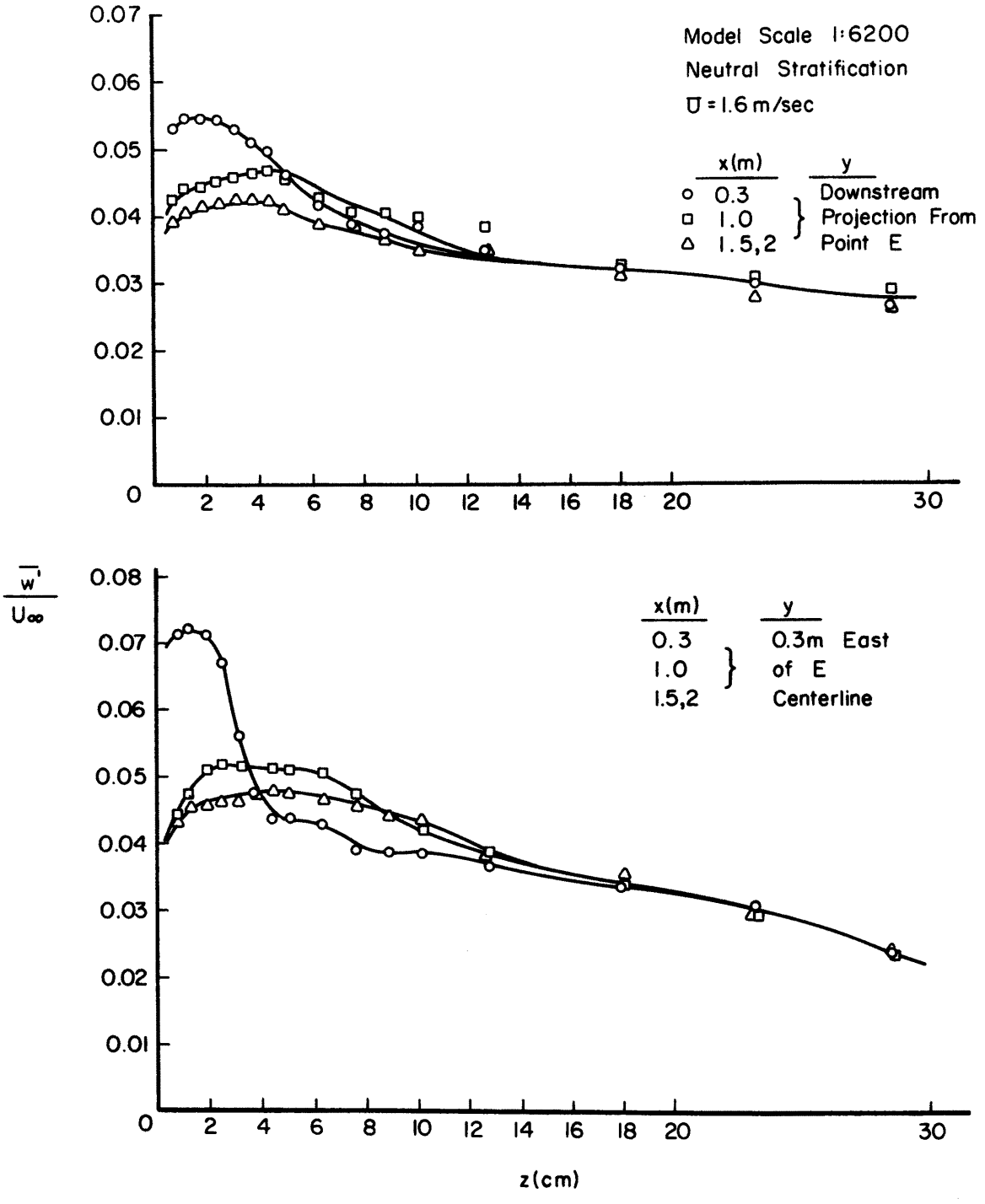

Figure 49. Vertical turbulent wake intensity - model scale: 1/6200

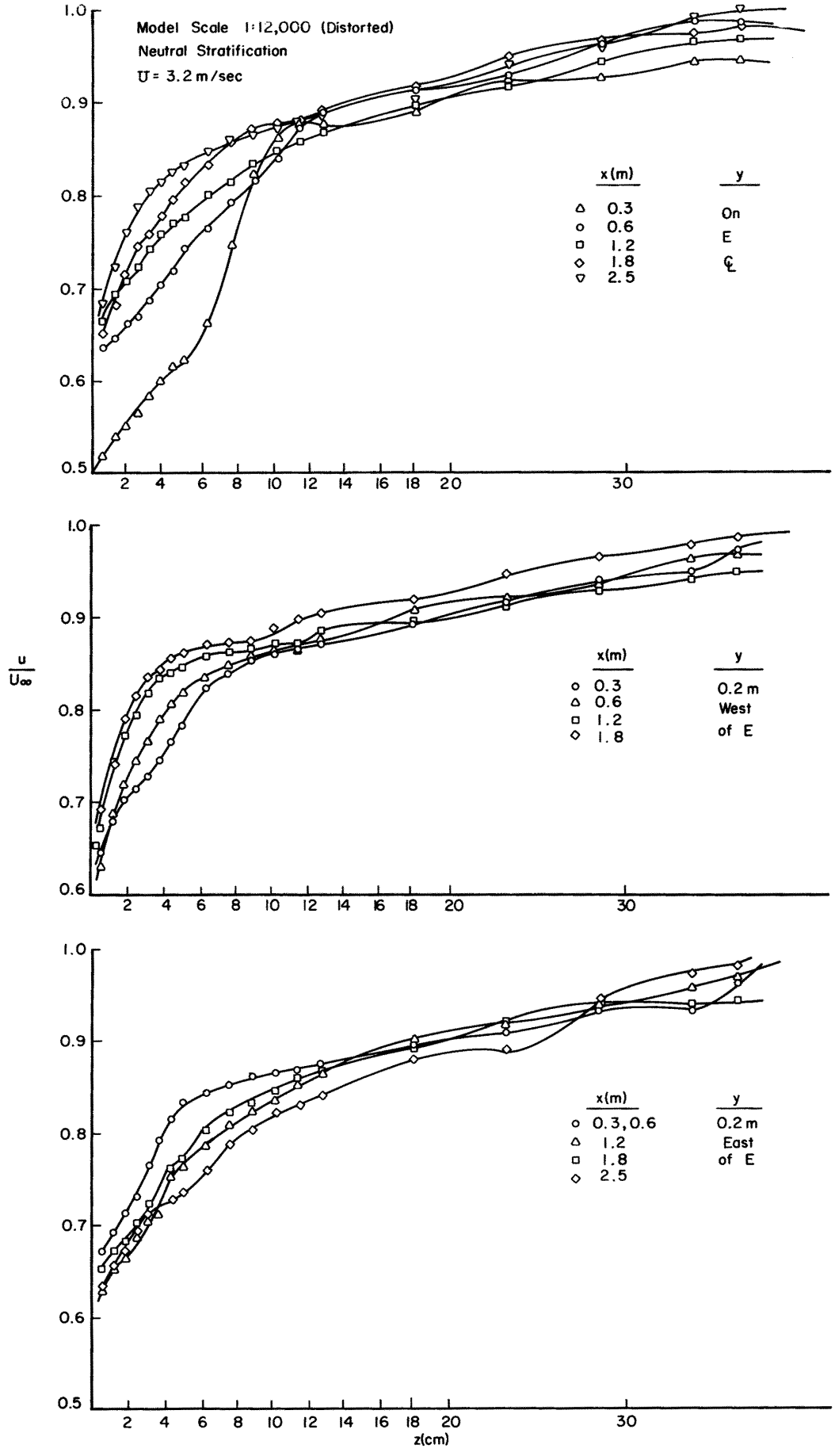

Figure 50. Velocity wake profiles - model scale: 1/12,000

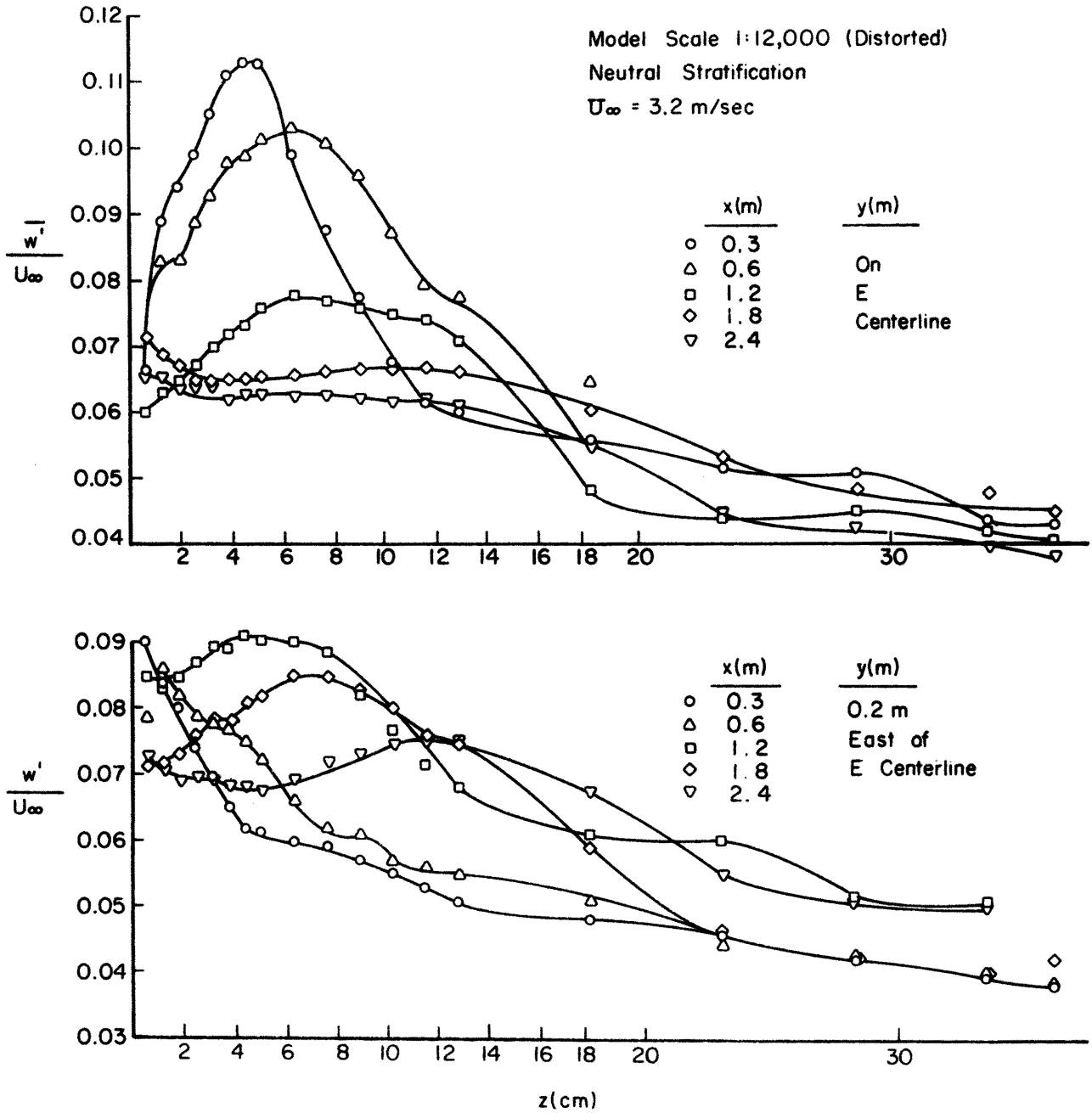

Figure 51. Vertical turbulent wake intensity - model scale: 1/12,000

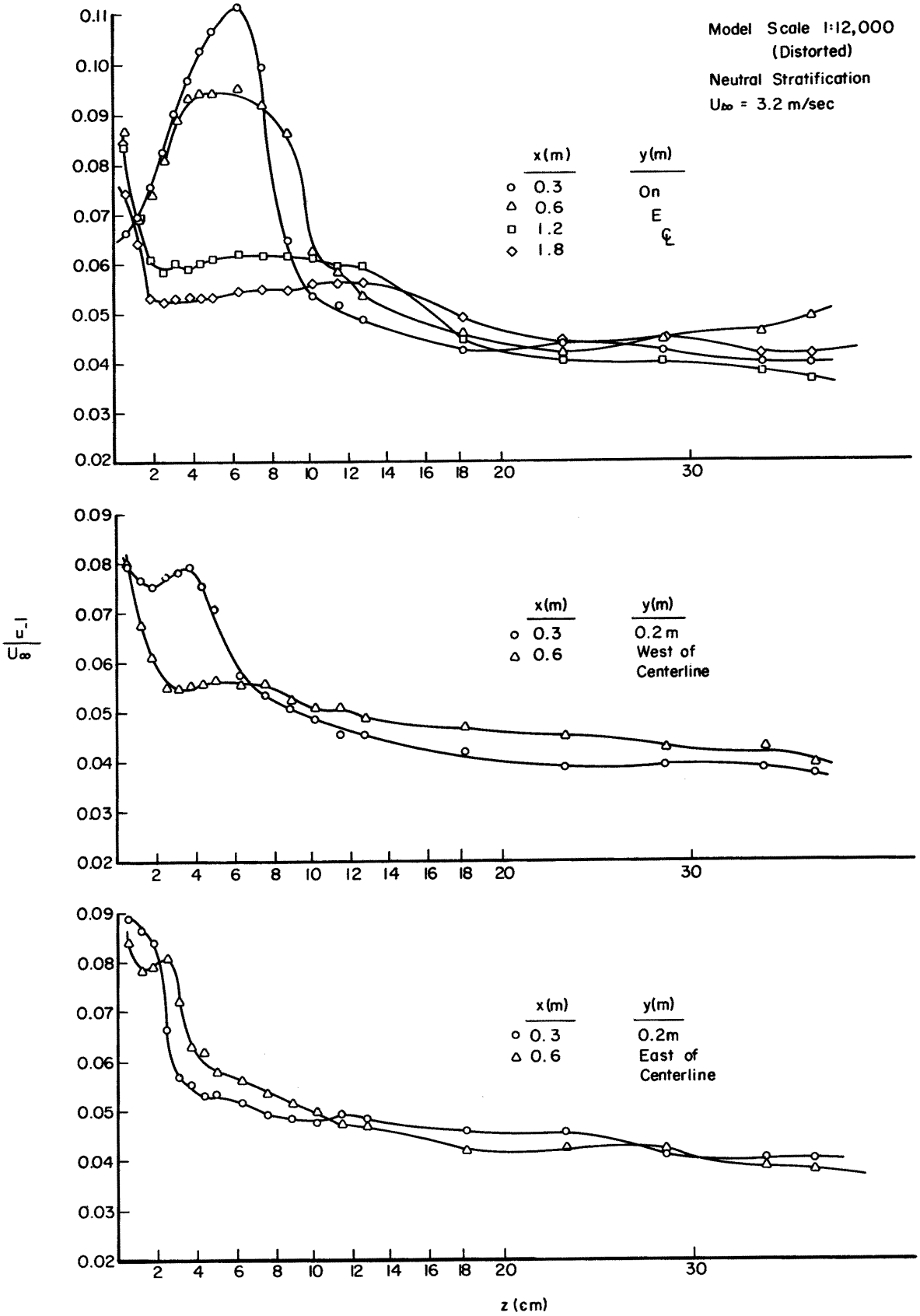

Figure 52. Longitudinal turbulent wake intensity - model scale: 1/12,000

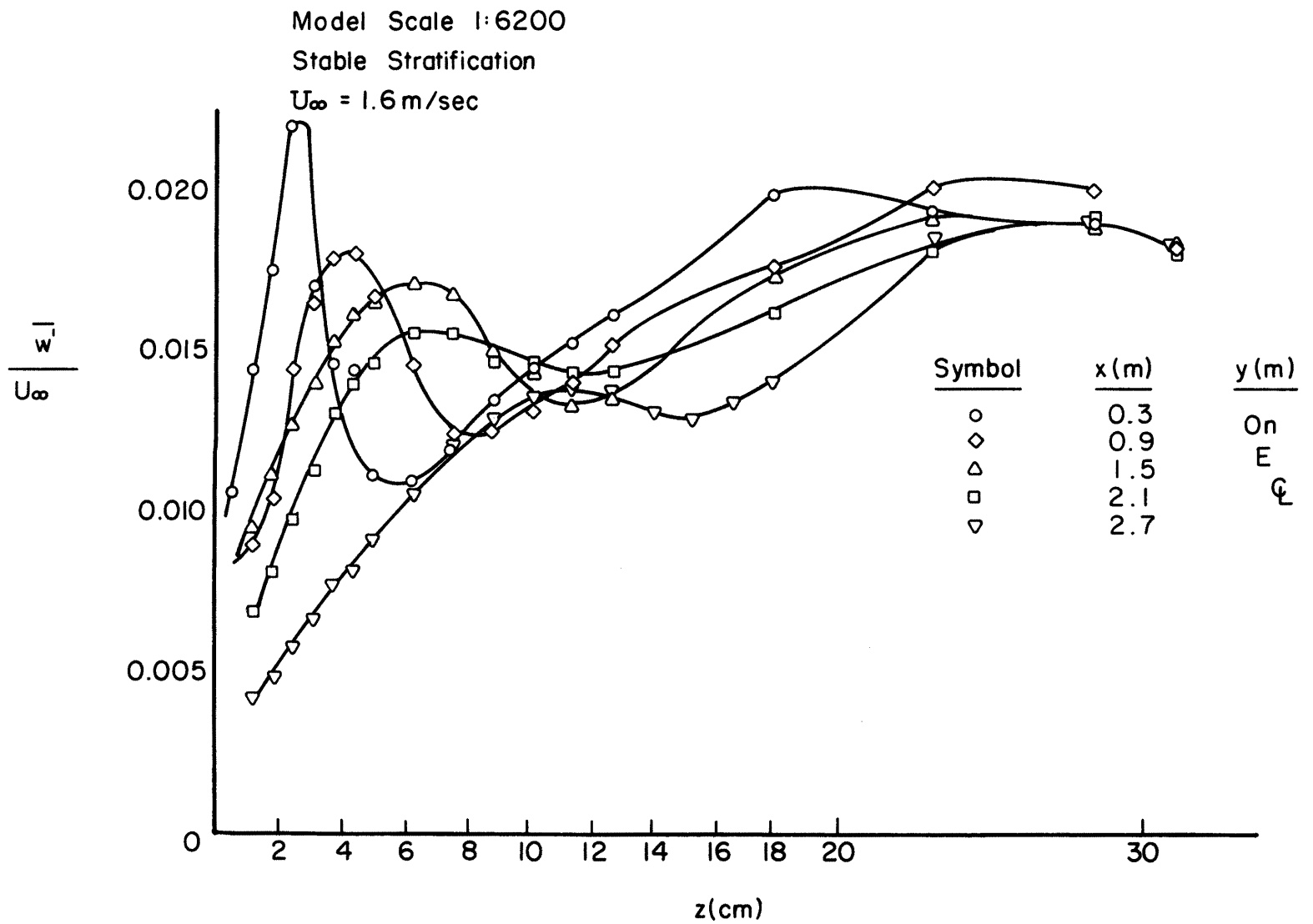

Figure 53. Vertical turbulent wake intensity - model scale: 1/6200

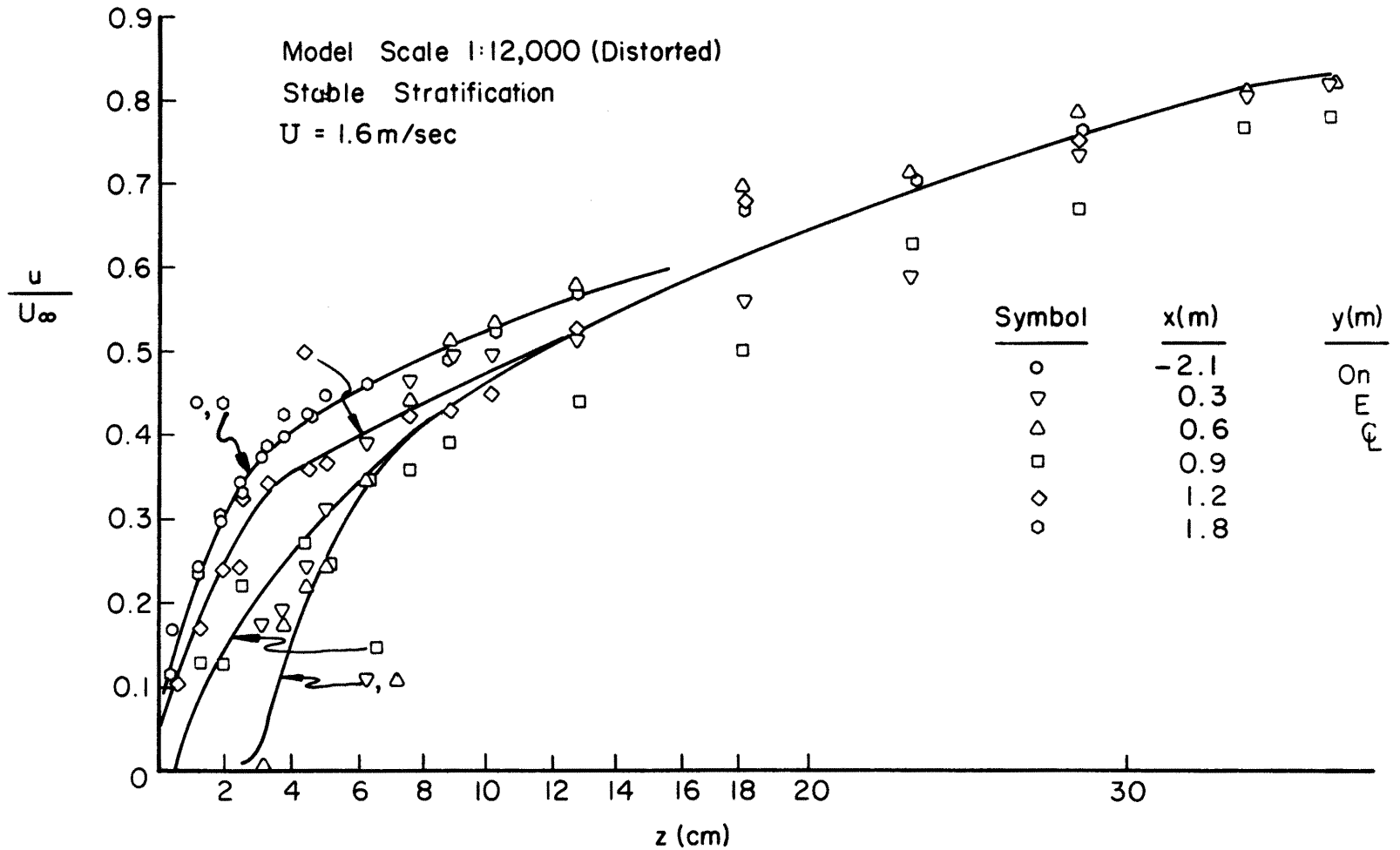

Figure 54. Velocity wake profiles - model scale: 1/12,000

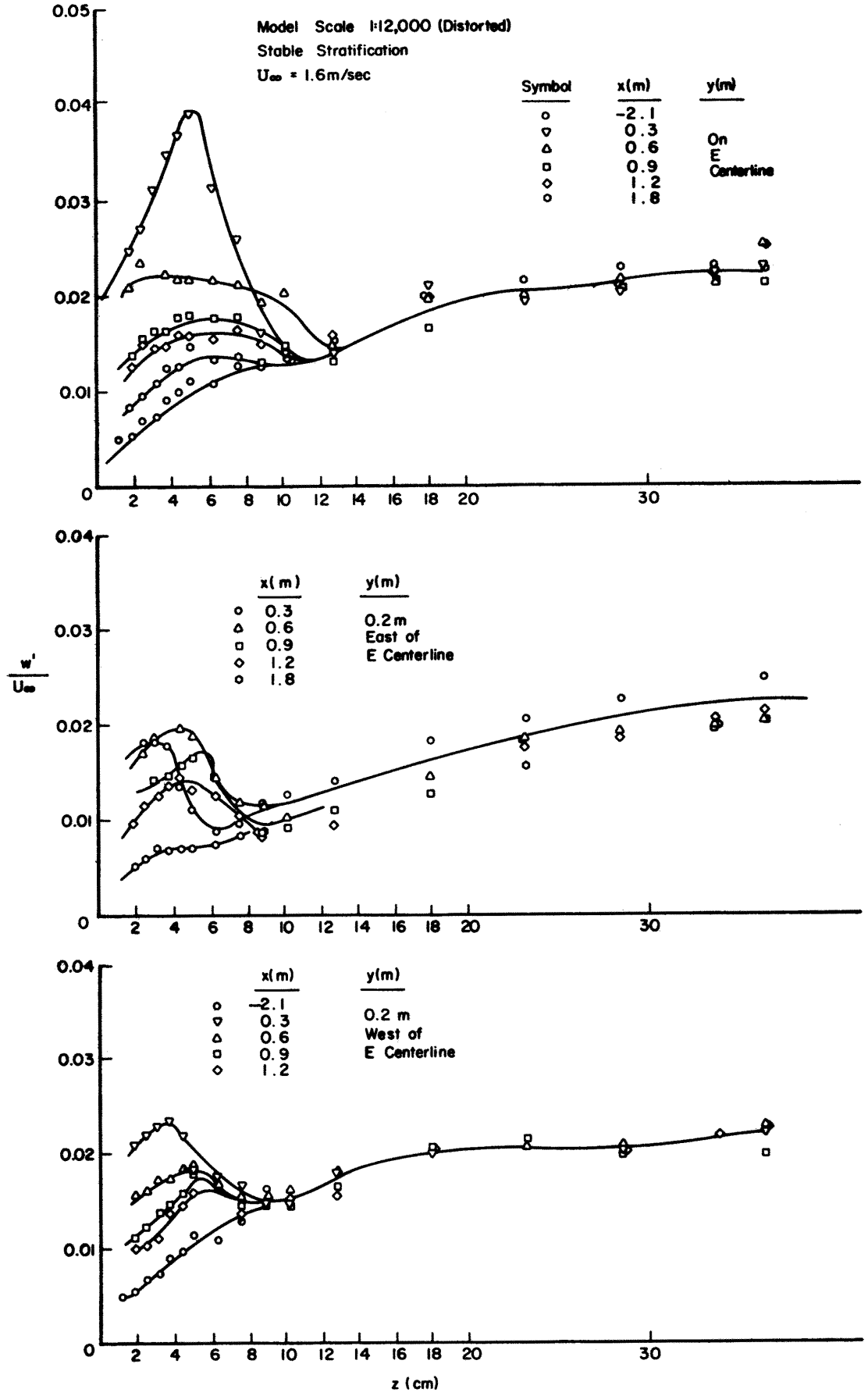

Figure 55. Vertical turbulent wake intensity - model scale: 1/12,000

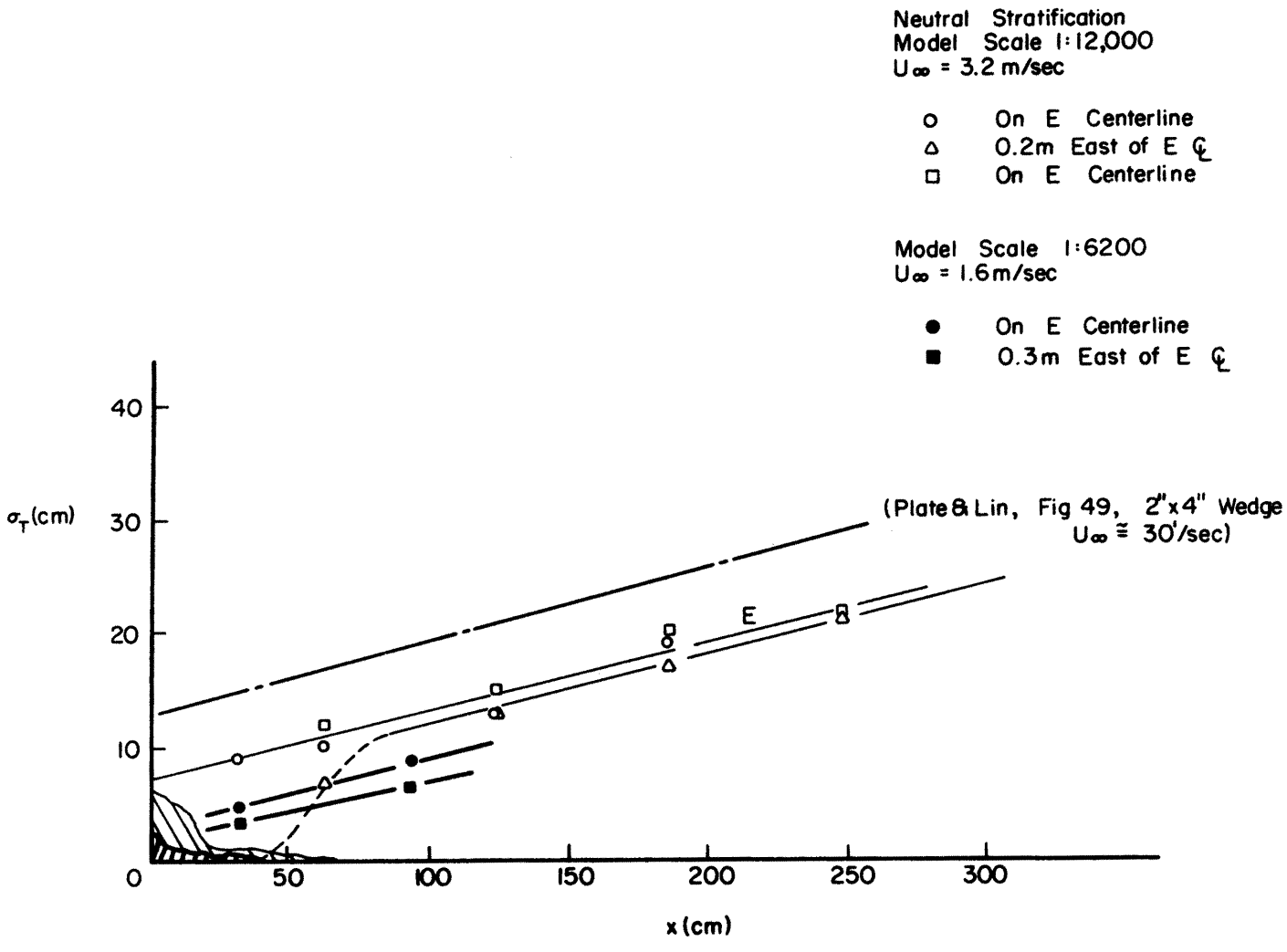

Figure 56. Characteristic length for wake vertical growth rate

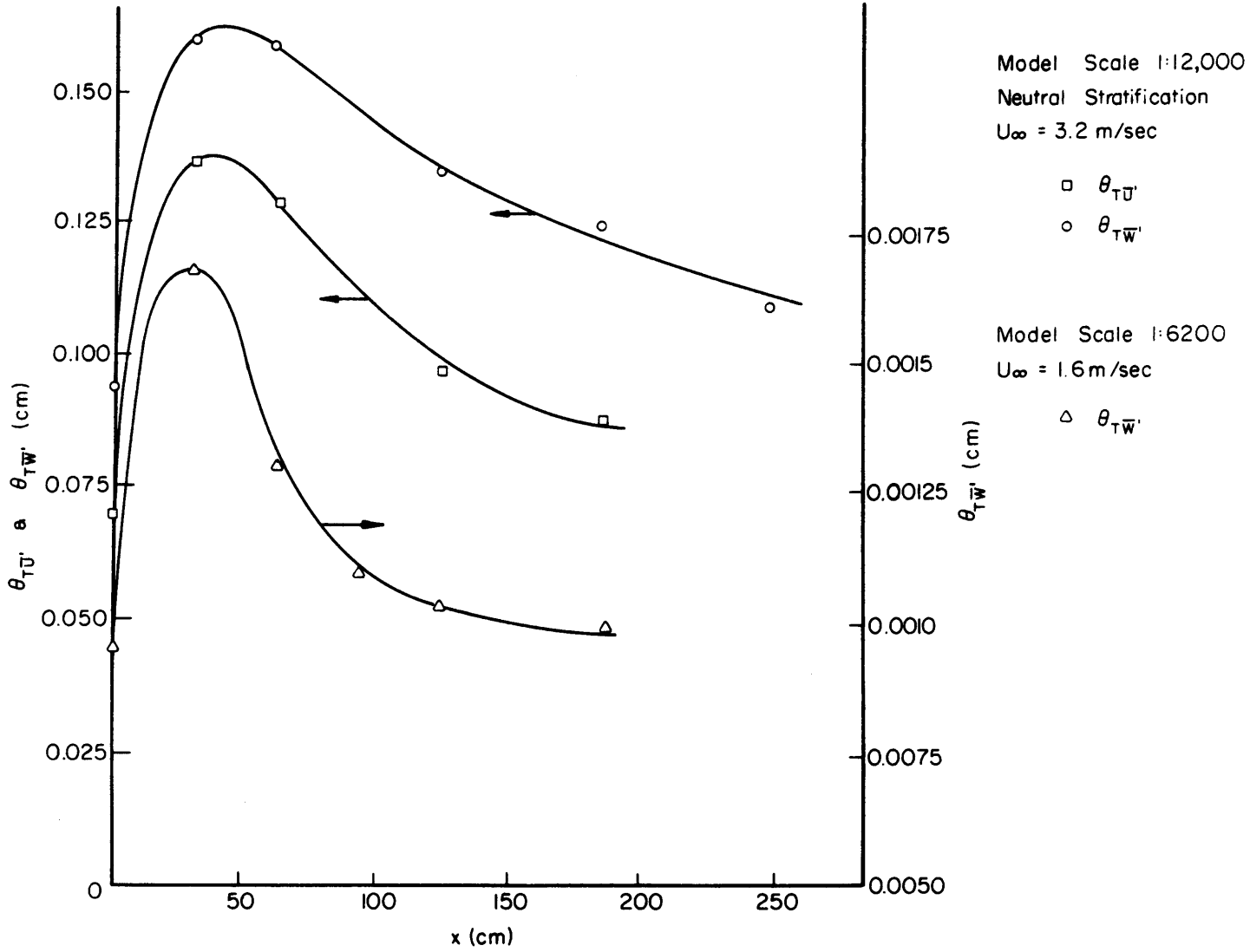

Figure 57. Wake energy scale

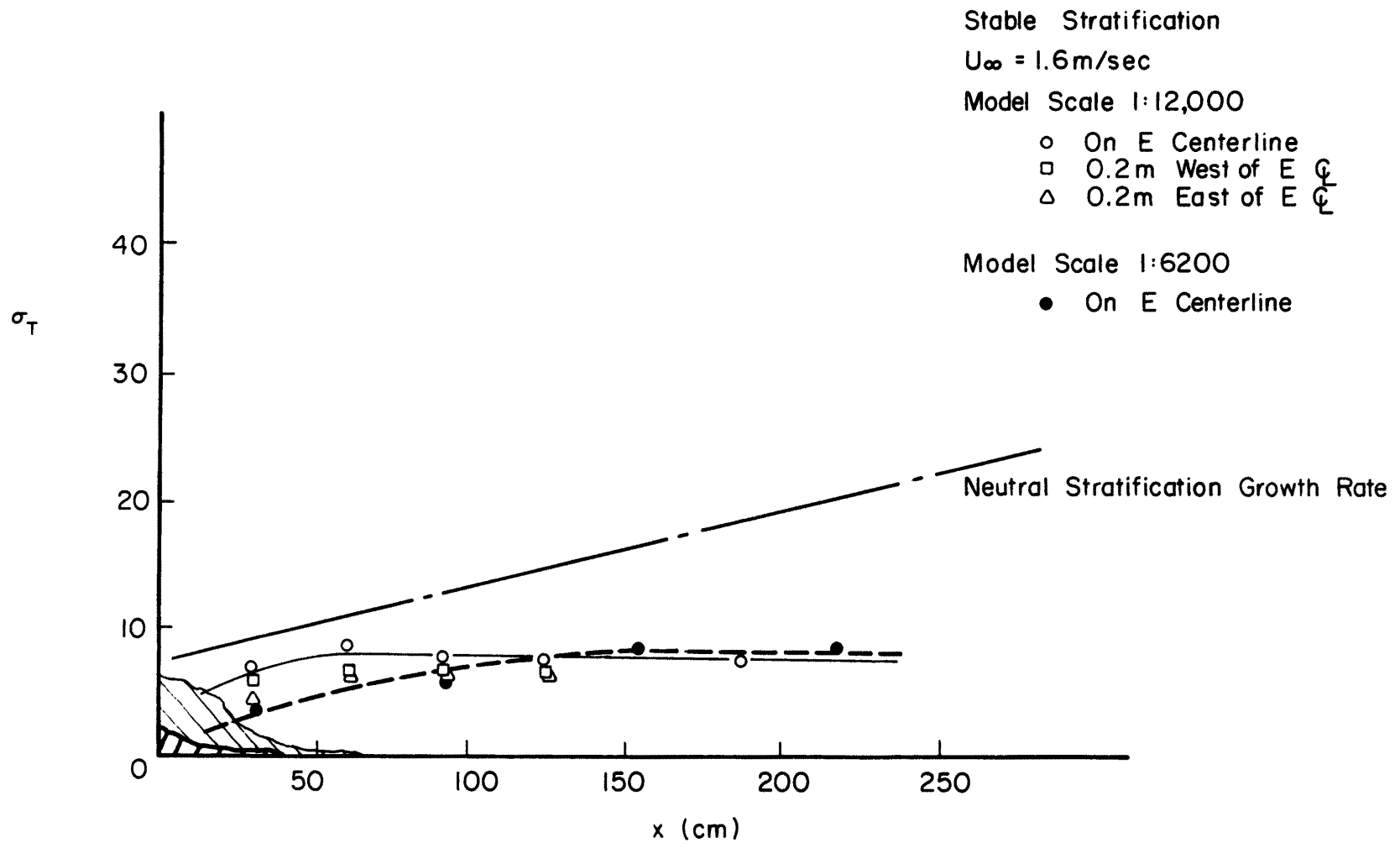

Figure 58. Characteristic length for wake vertical growth rate

Unclassified
Security Classification

DOCUMENT CONTROL DATA - R&D

(Security classification of title, body of abstract and indexing annotation must be entered when the overall report is classified)

1. ORIGINATING ACTIVITY *(Corporate author)* Fluid Mechanics Program, College of Engineering Colorado State University Fort Collins, Colorado	2a. REPORT SECURITY CLASSIFICATION Unclassified 2b. GROUP Unclassified

3. REPORT TITLE
Wind Tunnel Modeling of Flow and Diffusion over San Nicolas Island, California

4. DESCRIPTIVE NOTES *(Type of report and inclusive dates)*
Final Technical Report

5. AUTHOR(S) *(Last name, first name, initial)*
Meroney, R. N. and Cermak, J.E.

6. REPORT DATE	7a. TOTAL NO. OF PAGES	7b. NO. OF REFS
May 1967		30

8a. CONTRACT OR GRANT NO.	9a. ORIGINATOR'S REPORT NUMBER(S)
b. PROJECT NO.	CER66-67RNM-JEC44
c.	9b. OTHER REPORT NO(S) *(Any other numbers that may be assigned this report)*
d.	

10. AVAILABILITY/LIMITATION NOTICES
Distribution of this document is unlimited

11. SUPPLEMENTARY NOTES	12. SPONSORING MILITARY ACTIVITY
	U.S. Navy Purchasing Office, 929 South Broadway, Los Angeles, California 90055

13. ABSTRACT

Neutrally and stably stratified flow over a 1:6200 and a 1:12,000 scale model of San Nicolas Island, California, were studied in the Army Meteorological Wind Tunnel of the Fluid Dynamics and Diffusion Laboratory at Colorado State University. Surface characteristics of wind movement over the island were studied by the use of indicator paints, titanium tetrachloride smoke, and the measurement of mean velocity, mean temperature, mean concentration, and turbulent intensity profiles.

Available field data revealed that similarity was sufficiently achieved to give similar mean flow patterns. Flow in the wake region was self consistent, but no comparative field data are available. Concentration decay rates for diffusing tracers were comparable for neutral flow. Mean velocity, mean temperature, and Richardson number profiles were similar for stably stratified flows; however, the similarity of the diffusion plumes to plumes in the atmosphere is not clear. It is concluded that over complex terrain flow fields may be satisfactorily simulated for stable thermal stratification, but that the characteristics of diffusion in the stable stratifications produced by the Army Meteorological Wind Tunnel should be studied in greater detail.

DD FORM 1 JAN 64 1473

Unclassified
Security Classification

14. KEY WORDS	LINK A		LINK B		LINK C	
	ROLE	WT	ROLE	WT	ROLE	WT
Simulation Atmospheric Modeling Stratified Flow Diffusion Wind-Tunnel Laboratory Turbulent Flow Fluid Mechanics Micrometeorology Mesometeorology						

INSTRUCTIONS

1. ORIGINATING ACTIVITY: Enter the name and address of the contractor, subcontractor, grantee, Department of Defense activity or other organization *(corporate author)* issuing the report.

2*a*. REPORT SECURITY CLASSIFICATION: Enter the overall security classification of the report. Indicate whether "Restricted Data" is included. Marking is to be in accordance with appropriate security regulations.

2*b*. GROUP: Automatic downgrading is specified in DoD Directive 5200.10 and Armed Forces Industrial Manual. Enter the group number. Also, when applicable, show that optional markings have been used for Group 3 and Group 4 as authorized.

3. REPORT TITLE: Enter the complete report title in all capital letters. Titles in all cases should be unclassified. If a meaningful title cannot be selected without classification, show title classification in all capitals in parenthesis immediately following the title.

4. DESCRIPTIVE NOTES: If appropriate, enter the type of report, e.g., interim, progress, summary, annual, or final. Give the inclusive dates when a specific reporting period is covered.

5. AUTHOR(S): Enter the name(s) of author(s) as shown on or in the report. Enter last name, first name, middle initial. If military, show rank and branch of service. The name of the principal author is an absolute minimum requirement.

6. REPORT DATE: Enter the date of the report as day, month, year; or month, year. If more than one date appears on the report, use date of publication.

7*a*. TOTAL NUMBER OF PAGES: The total page count should follow normal pagination procedures, i.e., enter the number of pages containing information.

7*b*. NUMBER OF REFERENCES: Enter the total number of references cited in the report.

8*a*. CONTRACT OR GRANT NUMBER: If appropriate, enter the applicable number of the contract or grant under which the report was written.

8*b*, 8*c*, & 8*d*. PROJECT NUMBER: Enter the appropriate military department identification, such as project number, subproject number, system numbers, task number, etc.

9*a*. ORIGINATOR'S REPORT NUMBER(S): Enter the official report number by which the document will be identified and controlled by the originating activity. This number must be unique to this report.

9*b*. OTHER REPORT NUMBER(S): If the report has been assigned any other report numbers *(either by the originator or by the sponsor)*, also enter this number(s).

10. AVAILABILITY/LIMITATION NOTICES: Enter any limitations on further dissemination of the report, other than those imposed by security classification, using standard statements such as:

(1) "Qualified requesters may obtain copies of this report from DDC."

(2) "Foreign announcement and dissemination of this report by DDC is not authorized."

(3) "U. S. Government agencies may obtain copies of this report directly from DDC. Other qualified DDC users shall request through _____."

(4) "U. S. military agencies may obtain copies of this report directly from DDC. Other qualified users shall request through _____."

(5) "All distribution of this report is controlled. Qualified DDC users shall request through _____."

If the report has been furnished to the Office of Technical Services, Department of Commerce, for sale to the public, indicate this fact and enter the price, if known.

11. SUPPLEMENTARY NOTES: Use for additional explanatory notes.

12. SPONSORING MILITARY ACTIVITY: Enter the name of the departmental project office or laboratory sponsoring *(paying for)* the research and development. Include address.

13. ABSTRACT: Enter an abstract giving a brief and factual summary of the document indicative of the report, even though it may also appear elsewhere in the body of the technical report. If additional space is required, a continuation sheet shall be attached.

It is highly desirable that the abstract of classified reports be unclassified. Each paragraph of the abstract shall end with an indication of the military security classification of the information in the paragraph, represented as *(TS)*, *(S)*, *(C)*, *or (U)*.

There is no limitation on the length of the abstract. However, the suggested length is from 150 to 225 words.

14. KEY WORDS: Key words are technically meaningful terms or short phrases that characterize a report and may be used as index entries for cataloging the report. Key words must be selected so that no security classification is required. Identifiers, such as equipment model designation, trade name, military project code name, geographic location, may be used as key words but will be followed by an indication of technical context. The assignment of links, rules, and weights is optional.